Palacký University, Olomouc
Faculty of Science

Applications of Geochemical and Reactive Transport Modeling in Hydrogeology

Ondřej Šráček, Miroslav Černík, Zbyněk Vencelides

Olomouc 2013

Reviewers: Konstantin Raclavský
Zlatica Ženišová

INVESTMENTS IN EDUCATION DEVELOPMENT

"Innovation of the study program Environmental Geology"
Project OP VK CZ.107/2.2.00/15.0317

Acknowledgements
We thank Jaroslav Nosek for help with preparation of transport model.
The book was supported in part by the Project OP VaVpI Centre for Nanomaterials, Advanced Technologies and Innovation CZ.1.05/2.1.00/01.0005, and partly by the Project OP VK CZ.107/2.2.00/15.0317 "Innovation of the study program Environmental Geology". We also thank Konstantin Raclavský and Zlatica Ženišová for constructive reviews, which helped to improve this text.

First Edition

ISBN 978-80-244-3781-1

Content

1 Introduction

Application of geochemical modeling, frequently also coupled to reactive transport modeling, became an important part of many hydrogeological and geochemical investigations. This text intends to present some basic and typical applications of geochemical and reactive transport modeling. As stated in the title, focus of the text is on the modeling of geochemistry and reactive transport. This means that flow modeling and conservative tracer transport modeling principles are presented here only at the levels necessary for applications of geochemical and reactive transport types of modeling. Theoretical background in this text is limited and emphasis is placed on practical aspects of modeling, e.g. how to prepare a conceptual model, how to calibrate a model, how to choose mineral phases for geochemical modeling etc. Theoretical background can be found elsewhere in literature published in both English and Czech and some of these publications are included in references. Principal program used for geochemical calculations in this text is PHREEQC because it is available with no charge at web site of the U.S. Geological Survey.

Modeling in hydrogeology is sometimes considered not only a science, but also an art. We are trying to present here some rules of this "art". We hope this publication will be useful for modeling practitioners and we will be grateful for any feedback from readers, which could improve our text.

Authors

2 Flow modeling

2.1 Basic terms

The ability of an aquifer to transmit water is described by parameter called hydraulic conductivity K [m.s^{-1}], which also depends on properties of transmitted fluid. When hydraulic conductivity is integrated in vertical dimension, we obtain transmissivity T [m^2.s^{-1}], i.e. hydraulic conductivity multiplied by saturated thickness of aquifer. The volume of water released from storage in an aquifer per unit surface area per unit change in head is called storativity S [–]. In confined aquifer the property is characterized by the specific storage S_s [m^{-1}], which describes water release per unit volume of the aquifer, and in unconfined aquifer by the specific yield S_y [–], also known as drainable porosity (Domenico and Schwartz, 1998). Generally it holds that numerical value of $S_y >> S_s$.

A general form of governing equation for flow modeling in 2-D (i.e. in the aquifer view point in the terminology of Anderson and Woessner, 1992) is

$$\frac{\partial}{\partial x}\left(T_x \frac{\partial h}{\partial x}\right)+\frac{\partial}{\partial y}\left(T_y \frac{\partial h}{\partial y}\right)=S\frac{\partial h}{\partial t}-R+L \tag{2.1}$$

where leakage L is calculated as

$$L=-K_z \frac{h_{source}-h}{b'} \tag{2.2}$$

In these equations R represents source/sink term (e.g. pumping well discharge), b' is thickness of aquitard across which leakage takes place and h_{source} is hydraulic head in the source of leakage area (e.g. in overlying aquifer which leaks water across aquitard to the modeled aquifer).

When fully 3-D modeling of flow is considered the general form of governing equation is

$$\frac{\partial}{\partial x}\left(K_x \frac{\partial h}{\partial x}\right)+\frac{\partial}{\partial y}\left(K_y \frac{\partial h}{\partial y}\right)+\frac{\partial}{\partial z}\left(K_z \frac{\partial h}{\partial z}\right)=S_s\frac{\partial h}{\partial t}-R \tag{2.3}$$

This equation strictly applies for confined aquifer where saturated thickness remains constant. In unconfined aquifer situation is different because saturated thickness changes as a consequence of decreasing hydraulic head. Governing equation is

$$\frac{\partial}{\partial x}\left(K_x \frac{\partial h^2}{\partial x}\right)+\frac{\partial}{\partial y}\left(K_y \frac{\partial h^2}{\partial y}\right)=2S_y \frac{\partial h}{\partial t}-2R \tag{2.4}$$

The equation above is nonlinear because h appears to the second power at left side and to the first power at right side.

For more detailed treatment of the topic see Freeze and Cherry (1979), Domenico and Schwartz (1998) and in Czech Šráček and Kuchovský (2003).

2.2 Steps in preparation of a flow model

Principal steps in preparation of a flow model include:
(a) Establishing purpose of modeling,
(b) Development of conceptual model,
(c) Selection of computer code,
(d) Model design,
(e) Model calibration,
(f) Sensitivity analysis,
(g) Model verification,
(h) Model prediction,
(i) Postaudit.

Ad (a). In this step, called establishing of model purpose, we justify why we need modeling to achieve project's goals. In some cases a simple analytical solution can be used instead of more sophisticated and time-consuming numerical code.

Ad (b). Conceptual model is perhaps the most important part of modeling process. Errors in this step are the most common and they can spoil completely whole modeling effort (Bredehoeft, 2005). In this step we define hydrostratigraphy, hydraulic parameters of different units and also stresses on the modeled system.

Ad (c). In this step we have to select modeling code which is able to model processes included in conceptual model. This step should also include verification of a code, i.e. determination if the code solves correctly governing equations.

However, when we use well-established codes such as MODFLOW, we assume that the code has already been verified.

Ad (d). In model design step we turn conceptual model into a form suitable for modeling. In this step modeling grid is designed, boundary conditions and time steps are selected and preliminary values of hydraulic parameters and hydrological stresses are set up. When we want to use the model for later transport and/or reactive transport modeling, in flow modeling step we have to already consider criteria for transport modeling grid size including suitable values for Peclet number and Courant number (see chapter 3.1).

Ad (e). In calibration step a set of values for hydraulic parameters and hydrologic stresses is found which approximates well values of hydraulic heads and water fluxes. Calibration is generally performed in steady-state mode. Calculated and observed hydraulic heads are compared and calibration error is evaluated using several parameters presented, for example, by Anderson and Woessner (1992). Calibration can be done by trial-and-error or by the application of automated parameter estimation code.

Ad (f). In this step sensitivity analysis is performed to determine the effect of uncertainty on the calibrated model. By variation of selected model parameters, the most critical parameters are found, which have an impact on calculated hydraulic heads.

Ad (g). Purpose of this verification step is to establish more confidence in the model using the set of calibrated data to produce second set of calculated hydraulic heads. Commonly verification is performed in transient mode to calibrate strorativity values, which cannot be calibrated in steady-state mode. However, some modeling experts are arguing that verification of a model in the sense of Karl Popper's approach is impossible (Konikow and Bredehoeft, 1992) and, according to them, the term "verification" should be replaced, for example, by "history matching".

Ad (h). Prediction provides a quantitative response to events in future (e.g. pumping scenario). The model is run using parameters based on calibration and verification, but stresses in the modeling are based on values expected in future. This means that estimates of future stresses are necessary for this simulation. Prediction is generally the principal purpose of a modeling exercise.

Ad (i). Postaudit is frequently neglected part of modeling, but it is very important. Several years after modeling new data are collected to determine whether modeling provided correct results. The postaudit should be performed long enough to guarantee that there was sufficient time for changes to occur.

3 Transport modeling

3.1 Basic terms

There are several processes of contaminant transport in water (Table 3.1):

Diffusion is contaminant transport based on concentration gradient, which may also occur in standing water or even against flow direction. Steady state diffusion is described by the 1st Fick's Law. Principal parameter is effective diffusion coefficient D_e [$m^2.s^{-1}$], which is calculated from diffusion coefficient for free water D_w taking into account porosity and tortuosity of porous media (Fetter, 1999).

Advection is transport with bulk motion of flowing water on the basis of hydraulic gradient. Principal parameter is average linear velocity v [$m.s^{-1}$] determined by Darcy's Law equation. Advection is generally principal transport mechanism except very low permeability materials, where diffusion dominates.

Dispersion is contaminant spreading caused by velocity variations at different scales including pore scale, layer scale, and aquifer scale (Fetter, 1999). It is linked to advection and if there is no advection, there is no dispersion (but there still can be diffusion). Principal parameters are longitudinal dispersivity α_L, transversal dispersivity α_H, and vertical dispersivity α_V. Units for all dispersion parameters are [m]. Dispersivity is combined with effective diffusion coefficient into parameter called hydrodynamic dispersion D_L,

$$D_L\ [m^2.s^{-1}] = \alpha_L.v + D_e \qquad (3.1)$$

When flow velocity v is close to 0, $D_L = D_e$. Value of dispersivity can be determined by trace test (ideal case) or by empirical relations based on the increasing value of dispersivity with increasing length of contaminant plume, e.g. equation of Xu and Eckstein (Domenico and Schwartz, 1998),

$$\alpha_L\ [m] = 0.83\ [\log (L)]^{2.414} \qquad (3.2)$$

where L is length of plume in m (i.e. transport scale).

Adsorption is process of attachment of contaminant particles to the surface of solid phase. Reversed process is called desorption. Adsorption is frequently

described by distribution coefficient, K_d [$L.g^{-1}$], representing linear adsorption isotherm. It can be determined based on a batch test as a slope of straight line in graph

$$S\ [mg.g^{-1}] = f\{C[mg.L^{-1}]\} \tag{3.3}$$

where S is adsorbed amount of contaminant and C is equilibrium concentration in water (also see Fig. 4.3). The linear adsorption isotherm does not consider finite amount of adsorption sites, but there are other isotherms, which consider this effect, e.g. Langmuir adsorption isotherm. Linear adsorption isotherm is used to calculate **retardation coefficient** R,

$$R\ [-] = v_{conser}/v_{adsor} = L_{conser}/L_{adsor} = 1 + (\rho_b/n).K_d \tag{3.4}$$

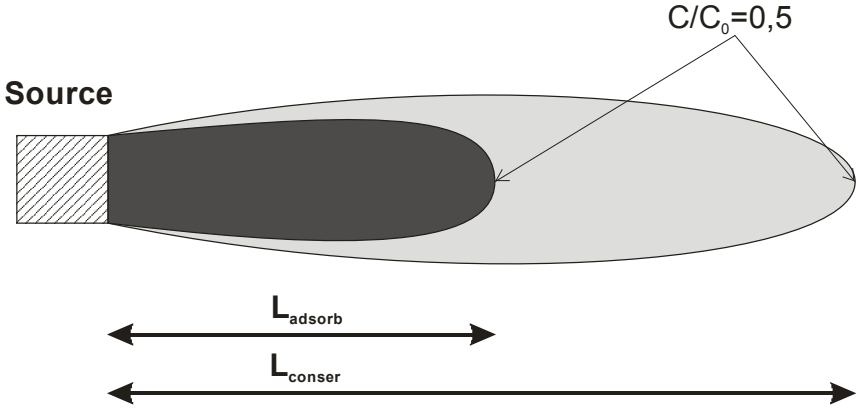

Fig. 3.1 Concept of retardation

where v_{conser} is velocity of advective transport of a conservative contaminant (i.e. contaminant with no sorption, decay or precipitation), v_{adsor} is velocity of advective transport of adsorbed contaminant, L_{conser} is the transport distance of conservative contaminant, L_{adsor} is transport distance of adsorbed contaminant (Fig. 3.1), ρ_b is bulk density of solid phase and n is porosity of porous media. As observed in Fig. 3.1, retardation coefficient is the ratio of respective transport distances for conservative and adsorbed contaminant and, because time is fixed, it is also the ratio of their advective velocities (i.e. approximated by their relative concentrations $C/C_0 = 0.5$).

For organic contaminants a different approach for determination of adsorption isotherm is used instead of batch test (Fetter, 1999; Šráček and Zeman, 2004). First of all, distribution coefficient octanol-water K_{ow} is taken from literature and

distribution coefficient organic carbon-water K_{oc} is calculated using an empirical equation such as the equation of Schwarzenbach-Westall (Fetter, 1999):

$$\log K_{oc} = 0.49 + 0.72 \log K_{ow} \tag{3.5}$$

Then value of K_d is calculated as

$$K_d = K_{oc} \cdot f_{oc} \tag{3.6}$$

where f_{oc} is a fraction of organic carbon in aquifer solids. Finally retardation coefficient R is calculated using equation 3.4 just like for inorganic contaminants.

Decay is decomposition of contaminant generally accompanied by formation of its daughter product. In fact, this process applies only for organic contaminants (and, of course, for radionuclides), but not to inorganic contaminants. For example, when benzene, C_6H_6 is transformed to CO_2, it is gone forever. In contrast, when Cr(III) precipitates as $Cr(OH)_3$, it remains in solid phase and can be re-mobilized in changing pH and Eh conditions. Principal decay parameters are decay constant λ [s^{-1}] and half-life $t_{1/2}$ [s]. They are linked by relation

$$\lambda = \ln 2 / t_{1/2} \tag{3.7}$$

All processes are implemented in **Advection-Dispersion Equation** (ADE) which has the following form for a conservative contaminant in 1-D:

$$D_x \frac{\partial^2 C}{\partial x^2} - v_x \frac{\partial C}{\partial x} = \frac{\partial C}{\partial t} \tag{3.8.}$$

The equation also has 2-D and 3-D forms and can be solved by analytical or numerical methods. Analytical solution of 1-D equation (i.e. applicable to laboratory column) is called solution Ogata-Banks (Freeze and Cherry, 1979). The Ogata-Banks solution of the ADE gives concentration C(x, t).

Principal sources of contamination can be constant source and instantaneous source. **Boundary conditions** for constant source can be constant concentration C_0 at the source point x = 0 or constant contaminant flux J_C (x = 0) at the boundary of solution domain. First boundary condition is more common, but both boundary conditions give converging solution in longer distance from a source.

Peclet number Pe = $\Delta l/\alpha_L$ is used to determine nodal spacing Δl in numerical modeling grid. Recommended value is less than 10.

Courant number C = v ($\Delta t/\Delta l$) is used to determine discretisation of time step Δt in numerical modeling. Recommended value is less than 1. This means that time step should be $\Delta t < \Delta l/v$, meaning shorter than time it takes for contaminant to move the distance Δl.

More detailed treatment of contaminant transport processes is in Fetter (1999) or in Czech in Šráček et al. (2002).

Table 3.1 Transport processes

Process	Characteristic parameter	Symbol and units
Diffusion	Effective diffusion coefficient	D_e [$m^2 \cdot s^{-1}$]
Advection	Flow velocity	v [$m \cdot s^{-1}$]
Dispersion	Dispersivities	α_L, α_H, α_V [m]
Adsorption	Linear adsorption isotherm	K_d [$L \cdot g^{-1}$]
Decay	Decay constant, half life	λ [s^{-1}], $t_{1/2}$ [s]

3.2 Example of transport modeling

As an example of mathematical modeling application, there is a modeling of a complex locality including extraction wells, impermeable barriers and remediation system. The purpose of the modeling was to estimate groundwater sources exposure due to existence of contamination. Groundwater flow model is based on MODFLOW (McDonald and Harbaugh, 1988) and transport model on MT3D (Zheng and Wang, 1999).

3.2.1 Introduction

The purpose of mathematical modeling at a model locality was to create a numerical flow and transport model with the aim of:

- building a model to interpret a map of measured groundwater isolines obtained in a state affected by:
  - the existence of underground barriers restricting the groundwater flow,
  - extraction groundwater from the Spring area at a total rate of 120 $L.s^{-1}$,
  - simultaneously pumping/infiltration on-site within the framework of the operation of a remedial system (pumping of 2.2 $L.s^{-1}$ and simultaneously infiltration of 0.8 $L.s^{-1}$),

- modeling the state unaffected by pumping based on the calibrated model in an affected state,
- defining the main groundwater flow directions based on the model,
- using the flow model to simulate the transport of substances and estimate the possible risks to the infiltration area in a 30 year horizon.

3.2.2 Used numerical tools

To meet the above-mentioned objectives, the modular three-dimensional mathematical tool Processing MODFLOW Pro® was used. This software uses the program MODFLOW 2000 to calculate the flow field as it allows the simulation of steady and unsteady groundwater flow in general multi-aquifer systems. The modular structure allows a number of hydrological problems to be solved and, if necessary, easy modification of input data. It is made up of the main program and a set of modules, through which it is possible to model the impact of pumping and infiltration wells, drainage systems, preferential pathways, sealing effects of tectonic faults, surface water courses, underground barriers, spatial dosage of groundwater from precipitation, evapotranspiration and to define special boundary conditions.

The PMPATH model was used to illustrate the main contamination migration pathways and to simulate advection transport. This module depicts the flow lines in the model flow field and tracks the migration without the influence of retardation using backward tracking and forward tracking methods.

The migration of the selected contaminants was simulated using the transport model MT3DMS, which enables the simulation of multiple substances at once.

The SURFER(TM) (Golden Software Inc.) program was used to evaluate the groundwater flow input and output data.

3.2.3 Input data and description of the model

The size of the modeled area was chosen to sufficiently cover the whole area of concern, which covers an area of 3 × 2.3 km. The model was designed so that its geometry, geological description, hydrological and hydrogeological characteristics describe the actual state of the site as closely as possible in regards to the information that was available during its design.

The following input data files were used to build and calibrate the groundwater flow model (Table 3.2):

Table 3.2 Flow model input data

Parameter	Value	Parameter	Value
Units and time steps		*Boundary conditions*	
units of time	[s]	Dirichlet	boundary of the model
units of length	[m]		
number of simulation periods	1 – steady state	Neumann	not used
		Cauchy	not used
Layers and elements		*Other parameters*	
number of layers	1	effective porosity	0.25
number of lines	213	hydraulic conductivity	1×10^{-5}–2.8×10^{-3} m.s^{-1}
number of columns	205	initial piezometer heads	208.9–214.6 m
length of element on *x* axis	20 and 4 m	infiltration	15–82 mm.year^{-1}
length of element on *y* axis	20 and 4 m		
Type of GW level	unconfined/ confined		
top of aquifer bottom of aquifer	208.3–212.5 m 200.6–208.1 m		

3.2.4 Boundary conditions

The selected types of model boundary conditions were taken into account when choosing the size of the model (Fig. 3.2). The size of the model was therefore chosen so that the western boundary of the model formed the water flow boundary, represented in the model by the boundary condition of a constant groundwater level. The northern and south-eastern boundary conditions were also simulated by the boundary conditions of a constant groundwater level, while the given values of the groundwater level under these boundary conditions are located on an imaginary flow line. The north-eastern boundary condition represents a line of pumping wells in the Spring area, which is interpreted in the model using constant groundwater head conditions with values measured when defining the affected state. The eastern boundary condition is represented by a water flow with constant groundwater heads at 212.5 meters above sea level.

Wells located within the model area, where pumping or infiltration of water occurs, were simulated using a constant flow to/from the elements and horizontal flow barrier with elements of substantially lower hydraulic conductivity.

The size of the modeled area with a designating model network, and the types of boundary conditions are shown in Fig. 3.2. An irregular model network with elements of 20×20, 20×4, 4×20 and 4×4 m was used. Because it is necessary to simulate the migration of substances throughout the model area as well as the influence of the detailed boundary conditions (local pumping), an irregular model

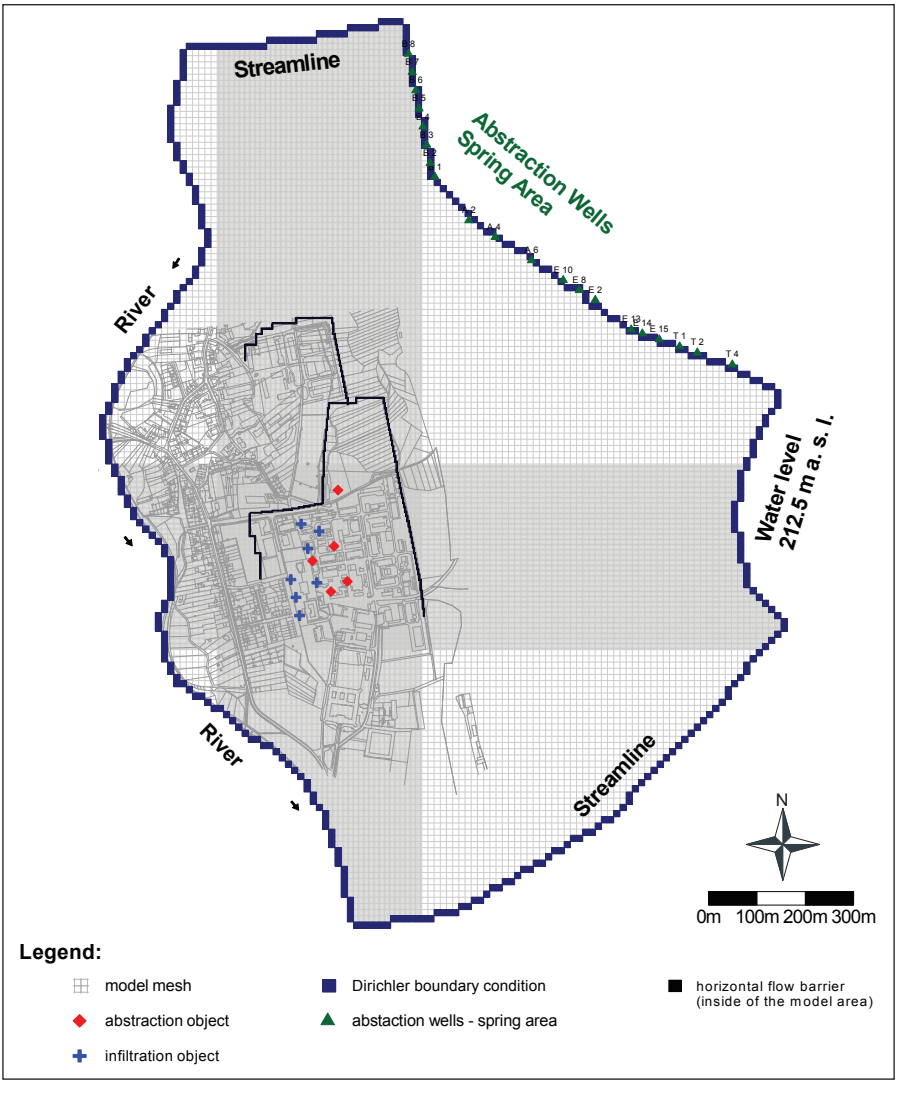

Fig. 3.2 Model area with boundary conditions

network had to be used. The basis is a model network with elements of 20 × 20 m. In areas where an underground sealing wall (hereinafter referred to as USW) is located and where the pumping/infiltration wells of the remedial system are being used the model network was decreased to 4 × 4 m (the size of the model grid is also shown in Fig. 3.2). Because MODFLOW model is based on the method of finite differences there are also model elements with sizes of 20 × 4 and 4 × 20 m. A total

of 66,690 model elements were used to describe the flow at the site, from which 12,156 were inactive (outside the model area beyond the boundary conditions).

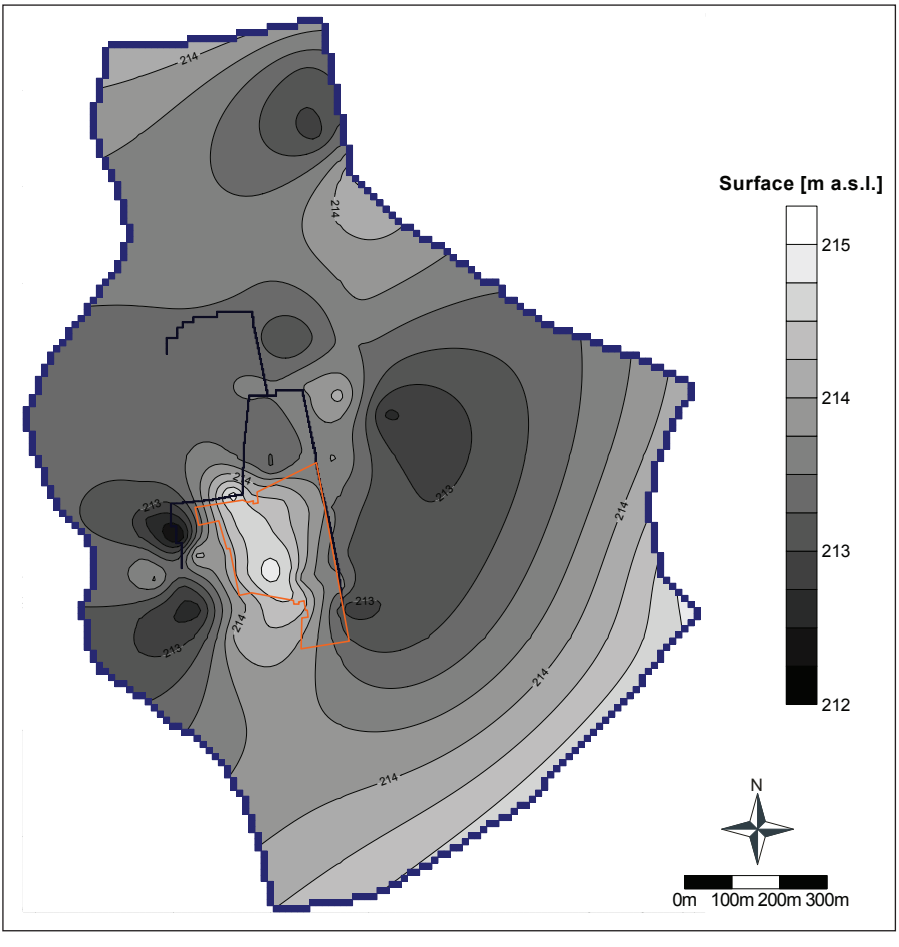

Fig. 3.3 Simulation of ground terrain in the model

Vertically, the model is designed as a one layer model with varied areal distribution of hydraulic conductivity based on the geological description of the site. For the design of the digital terrain maps, terrain elevation measurements of accessible wells were used and z-coordinates obtained by interpolation were used in areas without wells. The terrain representing the top of the aquifer is not relevant for the model as the groundwater level is unconfined throughout the study area. The terrain model is illustrated in Fig. 3.3.

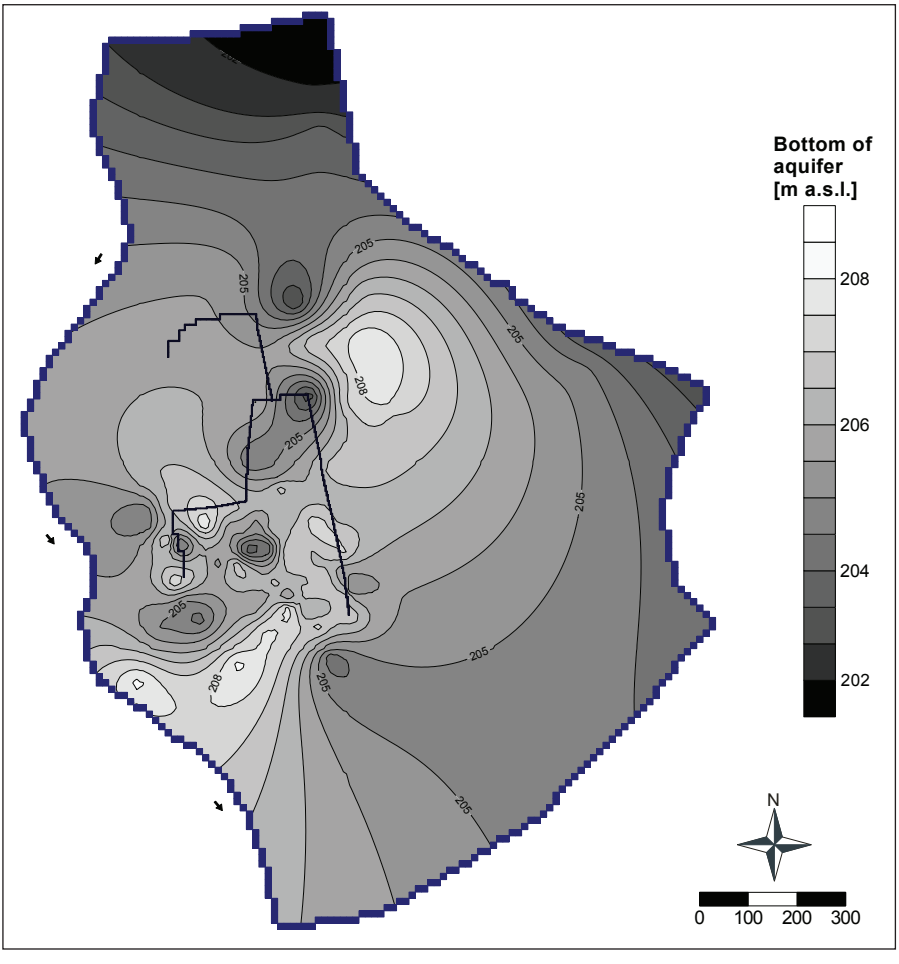

Fig. 3.4 Simulation of modeling domain bottom (top of impermeable clay layer)

The base of the aquifer is represented in the model by a bottom layer of sandy gravel, beneath which is a significantly less permeable clay layer. Geological profiles obtained from the available wells were used for the design of the model. The bottom of the model aquifer is shown in Fig. 3.4. Due to the fact that the level of geological exploration in the area is varied, the amount of data determining the base of the aquifer is also varied. The majority of the data and therefore the most accurate interpretation of the base of the aquifer are in the centre of the model area and the quality declines towards the edges. This is not such a problem for the mathematical modeling because the ultimate goal is to model the migration of substances from an area of greater exploration towards the edges of the model.

3.2.5 Flow model

The purpose of the flow model is to describe the current situation of groundwater flow and to simulate variations of change in this situation; also a well-calibrated flow model is the basis for the transport model.

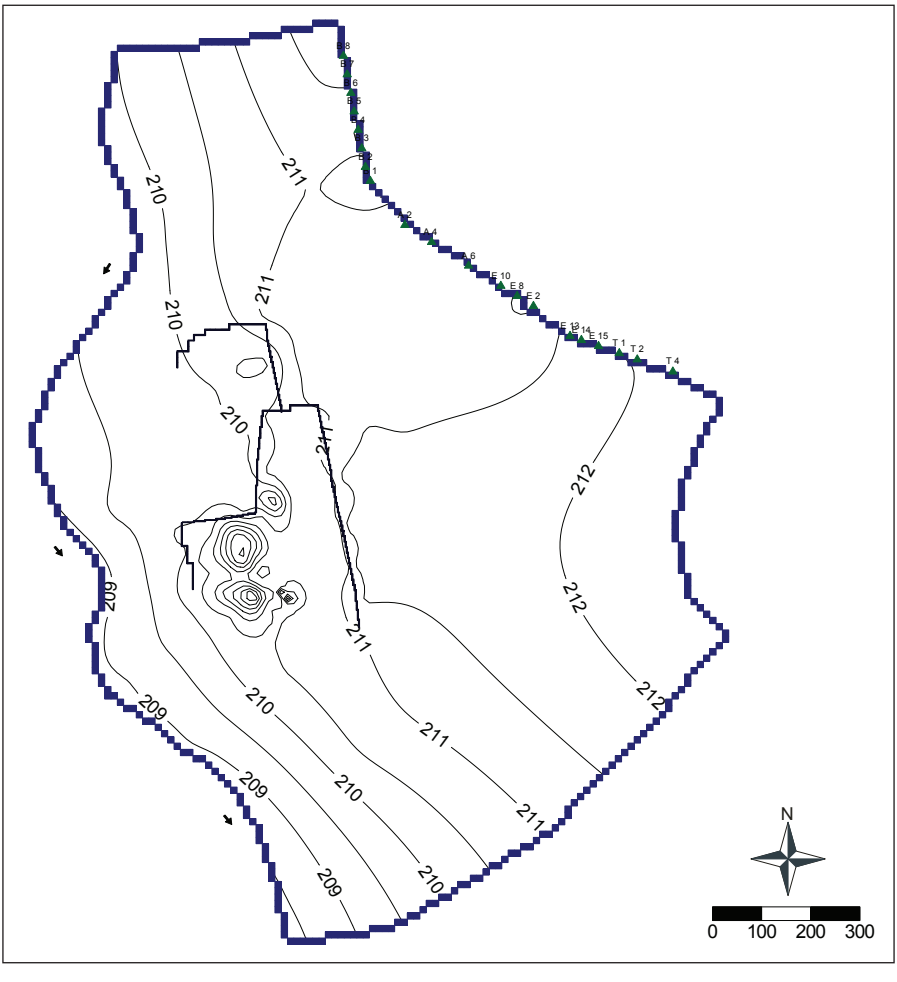

Fig. 3.5 Interpreted groundwater levels based on measured values

3.2.6 Calibration of the flow model

The flow model was calibrated to the measured affected state of the groundwater level included in Fig. 3.5. During this period, on-site remedial pumping/infiltration took place. Specific values of the volumes of pumped/infiltrated water are included in Table 3.3. Groundwater pumping in the infiltration area to the northeast of the area of concern has a major influence on the model flow field. This pumping is represented in the model by a decrease in the groundwater level in line of pumping wells: B1, A1, A2, A4, A6, E10, E2, E14, E15, T2, T3 (see Fig. 3.2, north-eastern boundary conditions).

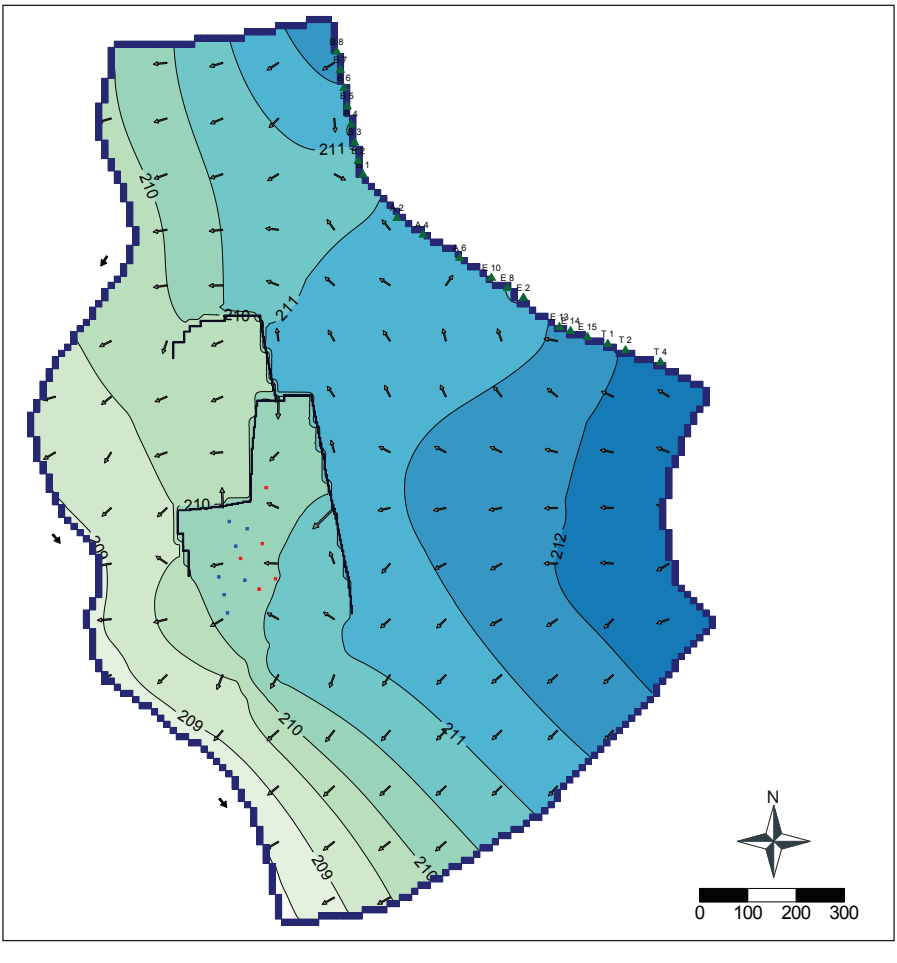

Fig. 3.6 Calculated groundwater levels and flow vectors (affected by local pumping and USW)

Table 3.3 On-site groundwater pumping/infiltration wells

Infiltration wells		Pumping wells	
Name of well vrtu	**Q (l.s^{-1})**	**Name of well**	**Q (l.s^{-1})**
R-50	0.06	AT-106	–0.58
R-211	0.16	P-32	–0.51
R-212	0.16	P-56	–0.19
R-213	0.16	SM-9	–0.36
SM-1	0.13	R-217	–0.60
SM-3	0.04		
SM-4	0.08		
Total	0.79		–2.24

Calibration of the flow model takes place by changing the spatial distribution of the hydraulic conductivity and then by comparing the calculated and measured groundwater levels so that the differences between the two levels are minimal. The hydraulic conductivity in the calibration was varied in the range of values for the expected type of aquifer material in the model area. Given the wide range of factors that have a large impact on the model (proximity of remedial wells and USW, the existence of underground storage tanks affecting groundwater flow, unsatisfactory state of some infiltration wells etc.), the wells around the site were assigned a lesser weight for the calibration or they were omitted from the flow model calibration altogether.

The result of the calibration of the flow model based on the measured groundwater level is included in Fig. 3.6, differences between the calculated and measured groundwater levels are shown in Fig. 3.7, the corresponding calibrated model distribution of hydraulic conductivity is illustrated in Fig. 3.8 and thickness of saturated layer is in Fig. 3.9.

The groundwater level in the aquifer decreases from east to west (towards the river) and the general character is influenced by local anthropogenic interference (Fig. 3.6). One of these is the pumping of water in the north-eastern part of the model (the Spring area), which is reflected in the significantly lower levels of groundwater than in general. Even more significant elements are the underground barriers at the site, which retain water on the inlet side (eastern part) forming a relatively important groundwater level plateau near the river. Local effects of pumping and infiltration of water at the site are not significantly reflected on the isolines and have limited extent. In terms of the overall balance of water this interference is unimportant because the difference between the infiltrated and pumped volumes is only about 1.5 l.s^{-1}. The flow direction shown in Fig. 3.6 is

also illustrated using flow velocity vectors. It is easy to see the pumping of water to the northeast of the model area (arrows pointing to the pumping locations), which is consistent with the isolines. The arrows can also be seen wrapping around the underground barriers and their effect on the local flow.

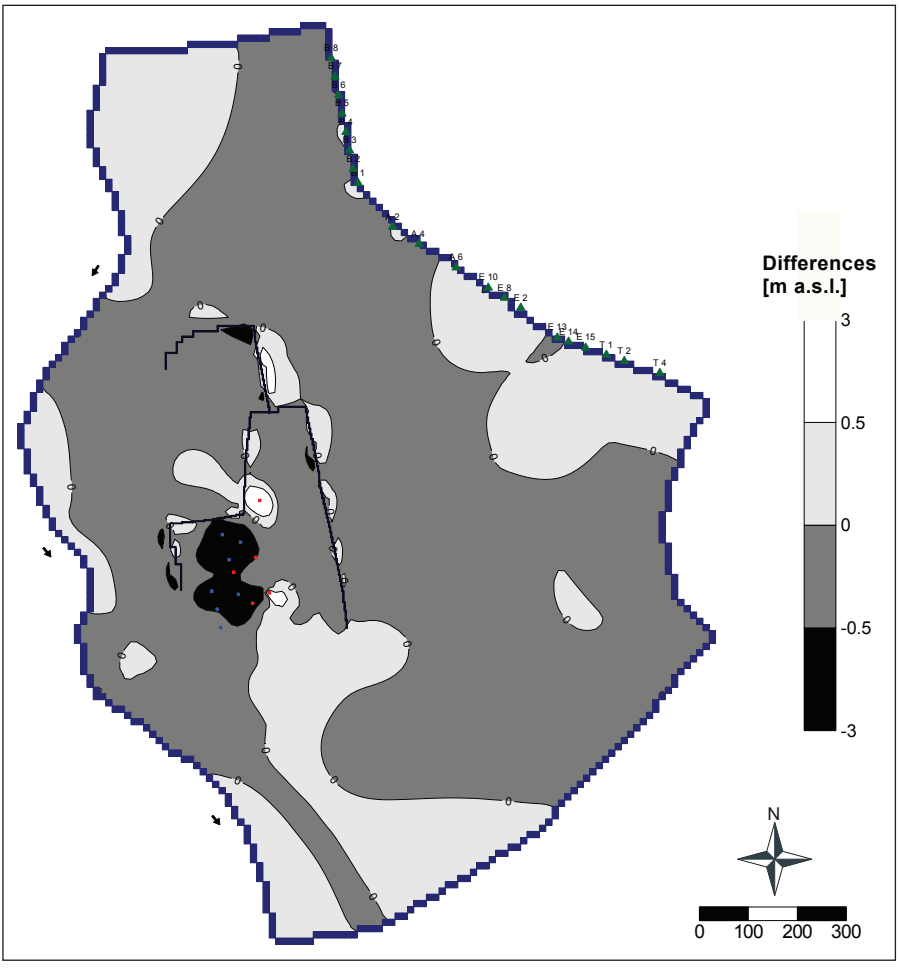

Fig. 3.7 Differences in the calculated and measured groundwater levels

When comparing all of the available groundwater level point measurements with the groundwater levels calculated by the model the average difference between the groundwater levels is 0.34 meters. The most common difference is around 0.2 m (Fig. 3.7). In seven of the monitored wells, however, this difference is greater

than 1.5 meters. These are on-site wells that are located on site and are part of the remedial system. This difference is not only due to the above described and poorly modeled heterogeneity, but also the fact that the remedial pumping takes place intermittently depending on the capacity of decontamination station and the measured groundwater levels representing the current state, not the long-term average. Another important factor is that the groundwater levels expressed in the individual elements are average values in the element 4 × 4 meters in contrast to the values found directly in the pumping (or infiltration) wells, where they are maximum values.

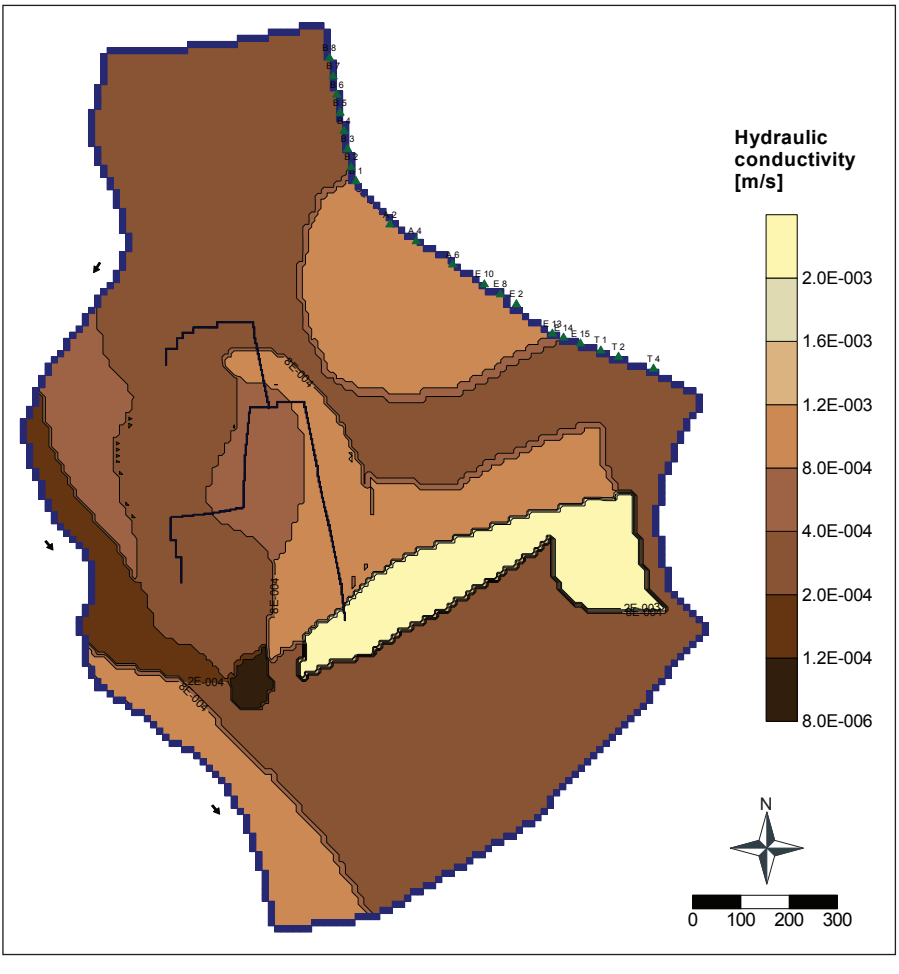

Fig. 3.8 Calibrated hydraulic conductivity

The distribution of hydraulic conductivity is based on the values corresponding to the nature of the geological environment. Detailed values for each model elements are based on the efforts to fit the measured groundwater levels by the model. The result is a map of the distribution of calibrated hydraulic conductivity of the aquifer shown on Fig. 3.8. As the basis there are values between 1.10^{-4}–1.10^{-3} m.s^{-1} with some extreme value areas, which are due to the geological profile.

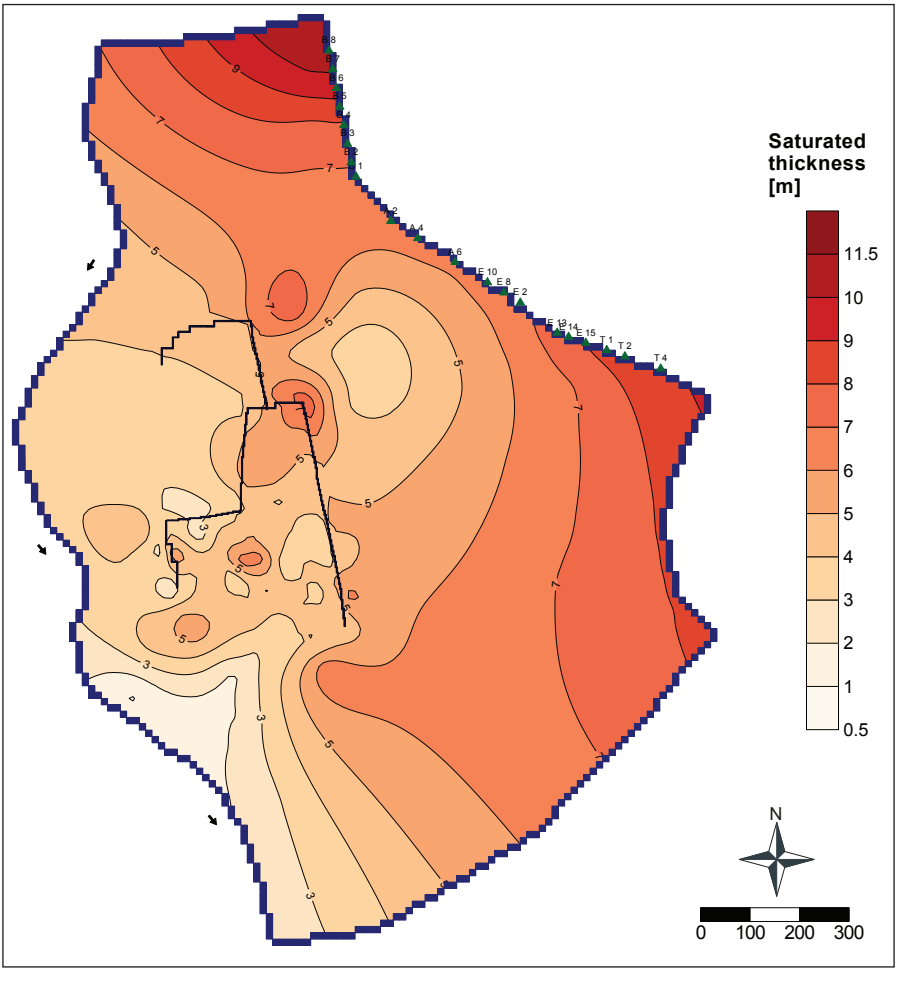

Fig. 3.9 Saturated aquifer

Another interesting result of the model is a map of saturated thickness of the aquifer, which is calculated as a difference between the calculated groundwater

level and the bottom of the aquifer (Fig. 3.9). Results show that in the area of remedial action (between USW) the saturated thickness is about 4 meters. Closer to the river the thickness of the aquifer declines, but on northern and eastern part rises. On the figure we can also see a decrease of the thickness in the Spring area, due to water extraction and local extremes in the remedial fields.

Another good way to display the groundwater flow direction is to use flow lines which depict in which direction the water flows from the selected model elements. These flow lines are shown for the calibration state in Fig. 3.10. The figure shows how the water flowing from the east deflects around the impermeable barriers and also how the water flows from the area of the remedial action.

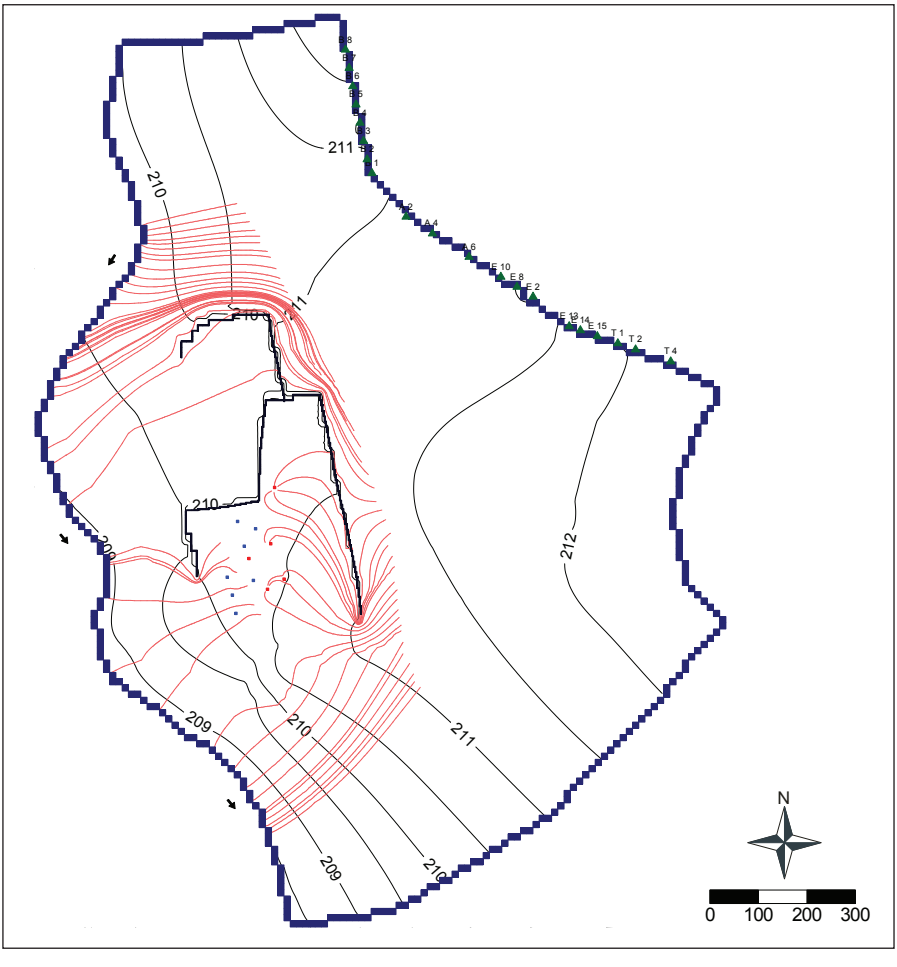

Fig. 3.10 Flow lines of calibrated model

3.2.7 Calculation of different hydraulic variants

There exists a requirement to test the possibility of increasing the pumping (to 250 l.s^{-1}) in the Spring area and the effect of this change on the flow in the model domain. Another change from the calibrated model is a stop of remedial system (pumping/infiltration on-site). The basic question is whether the contamination that occurs at the site can migrate to the groundwater resources in the Spring area and thereby threaten these resources.

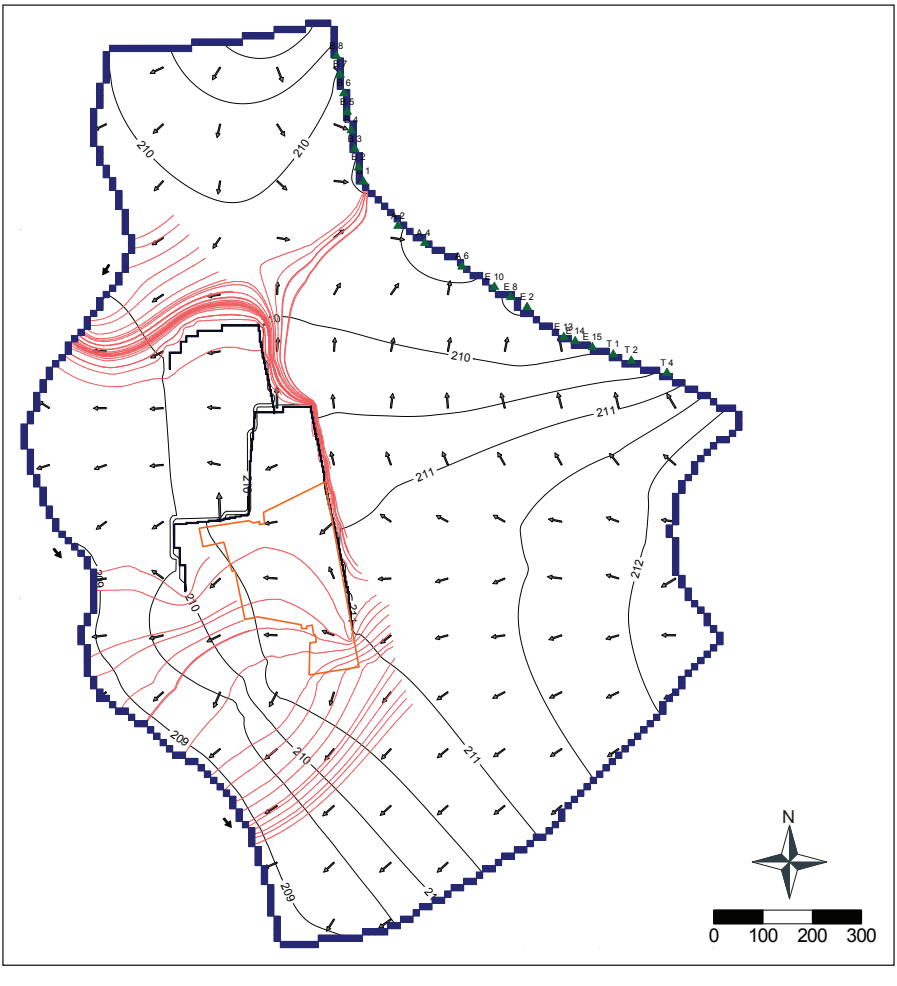

Fig. 3.11 Model results for the pumping of 250 L.s^{-1}

The result of the modeling scenario (Fig. 3.11) shows that due to the increased pumping the groundwater flow is deflected into the Spring area. Stopping the remedial work at the site has only a local effect on groundwater flow, which leads to a slight increase in the groundwater levels at the site due to the fact that the balance of water increases by stopping the pumping. The flow directions are not significantly changed.

The second model scenario is based on the previous one and in addition integrity of USW is compromised (i.e. USW is desintegrated). This scenario, which is well on the safe side, represents an unlikely future where the walls completely lose their ability, remedial works are stopped, but contamination is not yet removed. The result in Fig. 3.12 shows that even with this option, the water flows from the contaminated area towards the river and not to the infiltration area.

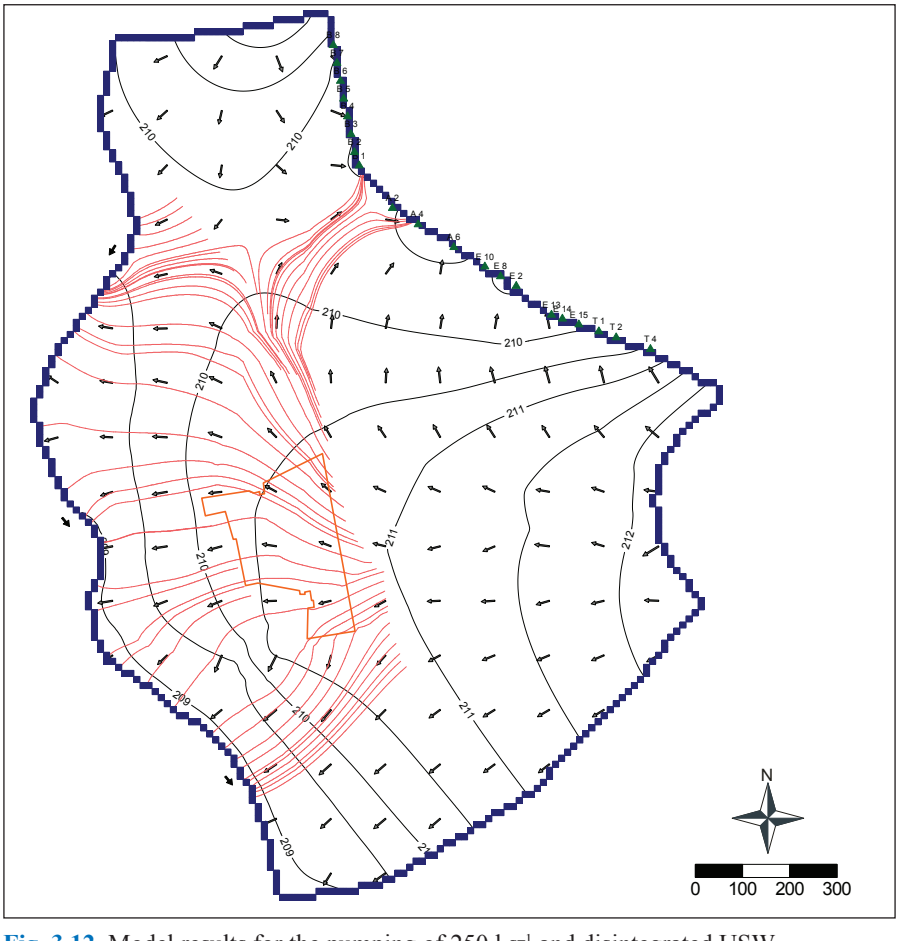

Fig. 3.12 Model results for the pumping of 250 $l.s^{-1}$ and disintegrated USW

3.3 Transport model

Two compounds were chosen as an example for transport modeling, namely ammonium ions, which represent a group of substances with very a low adsorption (migrate through the rock environment virtually without retardation), and chlorobenzene representing substances whose retardation is high due to sorption. Based on the results of the transport model it is possible to form an idea of the velocity of migration of other substances not simulated.

The migration of the selected contaminants was simulated using the transport model MT3DMS, which allows the simulation of multiple substances at once. The transport model parameters are listed in Table 3.4.

Table 3.4 Transport model input data

Parameter	Value	Parameter	Value
Sorption parameters		*Advection model parameters*	
bulk density (ρ)	1 800 kg.m^{-3}	method of calculating advection	upstream finite difference method
effective porosity (n_{ef})	0.25		
		Dispersion model parameters	
K_{OC}*		longitudinal dispersivity	2 m
– chlorobenzene	0.29 m^3.kg^{-1}	transverse dispersivity	0.2 m
– ammonium ions	1.61×10^{-7} m^3.kg^{-1}	vertical dispersivity	0.2 m
		Time parameters	
model value f_{OC}	0.0015; 0.01	length of simulation periods	30 year
distribution coef. K_D	$K_D = K_{OC}$* f_{OC}	time step	1 year
sorption type	linear ($R=1+K_D$* ρ/n_{ef})		

* Data source: EPI SuiteTM. U.S. EPA (http://www.epa.gov/reg3hscd/risk/human/rb-concentration_table/Generic_Tables)

In terms of the transport model design there are two key input parameters that significantly contribute to the behavior of the simulated substances: the effect of concentrations of organic carbon fraction in solid phase (f_{OC}) and the effect of modeled sources of contamination.

Sorption is simulated in the model as being linear; its size is specified by a distribution coefficient K_D for each of the individual contaminants. This distribution coefficient is calculated from the partition coefficient and the concentration of organic carbon (see Table 3.4). The higher the concentration of organic carbon, the greater is the sorption of the modeled substances onto the rock environment and therefore their slower migration. Two situations were simulated in terms of f_{OC}. The usual f_{OC} value is about 0.01. For safety reasons, value of 0.0015 was

also included in modeling, which is less favorable from the point of view of the hazardousness of contaminants (faster migration towards potential recipients).

Another input parameter to the transport model is the source of contamination. Besides initial distribution of contaminants in the aquifer, the model has a possibility to simulate a constant source of contamination. If constant sources are not used dilution leads to a rapid reduction of the contamination plume, which is often in conflict with observations at the site. This phenomenon is solved by using elements that serve as sources of contamination for the duration of the modeled period. These sources represent the contaminant in the unsaturated zone, where washing out leads to infiltration into the aquifer. This behavior is closer to the actual behavior at the site and hence it was also simulated.

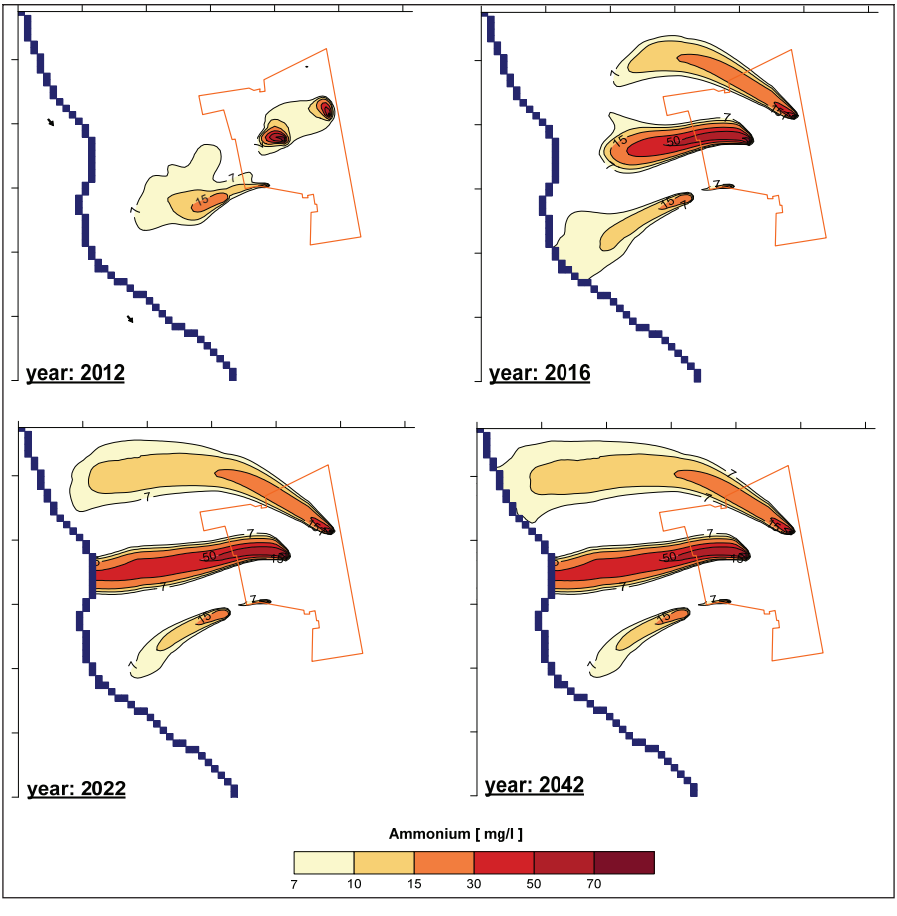

Fig. 3.13 Modeling of ammonium transport, model part

For the modeling, a situation was given where the impermeable barriers no longer fulfilled their function (the second modeling scenario, Fig. 3.12). In total, therefore, three transport model variants were calculated:

a) Modeling without retardation (ammonium ions) → Fig. 3.13;
b) Modeling with retardation (chlorobenzene), $f_{OC} = 0.01$ → Fig. 3.14;
c) Modeling with limited retardation (chlorobenzene), $f_{OC} = 0.0015$ → Fig. 3.15.

The first result is a model of the migration of ammonium ions. Fig. 3.13 shows the development of their concentrations over 30 years with a constant source. From the initial situation, which corresponds to the year 2012, there were three constant flows of ammonium ions towards the river due to migration in the direction of

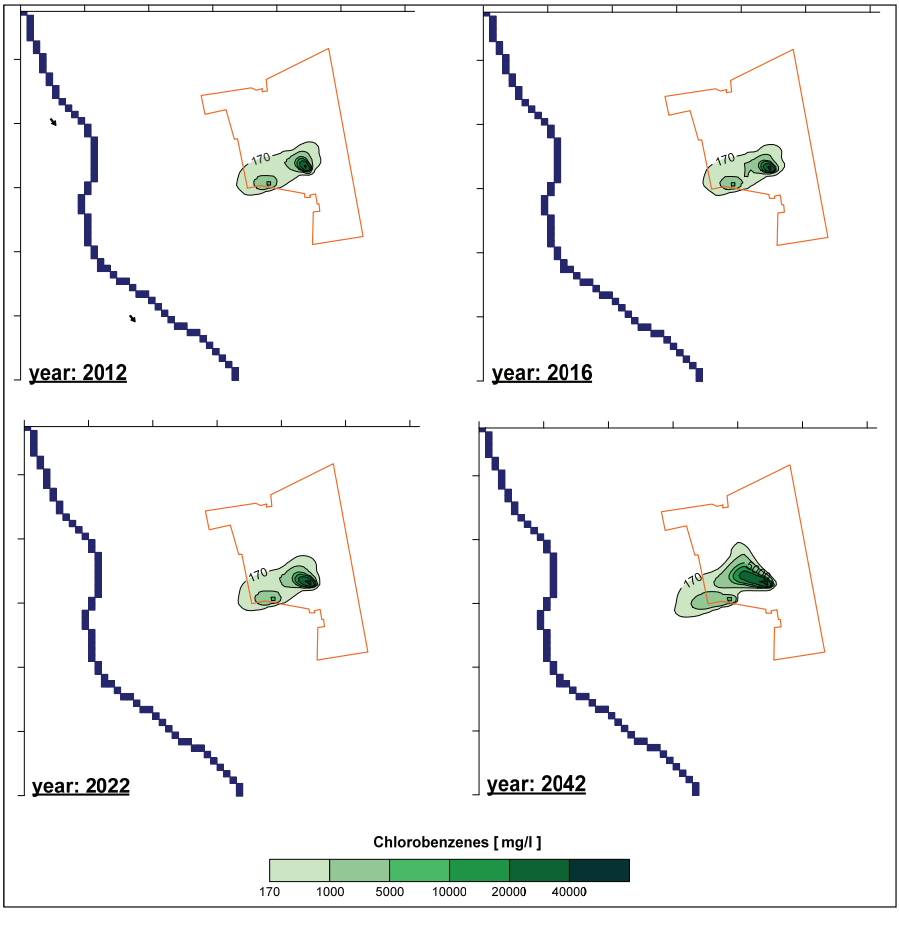

Fig. 3.14 Modeling of chlorobenzene migration ($f_{OC} = 0.01$), model part

the groundwater flow. These flows stabilize in time and represent a constant flow into the river. The concentration decrease is only due to dilution. For ammonium ions the variant with different f_{OC} was not modeled because the ammonium ions are not sorbed and therefore they are not affected by the f_{OC}.

A different situation exists for the sorbing chlorobenzene. Fig. 3.14 shows transport for f_{OC} values of 0.01, while Fig. 3.15 shows results for f_{OC} values of 0.0015. Since the initial distribution of chlorobenzene is different than that for ammonium ions, the shape of the contamination plume as it evolves over time is also different. In the case of f_{OC} values of 0.0015 the character of the contamination plume is analogous to that of the ammonium ions, because retardation of chlorobenzene is only 4.1 compare to 22 in case of $f_{OC} = 0.01$. Migration to the river also occurs thus affecting the quality of the water.

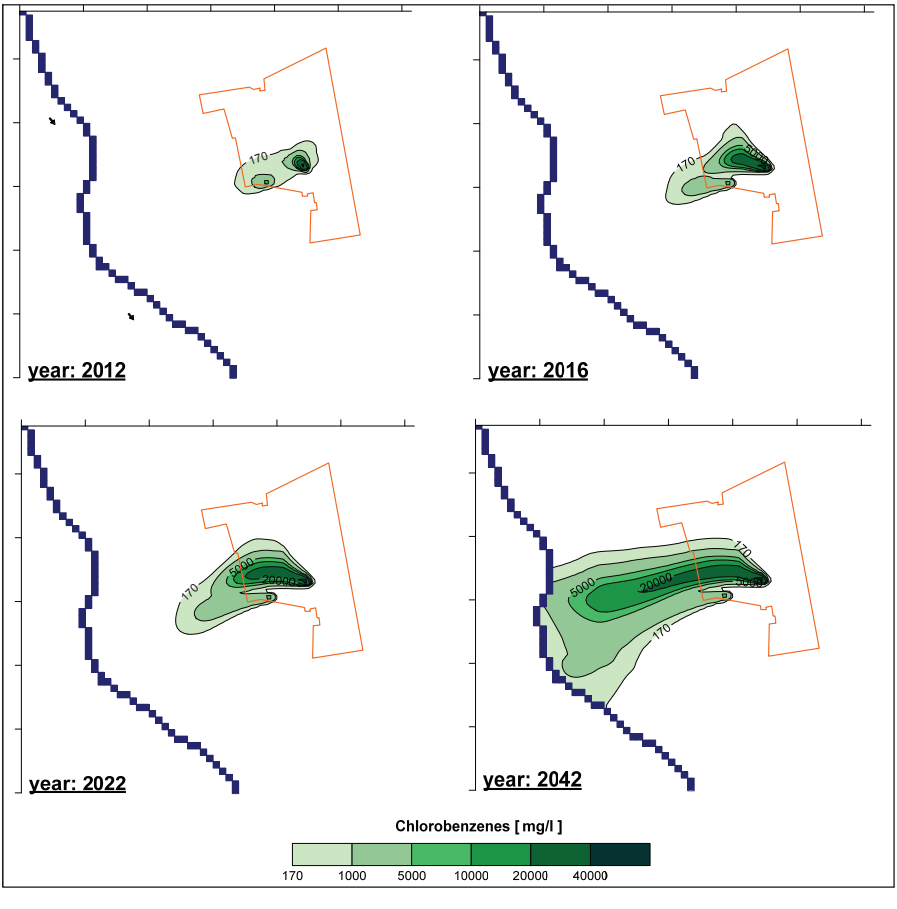

Fig. 3.15 Modeling of chlorobenzene migration (f_{OC} = 0.0015), model part

The situation is entirely different for f_{OC} values of 0.01 (which is most likely the real situation). The contamination plume grows very slightly over time and the final state, which is created after 10 years, is not too different from the initial situation (Fig. 3.13).

Again, it should be mentioned that all of the transport models are burdened by uncertainties associated with the flow model as well as uncertainties associated with the transport model, which have a major impact on the model results. However, the important result of the modeling is that even in unlikely unfavorable combinations of input data, the model results are favorable for proposed remedial action.

4 Principles of hydrogeochemistry

4.1 Sampling of water and solids

Sampling plays an important role in any geochemical investigation because when integrity of water or solid phase samples is compromised, results of interpretation and modeling might be incorrect. A principal objective is to obtain a water sample with the same chemical composition as those of water in its original environment (aquifer, surface water body etc.). When ground water is sampled in wells with long screen zone, then several redox zones may mix and irreversible chemical processes may occur. For example, when conditions close to water table are relatively oxic and dissolved oxygen is present, and conditions in deeper zone are reducing with dissolved iron, then there is mixing of ground water from both zones with resulting loss of both oxygen and iron in reaction like

$$Fe^{2+} + 0.25\,O_2(g) + 2.5\,H_2O = Fe(OH)_3(s) + 2\,H^+ \qquad (4.1)$$

In that case, not only iron and oxygen are lost, but other metals like Zn and Pb may be lost too because they are adsorbed on precipitated ferric hydroxide.

However, even when no reactions occur, there still is reduction of concentration due to conservative mixing. For example, when a plume of chloride considered as non-reactive tracer has a thickness of about 4 m and thickness of screen zone is of about 10 m, then there will be lower concentration of chloride in water sample, which will not correspond to its concentration in the aquifer. The only solution is the sampling with vertical resolution, using several piezometers with short screen zones open at different depths (Appelo and Postma, 2005) or multilevel samplers (MLS). Principal limitation is cost of such devices, which is higher compared to single wells.

Another problem is related to de-gassing of CO_2. In many cases, partial pressure of CO_2 (P_{CO2}) dissolved in ground water is higher than value corresponding to atmospheric value of $10^{-3.5}$ atm. Thus, when a sample is equilibrated with atmosphere, the reaction

$$Ca^{2+} + 2\,HCO_3 = CaCO_3(s) + CO_2(g) + H_2O \qquad (4.2)$$

goes to the right and calcite precipitates. Thus, a part of calcium and dissolved inorganic carbon (DIC) are lost. This process can be even accelerated as a consequence of increasing temperature of sample in the case of late measurement.

There is a controversy related to how many volumes of a water in well or piezometer should be pumped prior to collection of sample(s). It is generally assumed that 3 volumes should be enough, but this requirement cannot be sometimes met in the case of large diameter domestic wells. Thus, it is recommended to pump water until parameters like pH and EC are stabilized and then start the sampling (Appelo and Postma, 2005). There also is requirement of low rate pumping ($< 1 L.min^{-1}$) in the case of sampling of a contaminant plume because uncontaminated background water could dilute samples otherwise.

Field parameters: Several parameters have to be measured in the field because their values based on later measurement in laboratory are almost meaningless.

Temperature: this parameter changes quickly and has an impact on other parameters such as pH and Eh. Furthermore, temperature is necessary for geochemical speciation calculation. In an ideal case, temperature should be measured directly in a well by a down-hole probe. If it is impossible, then measurement should be performed in a flow-through cell, with minimized contact with atmosphere. Flow-through cell is a plexi-glass cylinder with hole for insertion of measurement electrodes, which is connected to pumping device.

Hydrogen ion activity (pH): this is an essential parameter because most geochemical processes are pH-sensitive. The value of pH is generally determined by distribution of carbonate species in water and, thus, it is strongly affected by equilibration with atmosphere. There is de-gassing (Equation 4.2) during sampling and resulting pH is generally higher than its correct value. Thus, measurement without contact with atmosphere is required. The pH-meter has to be calibrated using standard buffers prior to measurement.

Redox potential (Eh): the Eh value is generally lower in ground water compared to surface conditions. Thus, the contact of a sample with atmosphere ($\log P_{O2} = -0.68$ atm) causes changes in speciation such as oxidation of Fe(II) to Fe(III) (Equation 4.1). This means that any contact with atmosphere has to be avoided. Measurement is also performed in flow-through cell. The Eh value measured in field is measured with respect to Ag-AgCl (silver chloride) or Hg-Hg-Cl (saturated calomel) electrodes and the measured value has to be converted to a corresponding value for hydrogen electrode, E_{H2}:

$$E_{H2} = Eh_{field} + Eh_{correction} \tag{4.3}$$

where $Eh_{correction}$ is electrode type and temperature dependent and is indicated by manufacturer for different measurement devices. This correction Eh is +241 mV for saturated calomel electrode (25°•C). An alternative method to obtain $Eh_{correction}$

value is based on the measurement of Eh in both field sample and Zobell's solution with known E_{H2} value (Kehew, 2000).

Alkalinity: it is a measure of acid-neutralizing capacity of a solution. It is generally based on carbonate species, but there can be a contribution of other species:

$$\text{Alkalinity} = HCO_3^- + 2\,CO_3^{2-} + H_3SiO_4^- + H_3BO_2^- \ldots \text{ etc.} \quad (4.4)$$

Especially significant can be contribution of dissolved organic matter with deprotonated carboxylic acid groups, $R\text{-}COO^-$, in the proximity of a sanitary landfill. In that case, the value of alkalinity cannot be used to calculate distribution of carbonate species without corrections (Deutsch, 1997). In an ideal case, alkalinity is determined in the field by titration with acid like HCl and is reported in units like $mg.L^{-1}$ of $CaCO_3$ or $mg.L^{-1}$ of HCO_3^-. When field determination is impossible, then there should be collection of a special sample for later determination of alkalinity in laboratory. When a sub-sample is taken from a bigger sample later, there can be loss of alkalinity due to precipitation of calcite (Equation 4.2). Fritz (1994) concluded that most positive charge-balance errors (e.g., missing anions) were caused by errors in the measurement of alkalinity.

Dissolved oxygen (DO): this is a qualitative parameter only because the O_2/H_2O redox pair cannot be used for quantitative calculations. Detectable values indicate oxic environment where, for example, dissolved nitrate should be stable and ferrous iron should be absent. Measurements are often performed by oxygen electrode, but there are more precise methods like Winkler titration.

Electrical conductivity (EC): this is semi-quantitative parameter, which roughly corresponds to total dissolved solids (TDS) concentration. Thus, it can be used for delimitation of inorganic contaminants plumes, salt water intrusions etc. It is measured by conductivity meter in units such as $\mu S.cm^{-1}$. According to Appelo and Postma (2005), the EC divided by 100 gives a good estimate of the sum of anions or cations (in $meq.L^{-1}$):

$$\sum \text{anions} = \sum \text{cations } (meq.L^{-1}) = EC/100\ (\mu S.cm^{-1}) \quad (4.5)$$

This relation holds up to EC values of about 2000 μS/cm.

Collection and preservation of samples are very important. There is a controversy related to the filtration of samples. Generally, filtration is recommended in the

case of samples for cation and metal analysis. The filter used is generally 0.45 μm, but filter 0.1 μm is more convenient in some cases because some colloids can pass through 0.45 μm filter. Filtering is also recommended for anion samples because organic matter and some bacteria which could participate in reactions after collection of sample like sulfate reduction are removed. Filter is generally located on the output pipe of flow-through cell (so called on-line filter). Samples for cation and metal analysis should be acidified with acid such as HCl to pH less than 2.0 to avoid precipitation of iron (Equation 4.1). Samples for anion analysis are unacidified, but filtration is recommended.

If the presence of colloids is of interest, 2 samples are taken: one sample filtered and acidified and second one unfiltered and acidified. In the case of the presence of colloids concentrations in second sample should be higher.

After collection, samples should be kept at low temperature (about 4 °C) and analyzed as soon as possible. Conservation of samples is indicated in Table 4.1, based on Appelo and Postma (2005).

Table 4.1 Conservation of samples (adapted from Appelo and Postma, 2005)

Parameter	Conservation of sample
Ca, Mg, K, Na	Acidified to pH < 2.0 in polyethylene
NH_4, Si, PO_4	
Heavy metals	Acidified to pH < 2.0
SO_4, Cl	No conservation
NO_3, NO_2	Store at 4 °C and add bactericide like thymol
H_2S	Zn-acetate conservation or spectrophotometric field measurement
TIC	Dilute sample to TIC < 0.4 mmol.L^{-1} to prevent CO_2 escape
Alkalinity	Field titration using Gran method
Fe^{2+}	Spectrophotometric measurement on acidified sample
pH, T, Eh, O_2	Field measurement

Sampling of solids should be a common part of projects in hydrogeology and environmental geochemistry. The presence of reactive solids has a significant impact on concentrations of some contaminants in water. Also, concentrations of some minerals are required in geochemical modeling.

As a general rule, contact with atmosphere should be avoided after collection of samples and samples should be deposited in tight barrels, and, if possible, in nitrogen atmosphere. For example, de-gassing of CO_2 from pore water could cause precipitation of calcite and, thus, concentration of calcium in a sample would be

underestimated. There can also be oxidation of pyrite in a sample after its contact with atmospheric oxygen, with resulting precipitation of ferric hydroxide. Thus, reducing capacity of solids would be underestimated and adsorption capacity would be overestimated. Also, drying of samples should be prevented because secondary minerals previously not present in samples could be formed.

The following mineral phases are of principal interest:

Calcite: determines a neutralization capacity of a system and plays a significant role in the migration of acid mine drainage plume. Its dissolution is generally fast. Determination is by X-ray diffraction (for content > 5.0 wt %) and by acid digestion in carbonate step of sequential extraction.

Dolomite: plays the same role as calcite, but its dissolution is slower and may be kinetically constrained. Determination is the same as for calcite.

Ferric oxides and hydroxides: they are significant adsorbents of metals, may play a role in neutralization of acid mine drainage at low pH values (above 3.0), and they also are significant electron acceptors in hydrocarbon and landfill plumes. Their adsorption capacity is strongly pH-dependent. They can be determined by X-ray diffraction or by oxalate step of sequential extraction. Leaching in 0.5 M HCl can be used to determine readily available fraction of ferric oxides and hydroxides (Christensen et al., 2000). In general, ferric minerals and Mn(IV) minerals play a principal role in oxidation capacity (OXC) of solid phase. Methodology of the OXC determination is described in Heron et al. (1994) and Christensen et al. (2000).

Pyrite: contributes to the reducing capacity of aquifer solids (for example, may be an electron donor in denitrification) and can be determined by X-ray diffraction and by SEM. Pyrite content together with organic matter content are basis for determination of reduction capacity (RDC) of sediments, see discussion in Christensen et al., 2000.

Organic matter: contributes to reducing capacity and to pH-buffering capacity of aquifer solids. There is a special importance of fraction of organic carbon f_{oc} in adsorption of organic contaminants (Fetter, 1999). Determination is based on burning of samples of solids and on detection of CO_2 released during combustion. However, there has to be removal of carbonates by acid digestion prior to this analysis.

Clays (kaolinite, smectite)**:** contribute to adsorption capacity of solid phase and generally represent pH-independent component of adsorption (especially smectite). They also buffer acid mine drainage (Langmuir, 1997). They are determined by X-ray diffraction or by differential thermal analysis (DTA).

4.2 Introduction to thermodynamics

There are several approaches, which can be used in geochemical investigation. We will introduce basic terms first.

Thermodynamic approach: There is assumption of very fast reaction rate with instantaneous equilibrium and no time factor is included. This assumption may be valid in the case of slow ground water flow and long residence time in ground water system.

Kinetic approach: Time factor plus other factors which have an impact on the rate of reactions are considered. Kinetic approach is much less used than thermodynamic approach because data on reaction kinetics are limited. However, some slow reactions like silicate weathering and redox reactions require kinetic description. One of the best known reaction kinetics is the kinetics of pyrite oxidation.

Mass balance approach: It is based on the determination of concentration changes in different phases (compartments) of an investigated system. It cannot be applied in some situations because solid phase composition changes may be difficult or even impossible to determine.

Master variables: these are pH, redox potential (Eh) and ionic strength. They determine speciation (e.g., distribution of total concentrations among free ions and complexes) and behavior of dissolved species. Macrocomponents generally occur in high concentrations and influence master parameters of water. Examples are SO_4^{2-} and Fe^{2+} (only in acid mine drainage because in other environments Fe^{2+} generally has low concentration). The concentration of sulfate and Fe^{2+} in acid mine drainage, for example, has an impact on ionic strength (see later) and, thus, on activity coefficients, and Fe^{2+} concentration also has an impact on redox potential Eh. Macrocomponents influence behavior of microcomponents like Pb^{2+}, Zn^{2+} through ionic strength impact on activity coefficients and formation of complexes. When Pb^{2+} enters ground water, it has no influence on master parameters and macrocomponents. On the other hand, formation of complexes like $PbSO_4^0$ has strong impact on lead behavior, but not on sulfate behavior because generally concentration of lead is negligible compared to the concentration of sulfate. When only contamination by microcomponents takes place, we do not have to predict changes of master variables like in the case of contamination by macrocomponents and, thus, situation is much simpler.

Common concentration units in hydrogeochemistry are molarity M, defined as mass in moles in 1 litr of solution and molality m, defined as mass in moles in 1 kilogram of solution. In dilute solution molarity is approximately equal to molality. Concentration in miliequivalents per liter is concentration in milimoles per liter multiplied by charge of an ion. Activity a_i is "thermodynamic concentration"

or the fraction of total concentration which participates in geochemical reactions. It is calculated as a product of activity coefficient γ_i and concentration m_i:

$$a_i = \gamma_i \, . \, m_i \tag{4.6}$$

Activity coefficient is a function of ionic strength I, which is calculated as

$$I = 1/2 \sum m_i z_i^2 \tag{4.7}$$

where m_i is concentration and z_i is charge of ion i.

Ionic strength is a measure of mineralization of a solution. When ionic strength increases, activity coefficients decrease (Fig. 4.1). In very diluted solutions activity coefficient is @ 1.0 and activity is equal to concentration. The decreasing trend is related to the "cage" of opposite charge particles around ions. There is reversal of the trend in extremely concentrated solutions (brines) because beyond of ionic strength of about 1.0 mol/L there is an increase of activity coefficients with increasing ionic strength. This is related to decreasing amount of free water because most of water is already bound around dissolved species. In the case of uncharged species like $H_2CO_3^0$, $H_4SiO_4^0$ or $H_3AsO_3^0$ only second effect takes place and their activity coefficients are always ³ 1.0.

Activity coefficients are calculated using Debye-Hückel equation for ionic strength I < 0.1, Davies equation I < 0.5, and Pitzer's equations for very high ionic strength (Langmuir, 1997; Drever, 1997). However, Pitzer's parameters are generally available for 25 °C only.

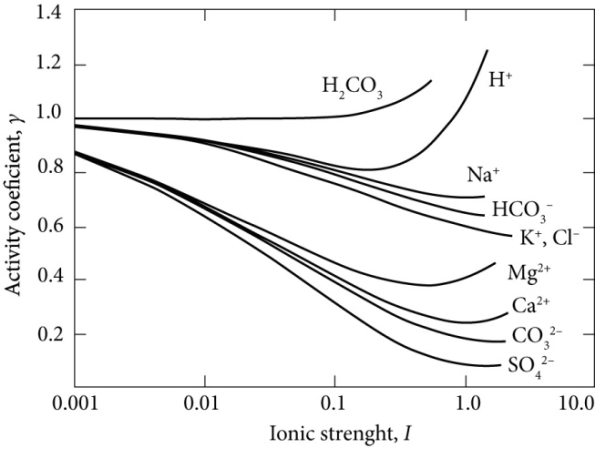

Fig. 4.1 Relation between ionic strength and activity coefficients (after Freeze and Cherry, 1979)

The Debye-Hückel equation in extended form is

$$\log \gamma_i = -Az_i^2 \frac{\sqrt{I}}{1 + Ba\sqrt{I}} \tag{4.8}$$

where γ_i is activity coefficient of ion i, z_i is its charge, A, B are temperature-dependent constant, and a is parameter corresponding to the size of an ion.

For higher ionic strength (I > 0.1), the Davies equation is used,

$$\log \gamma_i = \frac{-Az_i^2\sqrt{I}}{1+\sqrt{I}} + 0.2Az_i^2 I \tag{4.9}$$

where A is temperature-dependent constant, and the final term is purely empirical (0.3 is used instead of 0.2 sometimes). Constants and ion sizes used in both equations can be found, for example, in Stumm and Morgan (1996), and in Langmuir (1997). Hand calculation of activity coefficients becomes complicated and tedious when more species are involved. Thus, the equations above are used in speciation programs like PHREEQC (Parkhurst and Appelo, 1999) to calculate distribution of total concentrations among free ions and complexes.

Law of mass action: In reaction

$$aA + bB = cC + dD \tag{4.10}$$

where small letters indicate stoichiometric coefficients and capital letters are concentrations. The Gibbs free energy, which is driving force of the reaction, is expressed as

$$\Delta G_R = \Delta G^0{}_R + R.T.\ln \frac{[C]^c[D]^d}{[A]^a[B]^b} \tag{4.11}$$

where DG_R^0 is standard Gibbs free energy, R is universal gas constant, and T is temperature. For equilibrium applies that $DG_R = 0$ and

$$DG_R^0 = -R.T.ln\ K \tag{4.12}$$

where K is equilibrium constant for the reaction. The standard Gibbs free energy of a reaction is calculated as

$$DG_R^0 = DG_{f\ products}^0 - DG_{f\ reactants}^0 \tag{4.13}$$

where G_f^0 is Gibbs formation energy (from thermodynamic tables).

At equilibrium, there is no more change of reactants and products concentrations and $DG_R = 0$. If $DG_R < 0$, then a reaction proceeds from the left to the right, if $DG_R > 0$, then a reaction proceeds from the right to the left.

Van't Hoff equation is used to correct a value of equilibrium constant generally reported for 25 °C. When the constant is K_{T1} for temperature T_1, its value for temperature T_2 is

$$\log K_{T2} = \log K_{T1} + \frac{\Delta H^0{}_R}{2{,}303.R}\left(\frac{1}{T_1} - \frac{1}{T_2}\right) \tag{4.14}$$

where DH^0_R is enthalpy of reaction (from thermodynamic tables), and R is universal gas constant.

Solubility product K_{sp} is equilibrium constant for dissolution/precipitation of a mineral. Let us have dissolution of gypsum in water:

$$CaSO_4.2\,H_2O(s) = Ca^{2+} + SO_4^{2-} + 2\,H_2O \tag{4.15}$$

Mass action equation is

$$[Ca^{2+}]\,[SO_4^{2-}]\,[H_2O]^2/[CaSO_4.2\,H_2O] = K \tag{4.16}$$

where terms in brackets are activities K_{equil}. By definition, activities of pure solid phases and water (except for very mineralized solutions) are equal to 1.0, and we can write

$$[Ca^{2+}]\,[SO_4^{2-}] = K_{equil} = K_{sp} = 10^{-4.60} \text{ for } 25\,°C \tag{4.17}$$

where K_{sp} is equilibrium constant called solubility product. This constant applies for the reaction as it is written, e.g., for dissolution. For precipitation its value is $1/10^{-4.60} = 10^{4.60}$.

Saturation index SI indicates the degree of saturation with respect to a given mineral. It is defined as

$$SI = \log \frac{IAP}{K_{sp}} \tag{4.18}$$

where IAP is ion activity product, for example in the case of gypsum dissolution it is

$$IAP = [Ca^{2+}]\,[SO_4^{2-}] \tag{4.19}$$

where brackets denote activities. Sometimes degree of saturation $W = IAP/K_{sp}$ is used instead of SI.

When $IAP = K_{sp}$, the SI value is 0 and solution is at equilibrium with respect to a given mineral. If $SI > 0$, solution is supersaturated and mineral should precipitate, and if $SI < 0$, solution is undersaturated and mineral should dissolve (of course, if the mineral is present in solid phase in contact with water). It has to be emphasized that the SI value indicates direction, but does provide any information about rate of a reaction. Furthermore, there are reactions which never attain equilibrium and reactants are gradually transformed into products. An example is the oxidation of organic matter:

$$CH_2O + O_2 \rightarrow CO_2 + H_2O \qquad (4.20)$$

In this reaction, organic matter is consumed and even when concentration of products such as CO_2 increases, organic matter cannot be re-created. This means that this type of reactions requires kinetic description.

Only some minerals dissolve and precipitates relatively fast and they are called **reactive minerals**. In this case we can apply thermodynamic approach. Common reactive minerals are (adapted from Deutsch, 1997):

Carbonates: calcite, $CaCO_3$, dolomite, $CaMg(CO_3)_2$, siderite, $FeCO_3$, rodochrozite, $MnCO_3$;

Sulfates: gypsum, $CaSO_4.2H_2O$, jarosite, $KFe_3(SO_4)_2(OH)_6$, melanterite, $FeSO_4.7H_2O$, alunite $KAl_3(SO_4)_2(OH)_6$(questionable);

Oxides and hydroxides: ferrihydrite, $Fe(OH)_3$, goethite, FeOOH, gibbsite, $Al(OH)_3$, manganite, MnOOH, amorphous silica, SiO_2(am), brucite, $Mg(OH)_2$.

Congruent dissolution: when a mineral dissolves, the ratio between ions in solution is the same as in the mineral. For example, the ratio $Ca^{2+} : SO_4^{2-}$ is 1 : 1 in both gypsum and in water.

Incongruent dissolution: the ratio is different in dissolving mineral and in water. This is typical for dissolution of silicates, when secondary minerals are formed. An example is dissolution of orthoclase with formation of kaolinite:

$$CaAl_2Si_2O_8 + H^+ + H_2O = Al_2Si_2O_5(OH)_4 + Ca^{2+} \qquad (4.21)$$

The ratio $Ca^{2+} : Al^{3+} : Si^{4+}$ is 1 : 2 : 2 in orthoclase, but 1 : 0 : 0 in water because all Al^{3+} and Si^{4+} are retained in secondary mineral kaolinite.

Influence of complexation: there is formation of aquatic complexes of ions, for example calcium can be in solution as free ion Ca^{2+} and in the form of complexes like $CaSO_4^0$, $CaHCO_3^+$ etc. These complexes increase solubility of minerals of calcium, which would be lower if only Ca^{2+} would have been present in water.

Let us consider the dissolution of anglesite,

$$PbSO_4(s) = Pb^{2+} + SO_4^{2-} \qquad K_{sp} = 10^{-7.79} \tag{4.22}$$

If there are Mg^{2+} and Cl^- already present in water, there is formation of complexes

$$Mg^{2+} + SO_4^{2-} = MgSO_4^0 \text{ and } Pb^{2+} + Cl^- = PbCl^+ \tag{4.23}$$

and total dissolved lead concentration will be

$$(Pb)_{total} = (Pb^{2+}) + (PbSO_4^0) + (PbCl^+) \tag{4.24}$$

There also is an influence of ionic strength on dissolution of anglesite. In water with Mg^{2+} and Cl^-, the activity coefficients for Pb^{2+} and SO_4^{2-} are lower than in distilled water and more anglesite dissolves. In that case we can write that

$$\gamma_{Pb2+}.m_{Pb2+}.\gamma_{SO42-}.m_{SO42-} = K_{anglesite} \tag{4.25}$$

The value of solubility product of $K_{anglesite}$ is a constant, and, thus, when values of activity coefficients γ_i are reduced as a consequence of high ionic strength, then values of concentrations m_i have to increase to compensate for the change.

Common ion effect: if water is at equilibrium with less soluble mineral and encounters more soluble mineral, which contains an ion from the first mineral already dissolved in water, then the first mineral precipitates (Drever, 1997). An example is the precipitation of calcite during dissolution of gypsum:

$$Ca^{2+} + HCO_3^- + CaSO_4.2\,H_2O(s) = Ca^{2+} + SO_4^{2-} + CaCO_3(s) + H^+ + 2\,H_2O \tag{4.26}$$

When water of Ca-HCO_3 type at equilibrium with calcite encounters gypsum, the resulting water is of Ca-SO_4 type. Calcite is less soluble than gypsum and dissolu-

tion of gypsum with input of large quantity of Ca^{2+} forces precipitation of calcite and reduction of bicarbonate concentration. Similarly, if the water dissolving anglesite in the previous case contains SO_4^{2-} instead of Cl^-, there will be very limited dissolution of anglesite because sulfate is in both anglesite and in water.

Order of encounter refers to the order in which strata with different minerals are encountered by flowing ground water. Even when the same strata with the same mineral assemblage are encountered, resulting groundwater chemistry at outflow will be different if the order of strata is different (Palmer and Cherry, 1984). For example, if first sequence contains shale layer with Na-montmorillonite, limestone layer, and gypsum layer and second sequence contains limestone layer, gypsum layer, and shale layer with Na-montmorillonite and organic matter, the water at the first sequence outflow will have high Ca^{2+} and SO_4^{2-} concentrations and low Na^+ concentration, and the water at the second sequence outflow will have high Na^+, and low SO_4^{2-} and Ca^{2+} concentrations. This is a consequence of common ion effect, cation exchange, and sulfate reduction in different orders.

4.3 Redox reactions

In **redox reactions** there is a change of oxidation state of ions. Oxidation is a loss of electrons and reduction is a gain of electrons. Electrons cannot freely exist in solution, thus there is no oxidation without reduction and vice versa. An example is the oxidation of Fe^{2+} combined with precipitation of ferric hydroxide (Equation 4.1). In this reaction iron is oxidized from +2 state to +3 state and oxygen is reduced from 0 state to –2 state. On the other hand, dissolution of calcite,

$$CaCO_3(s) + CO_2 + H_2O = Ca^{2+} + 2\,HCO_3^- \qquad (4.27)$$

is not redox reaction because oxidation states of calcium and carbon are always +2 and +4, respectively.

Each redox reaction can be written as a combination of **2 half-reactions**, oxidation and reduction. For example, oxidation of Fe^0 by oxygen can be written as

$$Fe^0(s) = Fe^{2+} + 2\,e^- \qquad \text{oxidation of } Fe^0 \text{ to } Fe^{2+} \qquad (4.28)$$

$$0.5\,O_2 + 2\,H^+ + 2\,e^- = H_2O \qquad \text{reduction of } O^0 \text{ to } O^{-2}$$

$$Fe^0(s) + 0.5\,O_2 + 2\,H^+ = Fe^{2+} + H_2O \qquad \text{complete reaction}$$

In this reaction, Fe^0 is oxidized and is donor of electrons and reducing agent, and oxygen is acceptor of electrons and oxidizing agent.

There are two basic types of redox notation:

First of them is **redox potential, Eh [V]**, which is expressed with respect to hydrogen electrode. However, it is generally measured with respect to a different electrode (kalomel electrode etc.) and measured values have to be corrected for hydrogen electrode (see chapter 4.1). The potential of calomel electrode at 25 °C is about +0.245 V lower and therefore measured data should be increased by this number. The Nernst equation describes the relation between redox potential and activities of a redox couple. For example, for redox couple of iron the equation is

$$Eh = Eh^0 + \frac{RT}{nF} \ln \left[\frac{Fe^{3+}}{Fe^{2+}} \right] \qquad Eh^0 = 0.77 \text{ V} \qquad (4.29)$$

where Eh^0 is standard potential (from tables), n is number of transferred electrons, F is Faraday constant and terms in squared brackets are activities. The Eh^0 values for other redox reactions are e.g. in Appelo and Postma (2005).

Second type of notation is the **activity of electrons**. This is expressed in analogy with pH as $pe = -\log[e^-]$. However, in contrast to H^+, electrons cannot exist separately in a solution. Equation for iron redox couple in this notation is

$$pe = pe^0 + \log \left[\frac{Fe^{3+}}{Fe^{2+}} \right] \qquad pe^0 = 13.0 \qquad (4.30)$$

In this case the manipulation of equation is simpler than in the case of the Eh notation because the equation can be treated as an ordinary equilibrium equation. Conversion between both notations is

$$Eh\ [V] = 0.059\ pe \qquad \text{(for 25 °C)} \qquad (4.31)$$

Different forms of the same element with different oxidation number can have completely different behavior (soluble Fe(II) compared to insoluble Fe(III)) and toxicity (very toxic Cr(VI) compared to Cr(III) with low toxicity). Thus, information about oxidation state is necessary in investigation of contaminated sites.

Determination of oxidation state can be done:

a) Directly, by analytical determination on perfectly preserved (filtered and acidified in the field) sample. This determination has a priority.
b) By splitting of total concentration, for example Fe_{total}, on the basis of field Eh and pH values and the Nernst equation. This determination is problematic in case of more oxidation couples present simultaneously, because the measured Eh value can correspond to the strongest redox couple (which is often, but not always, Fe^{3+}/Fe^{2+} couple) and other redox couples may not be at equilibrium with this strongest couple. Especially poor is match between Eh and O_2/H_2O couple. Measurement of dissolved oxygen concentration gives mostly only very weak information on Eh.
c) By calculating Eh value from one redox couple like Fe(II)/Fe(III) and using the calculated Eh or pe value to determine concentration of second redox couple (for example, Mn(II)/Mn(IV)) by partition of the total concentration. This approach suffers of the same problem as the application of field Eh, e.g., there frequently is a lack of equilibrium between different redox couples. In geochemical programs like PHREEQC (Parkhurst and Appelo, 1999) it is possible to choose between all options mentioned above.

Redox sequence (also redox ladder): There is a natural sequence of redox reactions during oxidation of organic matter. Dissolved oxygen is consumed first and methane is generated last (Drever, 1997). The sequence is: $O_2 \rightarrow NO_3^- \rightarrow$ Mn(IV) $\rightarrow$ Fe(III) $\rightarrow SO_4^{2-} \rightarrow CH_4$. The sequence is based of free energy released at each redox reaction, which decreases from consumption of oxygen to methanogenesis. There is the same sequence observed along a flow path in a pristine flow system, e.g., dissolved oxygen is generally found close to recharge area and methane, if present, in deep confined zone. In the case of sanitary landfills and dissolved hydrocarbons plumes, the sequence is reversed, e.g., methane is found close to (or directly in) a source zone (landfill or free phase zone) and dissolved oxygen is found at the periphery of a plume.

4.4 Geochemical kinetics

Kinetic approach includes time factor. Let us have dissolution of halite, NaCl. When we plot concentration of Na^+ vs. time (Fig. 4.2), concentration of Na^+ increases initially, but at time $t = t_2$ reaches a maximum, and then remains constant. Since time t_2, the concentration of Na^+ does not depend on time and is determined by the solubility product of halite.

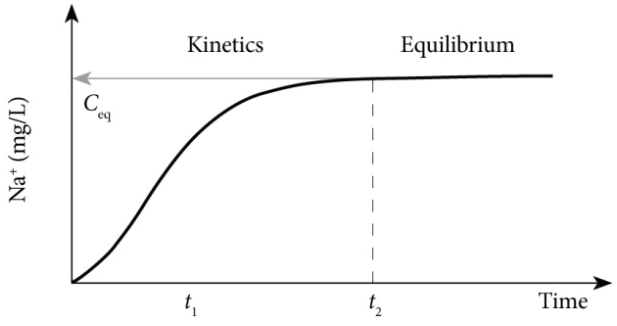

Fig. 4.2 Dissolution of halite (adapted from Appelo and Postma, 2005)

Behavior in the region where $t > t_2$ is described by thermodynamics, and behavior in region where $t < t_2$, e.g. at t_1, is described by kinetics. The time t_2 necessary to attain equilibrium is different for different minerals and conditions. It is relatively short for reactive minerals like calcite and gypsum and long for non-reactive minerals like quartz. However, if a reaction is "fast" or "slow" also depends on the relation between velocity of ground water flow and reaction rate (the faster the flow is, the less probable is equilibrium) and on the time scale of investigation (for example, predictions for radioactive disposal sites are for more than 10,000 years).

Order of reaction kinetics: depends on exponent of independent variable, for example reaction

$$-\frac{dC}{dt} = k.C \tag{4.32}$$

is of first order because the exponent of concentration C is one. In the reaction t is time and k is reaction constant linked to half-life $t_{1/2}$ as $k = ln2/t_{1/2}$. Solution of the equation obtained by integration for C_0 at t_0 is

$$C_t = C_0.e^{-kt} \tag{4.33}$$

where C_t and C_0 are concentrations at time t and at t_0 (initial concentration), respectively. Rate of reaction decreases with declining concentration and this reaction is used to describe radioactive decay of isotopes like ^{14}C and tritium and is also used for biodegradation of petroleum products like benzene and toluene and chlorinated solvents like PCE and TCE.

In the case of zero order kinetics, the reaction is

$$-\frac{dC}{dt} = k \tag{4.34}$$

and

$$C_t = C_0 - kt \tag{4.35}$$

Rate of zero order reaction is always the same and does not depend on concentration. In the case of second order reaction concentration is squared,

$$-\frac{dC}{dt} = k.C^2 \tag{4.36}$$

An example of second order reaction is the oxidation of Fe^{2+} by oxygen,

$$-\frac{dm_{Fe^{2+}}}{dt} = k.m_{Fe^{2+}}\left(OH^-\right)^2.P_{O_2} \tag{4.37}$$

This reaction is of 2nd order with respect to pH, but of 1st order with respect to Fe^{2+} concentration and partial pressure of O_2 (P_{O2}).

Homogeneous vs. heterogeneous reaction: Homogeneous reaction includes only one thermodynamic phase. Example is formation of $PbSO_4^0$ soluble complex in solution. Heterogeneous reactions include more phases and an example is dissolution of CO_2 in water, where CO_2 is gas phase and dissolved CO_2 in water is a liquid phase.

Rate of chemical reaction depends on temperature. Relation between reaction constant and temperature is given by **the Arrhenius equation**,

$$k = A.\exp\frac{-E_a}{R.T} \qquad (4.38) \tag{4.38}$$

where A is pre-exponential (Arrhenius) factor, E_a is activation energy, R is universal gas constant, and T is absolute temperature. If the reaction constants *k* for different temperatures is known, we can plot a graph log k = f(1/T) in order to determine activation energy from its slope equal to $-E_a/2.3R$.

4.5 Adsorption and cation exchange

Adsorption refers to the attachment of dissolved compounds to surface on adsorbent (clay, metal hydroxide etc.), whereas **absorption** refers to the penetration of dissolved compounds (or gases) into structure of an adsorbent. In many cases it is not possible to distinguish between both processes.

Clays have adsorption capacity relatively independent of pH. On the other hand, hydroxides and soil organic matter have adsorption capacity for inorganic species highly dependent on pH.

Clays have large specific surface, which generally has negative charge at close to neutral pH due to substitution of Si^{4+} and Al^{3+} in their crystal lattice by ions with lower valence.

Cation exchange capacity (CEC) characterizes adsorption capacity for cations. It is determined by saturation of exchange sites by a cation (generally NH_4^+) and then by determination of its concentration after expulsion from exchange sites by other cation (Na^+ in concentrated solution of NaCl). Values of CEC are reported in meq/100 g of soil (adsorbent) for specified pH (generally 7.0). Properties of clay minerals are in Table 4.2.

Table 4.2 Properties of clay minerals (adapted from Deutsch, 1997)

Property/clay mineral	Montmorillonite	Illite	Kaolinite
Particle size [µm]	0.01–1.0	0.1–2.0	0.1–5.0
Ion substitution	high	intermediate	low
Surface [m^2/g]	600–800	100–120	5–20
CEC [meq/100g]	80–100	15–40	3–15

Montmorillonite has the largest specific surface and the highest CEC values, and kaolinite exhibits the lowest values. In the case of clays also occurs protonation of surface at low pH values and thus, adsorption capacity changes. However, bulk adsorption capacity of clays is pH-independent: For example, for montmorillonite it is about 90 % of total adsorption capacity. Sand has relatively low CEC values, generally less than 1 meq/100 g or less. However, even this value is by no means negligible.

Organic matter in solid phase (SOM – solid organic matter) plays an important role in adsorption of non-polar organic contaminants, but also it is important ad-

sorbent for inorganic contaminants. This is related to de-protonation of carboxylic group –COOH and phenolic group –OH due to changes of pH, with resulting negative surface charge. Soil humus may have CEC up to 200 meq/100 g and can adsorb a significant fraction of metals. Appelo and Postma (2005) present an equation for calculation of CEC on the basis of both clay content and organic matter content:

$$\text{CEC [meq/100 g]} = 0.7 \times (\%\ \text{clay}) + 3.5 \times (\%\ \text{C}) \tag{4.39}$$

The **ion exchange** comprises replacement of one species adsorbed on solid phase surface by another species present initially in solution. Cation exchange is generally much more important than anion exchange because surface charge of minerals in aquifers is generally negative under common pH conditions. Ions with higher charge are preferentially adsorbed, but ion exchange also depends on concentrations in solution. For example, Ca^{2+} has higher affinity for adsorption than Na^{+} when dissolved concentrations are comparable, but Na^{+} is more adsorbed than Ca^{2+} in sea water with much higher Na^{+} concentrations. Adsorption affinity decreases in the sequence $Al^{3+} > Ca^{2+} > Mg^{2+} > K^{+} > Na^{+}$. When both charge and concentration of two ions are similar, then an ion with lower hydrated radius is preferred for adsorption. Hydrated radius is lower for ions with higher ion radius because in their case the ratio charge/ion radius (ionic potential) is lower. Thus, Ca^{2+} has higher ion radius and lower hydrated radius than Mg^{2+} and is preferentially adsorbed.

There often are **colloids** (particles of size < 1 μm) in water. Stability of colloids depends on electrostatic properties of their surface, which is very often modeled by electric double layer. This double layer has two distinguished parts – **Stern layer** with tightly held ions (generally cations) is close to surface of colloids and – **Gouy-Chapman layer** with mobile ions (cations still predominate) is further from surface, between Stern layer and bulk solution with the same concentrations of cations and anions. Stability of colloids depends on the thickness of the Gouy-Chapman layer which in turn depends on ionic strength of solution. When ionic strength increases, there is compression of the layer and flocculation of colloids occurs (for example, during mixing of river water and sea water in estuaries).

In the case of Fe- and Mn-oxyhydroxides the adsorption is strongly pH-dependent. When pH increases, there is **de-protonation of surface**,

$$\equiv SOH_2^{+} = \equiv SOH^{0} + H^{+} \tag{4.40}$$

$$\equiv SOH^{0} = \equiv SO^{-} + H^{+} \tag{4.41}$$

and adsorbed ions also change surface charge of adsorbent, for example, in the case of Zn^{2+} adsorption we can write

$$\equiv SO^- + Zn^{2+} = \equiv SOZn^+ \quad (4.42)$$

In equations above, the sign º indicates adsorption sites on solid phase and S indicates element in solid phase (in the case of ferric hydroxide it is Fe). When average charge at adsorbent surface is equal to zero, the numbers of positive and negative charge sites are equal and we can write that

$$\equiv SOH_2^+ = \equiv SO^- \quad (4.43)$$

Value of pH at the point is called **pH_{ZPC}** (pH of zero point of charge). Typical pH_{ZPC} values for different minerals are: clays 2.0–4.0, feldspars 2.0–2.5, $Fe(OH)_3$ 8.3, and calcite 8.4.

When pH of solution changes, there is also a change of electrostatic component of adsorption related to adsorption/desorption of H^+. This component of adsorption is expressed by **the coulombic (Boltzmann) term K_{coul}**,

$$K_{coul} = \exp\frac{-\Delta Z.F.\Psi}{R.T} \quad (4.44)$$

where ΔZ is change of surface charge, F is Faraday constant, Y is surface potential, R is universal gas constant and T is temperature. Bulk adsorption constant is a product of **intrinsic (chemical) constant K_{int}** and coulombic constant:

$$K_{bulk} = K_{int} \cdot K_{coul} \quad (4.45)$$

At pH_{ZPC} the numbers of positively and negatively charged sites are identical, bulk surface charge is equal to zero, and, thus, $K_{bulk} = K_{int}$. When pH increases, OH^- anions are adsorbing and negatively charged sites start to predominate. This causes adsorption of cations and desorption of anions. This behavior is called adsorption edge (Stumm, 1992; Langmuir, 1997).

However, it has to be emphasized that even at $pH < pH_{ZPC}$ some negatively charged sites exist, but they are less abundant than positively charges sites. Cations like Pb^{2+} are already adsorbed at pH much lower than pH_{ZPC}, usually at $pH < 6.5$ because their concentrations in water are generally small and they have strong affinity for adsorption.

Modeling of adsorption: The most common approach is based on the application of adsorption isotherms. They are either thermodynamic or empirical (not true thermodynamic) dependencies determined from batch experiments. In batch experiments a flask with known quantity of water and solid phase is spiked with known amount of a contaminant and after equilibration (usually after 24 hours) the partitioning between solid phase and water is determined as a difference between initial and final dissolved concentration. Adsorbed amount of contaminant (generally in mg/g) is plotted as a function of equilibrium water concentration (generally in mg/L). Adsorbed amount is calculated as

$$S = \frac{(C_i - C_r)V}{M} \tag{4.46}$$

where C_r is equilibrium concentration, C_i is initial concentration, V is volume of water and M is mass of solid phase adsorbents.

Linear distribution coefficient (isotherm) K_d is determined as a slope in the graph $S = f(C_r)$, (Fig. 4.3).

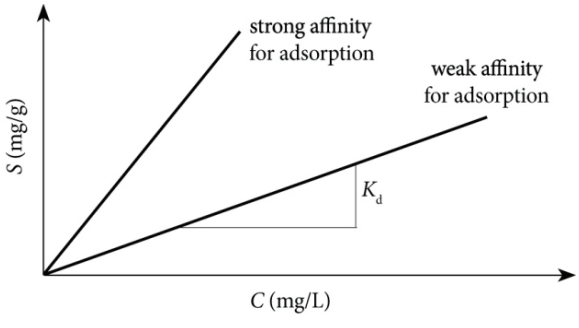

Fig. 4.3 Linear adsorption isotherm K_d

Linear isotherm is mainly applicable for low concentrations. Principal problem of linear adsorption isotherm is related to the lack of limit for adsorption with increasing concentration in water. This is not correct because number of adsorption sites is limited and there is a complete saturation of adsorption sites when concentration in water becomes too high.

Freundlich adsorption isotherm is expressed as

$$S = K_F.C^n \tag{4.47}$$

and takes into account decreasing growth of adsorption with increasing concentration in water. Therefore the exponent n, is generally < 1.0. However, there is no maximum adsorption limit either. Linear distribution coefficient K_d is special case of the isotherm for n = 1.0.

Langmuir adsorption isotherm is expressed as

$$S = \frac{S_{\max}.K_L.C}{1 + K_L.C} \tag{4.48}$$

where S_{max} is maximum amount of contaminant which can be adsorbed. When concentration in water is high, the product $K_L.C >> 1$, we obtain $S = S_{max}$, which is the asymptote of the graph S = f(C) or adsorption limit. The other limiting case is for low concentration insolution, where the product $K_L.C << 1$ and the isotherm changes to the linear one.

Adsorption isotherms can be implemented into advection-dispersion equation (ADE) and used to calculate **retardation factor R**, which is defined as

$$R = \frac{v_{water}}{v_{contam}} = 1 + \left(\frac{\rho_b}{n}\right).\frac{dS}{dC} \tag{4.49}$$

where v_{water} is velocity of ground water flow (or of a conservative, non-adsorbing tracer migration) and v_{contam} is velocity of adsorbing contaminant migration. Retardation factor for linear isotherm is (Fetter, 1999):

$$R = 1 + \left(\frac{\rho_b}{n}\right).K_d \tag{4.50}$$

For Freundlich isotherm, the resulting retardation factor is

$$R = 1 + \left(\frac{\rho_b}{n}\right).K_F.n.C^{(n-1)} \tag{4.51}$$

Note that retardation factor is constant for linear isotherm, but depends on concentration for Freundlich isotherm (and also for Langmuir isotherm).

We have discussed so far isotherms describing adsorption of only one ion on solid phase. **Selectivity coefficient** describes exchange between two ions of different charge in reaction expressed as

$$2\,\text{A-clay} + B^{2+} = \text{B-clay} + 2A^{+} \tag{4.52}$$

with selectivity coefficient (equilibrium constant) $K_{A\text{-}B}$. Selectivity coefficient $K_{A\text{-}B}$ just like adsorption isotherms is not a real thermodynamic constant because there is no thermodynamic description of adsorbed/exchanged ions behavior. Values are also valid for specified pH and water chemistry. In the case of the same concentrations in water divalent Ca^{2+} is preferentially adsorbed over monovalent Na^{+}. However, in sea water with high Na^{+} concentrations there is much more Na^{+} adsorbed on solid phase than Ca^{2+}. Applications of selectivity coefficient are discussed e.g. in Appelo and Postma (1999). In Table 4.3, there are selectivity coefficients for cation exchange with Na^{+},

$$Na^{+} + 1/i\ \text{I-X}_i = \text{Na-X} + 1/i\ I^{i+} \tag{4.53}$$

where X represents X fraction of ion I on exchange sites, and i is charge of the ion. When exchange without Na^{+} is considered, selectivity coefficients are determined by division of appropriate values for Na^{+} exchange, for example $K_{K/Ca}$ is 0.2/0.4 = 0.5. The notation in the Equation 4.53 is called Gaines-Thomas notation. There are other types of notation (Gapon, Vanselow), discussed in detail in Appelo and Postma (2005).

Table 4.3 Selectivity coefficients (Appelo and Postma, 2005)

Ion I^{+}	$K_{Na/I}$	Ion I^{2+}	$K_{Na/I}$
Li^{+}	1.2 (0.95–1.2)	Mg^{2+}	0.50 (0.4–0.6)
K^{+}	0.2 (0.15–0.25)	Ca^{2+}	0.40 (0.3–0.6)
NH_4^{+}	0.25 (0.2–0.3)	Sr^{2+}	0.35 (0.3–0.6)
Rb^{+}	0.10	Ba^{2+}	0.35 (0.3–0.6)
Cs^{+}	0.08	Fe^{2+}	0.6
–	–	Cu^{2+}	0.5
–	–	Zn^{2+}	0.4 (0.3–0.6)
Ion I^{3+}	–	Cd^{2+}	0.4 (0.3–0.6)
Al^{3+}	0.6 (0.5–0.9)	Pb^{2+}	0.3

Modeling of surface complexation takes into account changes in surface layer of adsorbent due to changes of pH and water chemistry. The most common is diffuse double layer (DDL) model. A common application of the modeling is

based on the adsorption on hydrous ferric hydroxide (HFO) with composition of goethite, molecular weight of 89 g/mol, surface area of 600 m^2/g, and number of adsorption sites 0.2 mol/mol HFO. It is possible to change these parameters. In some cases (adsorption of trace metals) second type of adsorption sites with number of 0.005 mol/mol HFO is also used (Dzombak and Morel, 1990; Stumm, 1992). More detailed description of the modeling is presented later.

5 Geochemical modeling

5.1 Types and strategy of geochemical modeling

In this text we discuss **geochemical models**, which consider geochemical reactions in the migration of dissolved species. There are **geochemical equilibrium models**, based on the assumption of thermodynamic equilibrium reached in a relatively short time (no time factor is included in calculation) and **geochemical kinetic models**, which include time factor. Basic division of equilibrium models is into: (**a) speciation models**, **(b) inverse models (also called mass balance models)**, **(c) forward models (also called reaction path models),** and **(d) reactive transport (coupled) models**. All these models are discussed in the following chapters in more detail. One of principal weaknesses of the equilibrium models is the assumption is that chemical equilibrium has been reached. However, kinetic models including chemical kinetics are not yet common in environmental geochemistry and there still is a lack of kinetic data for many geochemical processes.

On the basis of the relation to spatial coordinates models can be divided into **(a) batch models** in closed vessels (reactors), and **(b) reactive transport (coupled) models**, which calculate water chemistry evolution in time in spatial coordinates. Reactive transport geochemical (coupled) models can be in one, two, and three dimensions (1-D, 2-D, and 3-D).

It must be emphasized that the application of geochemical models is generally based on the assumption of known **flow pattern**. If sampling points used for the interpretation of geochemical evolution of ground water are not hydraulically connected, then the geochemical interpretation is in troubles. This means that generally we have to solve a flow model prior to a geochemical model.

Let us look at the influence of water sampling locations on the interpretation of geochemical evolution of ground water (Fig. 5.1). This is a plan view of a simple flow system with recharge area represented by point A. From point A ground water flow is diverted in 2 directions: towards river and points B and C, and in the opposite direction, towards point D and lake. When we investigate geochemical evolution of water, we can compare points A and B (and also C), but comparison of C and D does not make much sense from the viewpoint of the evolution of ground water chemistry.

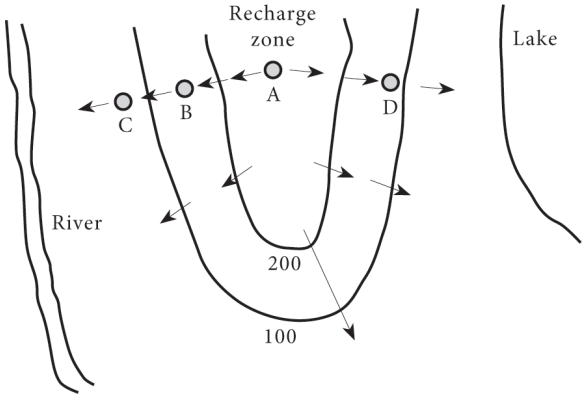

Fig. 5.1 Geochemical sampling of a hypothetical flow system (adapted from Chapelle, 1993)

Structure of input file differs between programs. There can be an **interactive input** based on question related parameter entry like in PRODEFA2 pre-processor of the program MINTEQA2 (Allison et al., 1991), **template type** of input, where data are written into pre-prepared forms like in program EQ3/6 (Wolery, 1992), and **script type** of input, where data are entered after a keyword like in program PHREEQC (Parkhurst and Appelo, 1999). Our objective in this chapter is to present an introductory background, which is necessary for simple geochemical and reactive transport modeling applications. More detailed information about applied geochemical modeling can be found in Deutsch (1997) and Zhu and Anderson (2002), and theoretical background can be found in Albarède (1995), and Bethke (1996).

Our modeling examples are generally based on the program PHREEQC, which represents a standard for geochemical and reactive transport modeling due to its availability and public domain character. Emphasis is on modeling strategy and structure of input files. Modeling results are discussed only briefly, when they are relevant for demonstration of general modeling principles.

5.2 Types of geochemical programs

Standard geochemical modeling program is PHREEQC (Parkhurst and Appelo, 1999). This program is produced by USGS and is based on former program WATEQ4F (Plummer et al., 1976). There are several modules which include speciation calculations, reaction path modeling including surface complexation adsorption modeling based on diffuse double layer (DDL) approach, inverse

geochemical modeling which includes uncertainty in input data, and 1-D reactive transport. This program can be downloaded with no charge from website http://www.usgs.gov. Database of PHREEQC, phreeqc.dat, is relatively limited, but data from other databases can be appended for modeling runs. The most comprehensive database is llnl.dat (Lawrence Livermore National Laboratory), which can be downloaded together with PHREEQC. The drawback of this database is that sources of data are not indicated. There is a version of PHREEQC with post processor for graphical plotting of results, prepared by Vincent Post. This version can be downloaded from http://www.geo.vu.nl/~posv/phreeqc/index.html.

Program MINTEQA2 (Allison et al., 1991) was produced by US EPA. This program is used for speciation calculations, batch-type reaction path modeling, ion-exchange, and surface complexation modeling using several approaches. Database of the program is very extensive, but no transport calculations are possible. The program includes an interactive module PRODEFA2 for preparation of input. The program can be downloaded with no charges from http://www.epa.gov. User friendly version Visual MINTEQ was prepared by Jon Petter Gustafsson and can be downloaded from http://www.lwr.kth.se/english/OurSoftWare/Vminteq/index.htm.

MINEQL+, Version 4.0, (Schecher and McAvoy, 1998), is a program similar to MINTEQA2. Speciation and forward modeling in batch mode and adsorption modeling can be performed.

Program EQ3/6 (Wolery, 1992) has two parts: EQ3 performs speciation calculations and can be used as a preparation of input for EQ6, which is then used for reaction path calculations. The program has an extensive database where sources of thermodynamic data are indicated.

Program NETPATH (Plummer et al., 1994) is used for inverse geochemical modeling, but a module for speciation calculations is also included. Unlike inverse modeling module of PHREEQC, the program does not include uncertainty in input data. Several models for ^{14}C dating corrections are included and calculation of isotopic fractionation in geochemical reactions for stable isotopes ^{13}C and ^{34}S can also be calculated. This program is combined with speciation program, which can be used to constrain inverse geochemical modeling results. The program can also be downloaded with no charge from USGS Home Page.

The Geochemical Workbench, GWB (Bethke, 1996) is capable of most options possible in PHREEQC (speciation, forward modeling, adsorption modeling etc.). Furthermore, the program includes post-processor for graphical output like Eh – pH diagrams. This program is not in public domain and can be purchased. More information is on www.rockware.com.

Program SOLMINEQ.88 (Kharaka et al., 1988) is a speciation and reaction path program, which includes options for high temperature systems (e.g. boiling).

Speciation and adsorption calculations in systems with organic matter can be performed by program WHAM (Tipping, 1994). Interactive version of WHAM prepared by Jon Petter Gustafsson is called WinHumic and can be downloaded from http://www.lwr.kth.se/english/OurSoftWare/WinHumicV/index.htm.

When ion strength is beyond the range of the applicability of Davies equation, activity coefficients should be calculated on the basis of the Pitzer virial coefficients approach. There is program PHRQPITZ (Plummer et al., 1988), which implements this approach and can be downloaded from USGS website, just like program PHREEQC. Another program with Pitzer's approach is SIMUL (Reardon, 1990), which has been originally designed for calculations in construction materials pore water. Both programs can be used for speciation and reaction path calculations.

Reactive transport modeling in 1-D is included in the program PHREEQC introduced above. There are several 3-D reactive transport programs including PHT3D (Prommer et al., 2003), PHAST (Parkhurst et al., 2004), MIN3P (Mayer et al., 2002) and HYDROGEOCHEM (Yeh and Tripathi, 1990). Both PHT3D and PHAST are based on the coupling of PHREEQC with a transport program, which usually is MT3DM (Zheng and Wang, 1999). Implementation of PHREEQC enables to perform almost any geochemical calculations, including kinetics of both organic and inorganic reactions. More recent version of PHT3D also comprises adsorption surface complexation modeling. Program MIN3P uses program MINTEQA2 in geochemical module, also includes large range of kinetic reactions and simplified diffuse double layer approach for surface complexation modeling of adsorption.

Outline of principal geochemical programs is in Table 5.1.

Table 5.1 Principal geochemical programs

Program	Speciation	Inverse model.	Forward model.	Reactive transport	Comment
PHREEQC	×	×	×	×	Free of charge from USGS
MINTEQA2	×		×		Free of charge from U.S. EPA
NETPATH	×	×			Free of charge from USGS
MINEQL+	×		×		
EQ3/6	×		×		
GWB	×		×	×	

5.3 Examples of geochemical modeling

5.3.1 Speciation modeling

5.3.1.1 Principles and modeling strategy

Speciation calculation represents most simple example of equilibrium based modeling. We know chemistry of water from one sampling point (for example, from a well or piezometer) and speciation program calculates distribution of dissolved species between free ions and aqueous complexes and also saturation indexes for different minerals. Lead, for example, can be present in water as free ion Pb^{2+}, and also in the form of complexes with anions:

$$Pb_{total} = Pb^{2+} + PbSO_4^0 + PbCl^+ + PbCO_3^0 \text{ etc.} \quad (5.1)$$

where Pb_{total} is total lead concentration from chemical analysis. In the terminology of Zhu and Anderson (2002), Pb_{total} is a **component** (e.g., chemical formula unit used to describe a system) and Pb^{2+}, $PbSO_4^0$ etc. are **species** (chemical entities which really exist in the system). Information about the distribution of dissolved species is important, for example, for risk assessment of contamination by metals because toxicity of metals depends on their speciation in solution. Carbonate complexes of metals, for example, are less toxic than their free ions.

Saturation index SI is used to determine the direction of geochemical processes. When $SI_{gypsum} > 0$, gypsum precipitates from the water and when $SI_{gypsum} < 0$, gypsum dissolves in contact with the water, if it is present in solid phase. Field data necessary for input of speciation program are temperature, pH, alkalinity, and results of laboratory chemical analysis.

Common problems solved using speciation programs are: (a) there is a sample with high concentration of dissolved aluminum and we need to know distribution of aluminum between Al^{3+} and different complexes (for example, $Al(OH)_4^-$, $AlSO_4^+$ etc.) because different forms of aluminum have different toxicity, (b) there are ground water samples from contaminant plume downgradient from mine tailing impoundment and we want to verify the possibility of precipitation of minerals like gypsum, $CaSO_4.2H_2O$, and jarosite, $KFe_3(SO_4)_2(OH)_6$.

A classical speciation program is WATEQ4F (Plummer et al., 1976). More advanced geochemical modeling programs like MINTEQA2 (Allison et al., 1991), and PHREEQC-2 (Parkhurst and Appelo, 1999) also include speciation module. There are countless examples of speciation modeling applications in geochemical and hydrogeological literature (for example, Blowes and Jambor, 1990; Robertson et al., 1991; Weaver and Bahr, 1991; Zhu et al., 2002, etc.).

Principal difficulties related to the application of speciation models are:

1. Calculations are based on assumption of thermodynamic equilibrium and do not include a time factor. This means that the SI values just determine the direction of a reaction, but not how long time it takes to complete the reaction. There are so called reactive minerals with fast dissolution/precipitation rate (however, expressions "fast" and "slow" depend on the velocity of ground water flow and on time scale of investigation). Examples of reactive minerals are listed in Chapter 4.2. On the other hand, dissolution of silicates like feldspars is slow and can be made even slower by the formation of secondary products layers on their surfaces. This type of reactions requires kinetic descriptions with a time factor. There are other reactions which never reach equilibrium, and in which reactants are gradually transformed into products. An example is the oxidation of organic matter by oxygen.
2. Equilibrium constants are defined for pure mineral phases, which seldom occur in nature. For example, there can be a gradual transition between K-jarosite $KFe_3(SO_4)_2(OH)_6$ and natro-jarosit $NaFe_3(SO_4)_2(OH)_6$ with changing value of equilibrium constant. A notorious example is ferric hydroxide because the value of equilibrium constant for the mineral phase changes several orders of magnitude depending on the degree of crystallinity (Langmuir, 1997).
3. Complexation with organic matter can highly increase concentrations of dissolved metals. In groundwater without organic matter metals would precipitate as mineral phases. Most modeling codes (except e.g. program WHAM introduced earlier) do not have data base of equilibrium constants for complexation with organic matter. Furthermore, the characterization of organic matter composition is complicated and expensive problem. Terms like humic and fulvic acids describe groups of organic acids with several hundred of members and only for some of them equilibrium constants are available.

There are several important parameters, which have to be entered in the input for speciation calculations. First of all, there has to be some indication of redox state of a water sample. A speciation program has to split somehow concentration of a redox-sensitive species. For example, when only total Fe_{total} concentration is available, program has to determine concentrations of Fe(II) and Fe(III) to calculate SI values for minerals of Fe(II) like siderite, vivianite, and melanterite and for minerals of Fe(III) like goethite and jarosite. In program PHREEQC redox state is generally described by value of pe. This parameter can be calculated from field value of Eh corrected for hydrogen electrode (Chapter 4.3). Alternatively, value of Eh and then pe can be determined from a redox couple with concentrations determined analytically (for example, from Fe(II)/Fe(III) couple) and then used to split total concentration of other redox sensitive element (for example, Cr_{total} to Cr(III)/Cr(VI)). As indicated in Chapter 4.3, redox equilibrium is rather

an exception than a rule and analytical determination of speciation should be preferred whenever possible. However, in some situations the Eh/pe approach is applicable, like in the case of acid mine drainage when the Fe(II)/Fe(III) couple corresponds well to the measured Eh values.

Another important parameter is alkalinity, which is linked to the input of dissolved inorganic carbon (DIC). Concentrations of carbonate species and DIC are generally calculated from alkalinity and pH value. Thus, alkalinity is very important parameter for water with pH > 4.5. Its value is obtained from titration of a sample with strong acid like HCl to an arbitrary pH value (generally 4.5) or the amount of acid is determined by the Gran plot (Appelo and Postma, 2005). Units of alkalinity used in the speciation input can be mg/L HCO_3 or mg/L $CaCO_3$. When mg/L HCO_3 are used, alkalinity value is higher by a factor of 1.22 than in the case of mg/L $CaCO_3$ (see example). Also, alkalinity value based on titration with acid may not always represent carbonate alkalinity. When concentration of organic acids is high (in plumes from landfills, BTEX plumes etc.), their contribution to titration may be significant and this results in overestimation of carbonate alkalinity.

Example: Sample of 200 mL with pH 7.2 required addition of 6.3 ml of 0.2 M HCl to lower pH to 4.5. Determine carbonate alkalinity in meq.L^{-1}, mg.l^{-1} as $CaCO_3$, and mg.L^{-1} as HCO_3^-.
Solution:
0.0063 liters of acid × 0.2 mol H^+ per liter × 1 000 mL/200 mL = 0.0063 moles H^+ per liter
Carbonate alkalinity = 6.3 meq.L^{-1}
= 6.3 × 50 = 315 mg.L^{-1} as $CaCO_3$
= 6.3 × 61 = 384.3 mg.L^{-1} as HCO_3

In some situations the approach called **swapping** can be used to enter data in input file. In this case, water sample is equilibrated with a mineral phase or with a specified gas pressure to obtain concentrations of dissolved species. For example, water assumed to be at equilibrium with atmosphere is equilibrated with $P_{CO2} = 10^{-3.5}$ atm and the distribution of carbonate species is calculated.

5.3.1.2 Case study: speciation in arsenic affected aquifers in Bangladesh

There are high arsenic concentration in Holocene fluvial sediments in Bangladesh and West Bengal, India. They seem to be linked to reductive dissolution of

Fe(III)-oxyhydroxides in buried sediments rich in organic matter (Ahmed et al., 2004; Sracek et al., 2004). Concentrations of reduced species like Fe(II), Mn(IV), NH_4^+, and CH_4 are generally high.

Earlier speciation calculations have suggested that low concentrations of Fe_{tot} in groundwater with high arsenic concentrations observed at some sites in Bangladesh could be due to the precipitation of Fe-mineral phases such as siderite ($FeCO_3$) or vivianite ($Fe_3(PO_4)_2.8H_2O$) (Sracek et al., 2001; Sracek et al., 2005). Speciation calculations using program PHREEQC were performed to evaluate the possibility of solubility control of several dissolved species. Thermodynamic data for arsenic, which is not included in PHREEQC database, were taken from the database of program MINTEQA2. Typical input file for speciation calculation of ground water samples from site Brahmanbaria located northeast of Dhaka is in Fig. 5.2.

```
      SOLUTION 1
      temp   11.1
      pH     6.87
      pe     1.39
      redox  pe
      units  mg/kgw
      Alkalinity 138.1 as HCO3
      Cl     5.37
      S      169.54 as SO4
      P      0.026 as HPO4
      Na     16.3
      K      5.13
      Mg     24.44
      Ca     50.46
      Fe     9.27
      Mn     0.445
      Al     1.32
      Si     15
      As     0.091
      Zn     0.083
      N(5)   0.9 as NO3
      N(-3)  0.46 as NH4
SOLUTION_MASTER_SPECIES
As            H3AsO4 -1.0        74.9216      74.9216
As(+3)        H3AsO3 0.0         74.9216
As(+5)        H3AsO4 -1.0        74.9216
```

```
SOLUTION_SPECIES 1
H3AsO4 = H3AsO4
       log_k  0
       delta_h      0      kcal
H3AsO4 + 2e- + 2H+ = H3AsO3 + H2O
       log_k  19.444
       delta_h      -30.015      kcal
H3AsO3 = H2AsO3- + H+
       log_k  -9.228
       delta_h      6.56   kcal
.
.
.
PHASES
Scorodite
       FeAsO4:2H2O = Fe+3 + AsO4-3 + 2H2O
       log_k        -20.249
Arsenolite
       As4O6 + 6H2O = 4H3AsO3
       log_k        -2.801
       delta_h 14.330 kcal
Claudetite
       As4O6 + 6H2O = 4H3AsO3
       log_k        -3.065
       delta_h 13.290 kcal
Orpiment
       As2S3 + 6H2O = 2H3AsO3 + 3HS- + 3H+
       log_k        -60.971
       delta_h 82.890 kcal
```

Fig. 5.2 Input of speciation calculation in PHREEQC, see text

In bloc SOLUTION 1 concentrations of dissolved ions are specified together with field temperature, pH, and pe based on measured Eh corrected with respect to hydrogen electrode. Since concentrations are in mg/kgw (kgw – kilogram of water), there is a difference, for example, between S(6) and SO_4 and form of an ion is specified. If concentrations are in mmol/kgw and mol/kgw, there would be no difference between S(6) and SO_4. Redox state is based on pe, but concentrations of NH_4^+ and NO_3^- are also specified and program automatically calculates Eh/pe values based on this redox couple.

Arsenic is not in PHREEQC database and its thermodynamic data have to be entered in input. First, definition of arsenic species is in SOLUTION_MASTER_SPECIES. Then aqueous complexes of arsenic are defined in SOLUTION_SPE-

CIES. The parameter delta_h is enthalpy, which is used to correct equilibrium constants log_k (given for 25 °C) for temperature specified in input file. Similarly, thermodynamic data for formation of minerals are entered in bloc PHASES. When value of enthalpy is not available (here, for example, for mineral scorodite) value of equilibrium is constant for any temperature. Equilibrium constants are applied for reactions as written. When reactants become products and vise versa, log k changes to $(\log k)^{-1}$.

Selected output is shown in Fig. 5.3. In Description of solution there is total carbon presented as CO_2. Another important parameter is charge balance error, which indicates quality of water chemistry analyses. In Redox couples, value of Eh based on N(–3)/N(5) redox couple determined analytically is shown. This value of +0.400 V is different from Eh/pe value of +0.082 V based on field measurement. Thus, there is a strong redox disequilibrium in this sample. In Distribution of species concentrations of free ions and aquatic complexes are shown. For example, most of total Al is present as $Al(OH)_4^-$ and concentration of free ion Al^{3+} is negligible. Total arsenic concentration has been entered in input and program split this concentration into As(3) and As(5) concentration. Finally, in Saturation indices values of SI for different minerals are shown. SI values for all arsenic minerals are negative, indicating that principal arsenic attenuation process probably is adsorption. Principal minerals of interest here are siderite and vivianite because they may incorporate Fe(II) and thus disturb correlation between dissolved iron and arsenic. The calculation results indicate that siderite may precipitate from the sample, but vivianite not. Summary of speciation calculation results from Brahmanbaria site in Bangladesh can be found in Sracek et al. (2005).

```
-----------------------------------Description of solution-----------------------------------

                                       pH = 6.870
                                       pe = 1.390
                          Activity of water = 1.000
                             Ionic strength = 8.869e-003
                            Mass of water (kg) = 1.000e+000
                         Total carbon (mol/kg) = 2.794e-003
                            Total CO2 (mol/kg) = 2.794e-003
                           Temperature (deg C) = 11.100
                       Electrical balance (eq) = -6.866e-005
  Percent error, 100*(Cat-|An|)/(Cat+|An|) = -0.66
                                    Iterations = 11
                                       Total H = 1.110158e+002
                                       Total O = 5.552217e+001

-------------------------------------Redox couples-------------------------------------

        Redox couple                pe       Eh (volts)
        N(-3)/N(5)              7.1055           0.4007

-----------------------------------Distribution of species-----------------------------------

                                                                  Log          Log          Log
        Species                Molality        Activity      Molality     Activity        Gamma

        H+                   1.468e-007       1.349e-007        -6.833       -6.870       -0.037
        OH-                  2.634e-008       2.390e-008        -7.579       -7.622       -0.042
        H2O                  5.551e+001       9.999e-001         1.744       -0.000        0.000
Al                  4.892e-005
        Al(OH)4-             3.688e-005       3.352e-005        -4.433       -4.475       -0.042
```

```
        Al(OH)2+            8.492e-006      7.717e-006       -5.071      -5.113      -0.042
        Al(OH)3             2.729e-006      2.734e-006       -5.564      -5.563       0.001
        AlOH+2              7.292e-007      4.973e-007       -6.137      -6.303      -0.166
        AlSO4+              5.114e-008      4.647e-008       -7.291      -7.333      -0.042
        Al+3                3.674e-008      1.715e-008       -7.435      -7.766      -0.331
        Al(SO4)2-           1.564e-009      1.422e-009       -8.806      -8.847      -0.042
        AlHSO4+2            7.405e-016      5.050e-016      -15.130     -15.297      -0.166
As(3)                   8.083e-008
        H3AsO3              8.060e-008      8.077e-008       -7.094      -7.093       0.001
        H2AsO3-             2.268e-010      2.061e-010       -9.644      -9.686      -0.042
        H4AsO3+             5.940e-015      5.398e-015      -14.226     -14.268      -0.042
        HAsO3-2             9.431e-016      6.431e-016      -15.025     -15.192      -0.166
        AsO3-3              2.639e-022      1.115e-022      -21.579     -21.953      -0.374
As(5)                   1.134e-006
        HAsO4-2             7.008e-007      4.779e-007       -6.154      -6.321      -0.166
        H2AsO4-             4.330e-007      3.935e-007       -6.364      -6.405      -0.042
        AsO4-3              1.484e-011      6.272e-012      -10.829     -11.203      -0.374
        H3AsO4              8.062e-012      8.079e-012      -11.094     -11.093       0.001
.
.

-----------------------------------Saturation indices-----------------------------------

        Phase                          SI  log IAP   log KT

        Al(OH)3(a)                   1.09    12.84    11.75   Al(OH)3
        Albite                       0.46     5.72     5.26   NaAlSi3O8
        Alunite                      7.62     8.03     0.40   KAl3(SO4)2(OH)6
        Anhydrite                   -1.77    -6.10    -4.33   CaSO4
        Anorthite                    0.86    29.11    28.25   CaAl2Si2O8
```

Aragonite	-1.19	-9.45	-8.26	CaCO3
Arsenolite	-25.06	-110.45	-85.39	As4O6
As2S3(am)	-108.19	-303.64	-195.45	As2S3
Ca-Montmorillonite	9.22	18.46	9.24	Ca0.165Al2.33Si3.67O10(OH)2
Calcite	-1.04	-9.45	-8.41	CaCO3
Chalcedony	0.12	-3.60	-3.72	SiO2
Chlorite(14A)	-6.28	67.53	73.81	Mg5Al2Si3O10(OH)8
Chrysotile	-9.62	24.39	34.01	Mg3Si2O5(OH)4
Claudetite	-24.83	-110.45	-85.62	As4O6
CO2(g)	-1.86	-20.08	-18.21	CO2
Dolomite	-2.25	-19.00	-16.75	CaMg(CO3)2
Fe(OH)3(a)	-0.29	17.97	18.26	Fe(OH)3
FeS(ppt)	-33.38	-73.10	-39.72	FeS
Gibbsite	3.92	12.84	8.93	Al(OH)3
Goethite	5.08	17.97	12.89	FeOOH
Gypsum	-1.51	-6.10	-4.59	CaSO4:2H2O
H2(g)	-16.52	-16.52	0.00	H2
H2O(g)	-1.89	-0.00	1.89	H2O
H2S(g)	-39.02	-82.80	-43.79	H2S
Halite	-8.60	-7.05	1.55	NaCl
Hausmannite	-22.94	41.70	64.64	Mn3O4
Hematite	12.10	35.93	23.83	Fe2O3
Hydroxyapatite	-7.86	-47.40	-39.54	Ca5(PO4)3OH
Illite	7.93	21.33	13.41	K0.6Mg0.25Al2.3Si3.5O10(OH)2
Jarosite-K	-8.62	23.39	32.01	KFe3(SO4)2(OH)6
K-feldspar	2.47	4.98	2.51	KAlSi3O8
K-mica	15.84	30.67	14.83	KAl3Si3O10(OH)2
Kaolinite	9.78	18.48	8.70	Al2Si2O5(OH)4
Mackinawite	-32.65	-73.10	-40.45	FeS

Manganite	-8.69	16.65	25.34	MnOOH
Melanterite	-4.63	-7.02	-2.39	FeSO4:7H2O
NH3(g)	-9.53	2.23	11.76	NH3
O2(g)	-54.98	33.04	88.02	O2
Orpiment	-91.24	-303.64	-212.40	As2S3
Pyrite	-48.89	-139.38	-90.50	FeS2
Pyrochroite	-6.81	8.39	15.20	Mn(OH)2
Pyrolusite	-18.80	24.91	43.71	MnO2
Quartz	0.59	-3.60	-4.20	SiO2
Realgar	-41.51	-118.68	-77.17	AsS
Rhodochrosite	-0.60	-11.68	-11.08	MnCO3
Scorodite	-6.97	6.87	13.84	FeAsO4:2H2O
Sepiolite	-5.89	10.25	16.14	Mg2Si3O7.5OH:3H2O
Sepiolite(d)	-8.41	10.25	18.66	Mg2Si3O7.5OH:3H2O
Siderite	0.43	-10.37	-10.80	FeCO3
SiO2(a)	-0.77	-3.60	-2.83	SiO2
Smithsonite	-2.70	-12.54	-9.84	ZnCO3
Sphalerite	-27.55	-75.27	-47.72	ZnS
Sulfur	-28.55	-66.28	-37.73	S
Talc	-5.88	17.18	23.06	Mg3Si4O10(OH)2
Vivianite	-1.89	-37.89	-36.00	Fe3(PO4)2:8H2O
Willemite	-5.05	11.47	16.53	Zn2SiO4
Zn(OH)2(e)	-3.96	7.54	11.50	Zn(OH)2

Fig. 5.3 Selected output of speciation calculation for sample from Brahmanbaria site discussed in text

5.3.2 Inverse geochemical modeling

5.3.2.1 Principles and modeling strategy

This type of modeling (also called mass balance modeling) is used in cases, when chemistry of groundwater and solid phase composition are already known, and reactions that have already happened between hydraulically connected sampling points should be determined. There are two types of inverse geochemical modeling: evolution of groundwater chemistry between 2 sampling points and mixing problem. In the case of chemical evolution, the input includes groundwater chemistry of 2 samples located on the same flowline and composition of solid phase in the aquifer between these 2 points. In the case of mixing problem, the required input are 3 samples, which represent chemistry of 2 waters prior to the mixing and chemistry of final water after mixing and completion of geochemical reactions. Typical models of the type are NETPATH (Plummer et al., 1994) and inverse modeling module of PHREEQC (Parkhurst and Appelo, 1999). Program is based on mass balance equation:

$$\Delta m_{T,K} = \sum \alpha_p b_{p,k} \; k = 1,j \tag{5.2}$$

where $\Delta m_{T,K}$ is change of total dissolved concentration of k^{th} component between sampling points, α_p is the quantity of component p (for example, in mol/kg of water) which dissolved or precipitated and $b_{p,k}$ is stoichiometric coefficient of k^{th} component in p^{th} mineral. For example, for dissolved inorganic carbon change along flowpath with reacting phases including calcite, dolomite and CO_2(g), we can write

$$\Delta m_{T,C} = \alpha_{calcite} + 2\alpha_{dolomite} + \alpha_{CO2} \tag{5.3}$$

The program solves a set of equations for specified components and the goal is to calculate mass transfer coefficient a for each phase. Similar equations are solved for mass balance of electrons and isotopes. An advantage of inverse modeling module in PHREEQC is the possibility to include uncertainty in input data. Range of possible concentrations can be entered by user and then range of mass transfer coefficient is calculated.

The output has the following form:

Water A + Reactants = Water B + Products (5.4)

Example of mass balance model output is the interpretation of water chemistry in the Madison Aquifer in Wisconsin, USA (Plummer et al., 1984):

Recharge water + 20.15 gypsum + 3.54 dolomite + 0.87 CH_2O + 15.31 NaCl + 2.52 KCl + 0.09 FeOOH + 8.28 Na_2-X = Mysse water + 5.33 calcite + 0.09 pyrite + 8.28 Ca-X (5.5)

where mass transfer coefficients are in mmol/L and X indicates exchange sites on solid phase. Generally, solution is non-unique and several possible models of reactions (sometimes none model of reactions as well) are suggested by a program. Less probable models can be eliminated on the basis of mineralogical data (for example, when dissolution of calcite is suggested, this mineral must be present in solid phase) and speciation calculation results (similarly, when calcite should dissolve, its SI value should be negative at initial sampling point). The type of models is generally used for the interpretation of regional water chemistry evolution (examples include Gerla, (1992), and Sracek and Hirata (2002)), but it has also been used for interpretation of reactions in aquifers contaminated by petroleum hydrocarbons and organic matter from landfills (Baedecker et al., 1993; van Breukelen et al., 2003; Vencelides et al., 2007).

5.3.2.2 Case study: inverse geochemical modeling of the Guarani Aquifer system in Brazil

The Guarani system is one of the largest aquifer systems in the world. It is so called transboundary aquifer, which is located in several countries including Brazil, Argentina, Uruguay, and Paraguay. In São Paulo state, Brazil, the Guarani system comprises Botucato and Piramboia Aquifers (Fig. 5.4), which are confined by underlying Passo Dois Aquitard and overlying Serra Geral Formation. The aquifer is dipping towards the west, e.g., towards the River Paraná. There is evolution from Ca-HCO_3 groundwater type with low mineralization and neutral pH in recharge zone towards Na-HCO_3 groundwater type with high mineralization and high pH values (above 9.0) in deep confined zone. Simultaneously, concentration of F^- increases up to 13 mg/L and temperature reach 63 °C at site Presidente Prudente close to the River Paraná (Sracek and Hirata, 2002).

On the basis of ionic ratios it has been concluded that the increase of Na concentration cannot be caused only by dissolution of evaporites like halite, NaCl, and thenardite, $NaSO_4$, and an alternative source of Na has to be present. It has been suggested by Sracek and Hirata (2002) that cation exchange combined with dissolution of carbonates may explain formation of Na-HCO_3 groundwater. Conceptual model of groundwater chemistry evolution can be summarized as

$CaCO_3 + CO_2 + H_2O + Na_2\text{-X} = 2\,Na^+ + 2\,HCO_3^- + \text{Ca-X}$ (5.6)

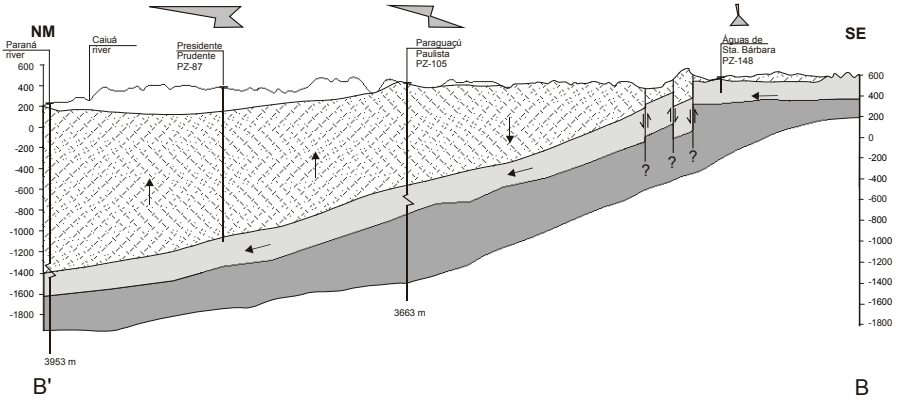

Fig. 5.4 Cross section of the Guarani Aquifer in Sao Paulo state, Brazil (after Sracek and Hirata, 2002). Water chemistry is indicated by Stiff diagrams above the profile. Principal aquifer sliced between aquitards is indicated by light gray shading (Published with permission of Springer, License Number 32669440781135)

This reaction removes from groundwater Ca^{2+} produced by dissolution of calcite and increases pH and dissolved inorganic carbon (DIC) concentrations. Fluorite, CaF_2, also dissolves due to low Ca^{2+} concentrations. Selected results of speciation calculations for wells are shown in Table 5.2.

Table 5.2 Selected results of speciation calculation for water in the Guarani Aquifer

Parameter/well	$SI_{calcite}$	SI_{gypsum}	$SI_{fluorite}$	PCO_2 [atm]	DIC [mmol/L]
PZ-148	–1.21	n.a.	–3.91	–3.22	1.45
PZ-105	–0.70	–4.67	–2.83	–2.75	4.68
PZ-87	0.63	–2.93	–0.48	–3.47	3.13

There is a decrease of P_{CO2} and increase of DIC between wells PZ-105 and PZ-148. This behavior indicates dissolution of calcite, which is also supported by negative $SI_{calcite}$ value. Inverse geochemical modeling performed in program NETPATH included Ca, Na, C, S, and Cl as elements (constraints in NETPATH terminology) and calcite, halite, gypsum, CO_2(g), and Ca/Na exchange as phases. Results of inverse geochemical modeling are in Table 5.3. These results indicate that dissolution of calcite and Na-input from exchange sites may explain changes of ground water chemistry between recharge zone and deep confined zone. Deep geothermal well PZ-87, located behind cation exchange front, is already influenced by CO_2 de-gassing and precipitation of calcite.

Table 5.3 Output of inverse geochemical modeling for zone between PZ-148 and PZ-105, sign minus indicates removal from ground water

Phase	Mass transfer [mmol/.L^{-1}]
Halite	0.45
Calcite	2.25
Gypsum	0.10
CO_2(g)	0.97
Na_2-X	2.36
Ca-X	–2.36

5.3.2.3 Case study: inverse geochemical modeling at site contaminated by petroleum hydrocarbons at Hnevice, Czech Republic

There is a contamination by petroleum hydrocarbons (PHC) at Hnevice site close to the river Labe (Elbe), north of Prague in the Czech Republic. Several PHC releases occurred since 1940's (Vencelides et al., 2007). In late 1980's, the free phase plume shrinked as a consequence of dissolution and remediation pumping. Currently (2004) there are 4 different geochemical zones: background zone never invaded by NAPL, former NAPL zone, now reoxidation zone; recent NAPL plume, and fringe zone between recent free phase plume and deep uncontaminated zone (Fig. 5.5). The detailed study site was located at the rear of the plume, where background groundwater with high concentrations of electron acceptors mixes with contaminated groundwater. Conceptual model of this site includes (a) initial dissolution of free phase, dissolution of Fe(III) minerals such as ferrihydrite, precipitation of mixed Fe(II)-carbonates and possibly Fe-sulfides, de-gassing of CO_2 and CH_4, and (b) later flux of electron acceptors into the former free phase zone and oxidation of Fe(II) minerals.

Inverse modeling was performed for the segment between sampling points PJ519 and PJ520 (Fig. 5.5). This segment is located in the zone between margin and central zone of the recent contaminant plume. Selected phases were: goethite, manganite, solid solution mineral $Fe_{0.8}Ca_{0.2}CO_3$, organic matter with composition $CH_{1.15}$ (toluene), mackinawite, and de-gassing of CO_2(g), N_2(g), and CH_4(g). The composition of Fe(II) carbonate mineral composition is consistent with data from Bemidji (Tuccillo et al., 1999) and gave the best results. Any other Ca/Fe ratios generally caused convergence problems during the inverse modeling calculations. The organic matter composition roughly corresponds to toluene. Data on δ^{13}C(DIC), were used for calibration of inverse geochemical modeling. The δ^{13}C values for the mineral phases used in the model were (in per mil.): Fe(II) carbonate –1.0, $CH_{1.15}$ –27.0, CO_2(g) –15.0, and CH_4(g) –60.0. The ranges of uncertainties were ±2 per mil. for all C phases except for methane, were the

value was ± 5 per mil. The uncertainty for dissolved concentrations was 0.165 (e.g., 16.5 % range around entered concentration values was allowed). The input file is given in Fig. 5.6.

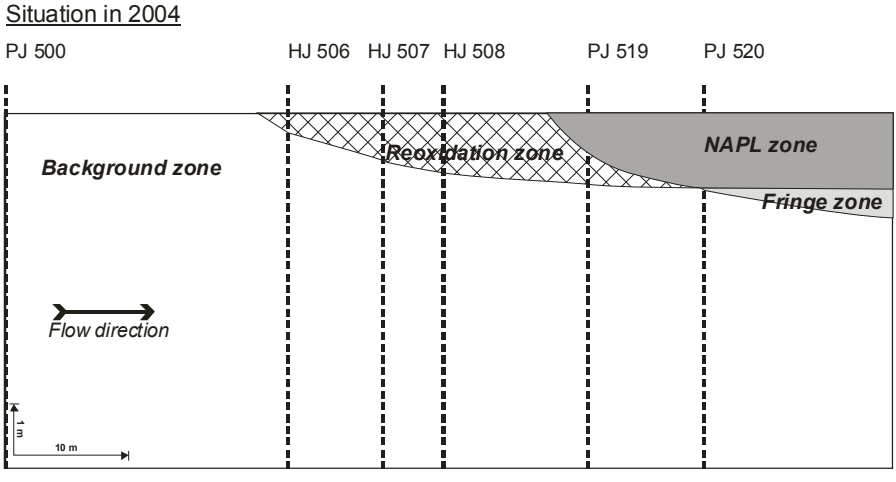

Fig. 5.5 Conceptual model of geochemical zones at Hnevice site (after Vencelides et al., 2007)

First, SOLUTION 1 and SOLUTION 2 are defined. Isotopes are included in option –i (here ^{13}C values for DIC). Samples should be located on the same flowline. Then in INVERSE_MODELING bloc –solutions defines initial and final solution, -uncertainty indicates range of possible values around entered concentrations, and –balances include ions (here Na and Cl), which are not comprised in entered phases. Command –phases includes minerals which may dissolve or precipitate. If not stipulated in input, both reactions are allowed. Also, values of ^{13}C isotope with range of possible values are entered for relevant phases (carbonate minerals, toluene, and methane). Then in bloc PHASES mineral phases, which are not included in phreeqc.dat database are defined (here toluene, C_7H_8, and mixed Ca-Fe(II) carbonate). The values of log k are not important because this constant is not used in inverse modeling, but the stoichiometry of equations does matter.

Selected output of inverse modeling is in Fig. 5.7. First column shows mass transfer in mol/L. Sign minus plus indicates dissolution or degradation (for example, $Fe(OH)_3(a)$ and toluene), sign minus indicates precipitation (for example, mackinawite and manganite). Sign minus for gases (here N_2 and CH_4) indicate de-gassing. Minimum and maximum mass transfers are shown for ranges of concentrations defined in uncertainties. Redox mole transfers are shown for redox reactions.

```
TITLE Hnevice-inverse modeling
SOLUTION 1 Sample 519/5.4m
units mg/kgw
temp  9.3
pH 6.8
pe 2.03
Alkalinity 366 as HCO3
Ca    196.4
Na    50
Cl    50
S(6) 270 as SO4
Fe    6.2
Mn    0.87
N(5)  20 as N
N(-3) 0.005 as N
density 1
-i    13C   -14.5   2.0
SOLUTION 2 Sample 520/5.4m
units mg/kgw
temp  9.3
pH 7.63
pe 1.78
Alkalinity 634 as HCO3
Ca    176.3
Na    50
Cl    50
S(6) 184 as SO4
Fe    9.18
Mn    8.48
N(5)  7 as N
N(-3) 0.015 as N
density 1
-i    13C   -7.66   2.0
INVERSE_MODELING
-solutions 1 2
-uncertainty 0.165
-balances
 Na
 Cl
-range
-isotopes
      13C
-phases
      Fe0.8Ca0.2CO3 precip     13C   -1.0   5
      Fe(OH)3(a) dissolve
```

```
      C7H8 dissolve             13C - 27.0     1
      Manganite dissolve
      Mackinawite precip
      N2(g)  precip
      CO2(g) precip             13C    -18.0    5
      CH4(g) precip             13C    -70.0   20
PHASES
C7H8
      C7H8 + 14H2O = 7CO2 + 36H+ + 36e-
      -log_k 0.0
Fe0.8Ca0.2CO3
      Fe0.8Ca0.2CO3 + H+ = 0.2Ca+2 + 0.8Fe+2 + HCO3-
      -log_k 0.0
END
```

Fig. 5.6 Input of inverse modeling at Hnevice site

```
Phase mole transfers:          Minimum     Maximum
  Fe0.8Ca0.2CO3 -3.058e-003 -3.059e-003 -3.011e-003
     Fe(OH)3(a)  4.175e-003  4.151e-003  4.221e-003 Fe(OH)3
           C7H8  9.915e-004  9.808e-004  9.951e-004 C7H8
      Manganite  1.640e-004  1.600e-004  1.666e-004 MnOOH
    Mackinawite -1.630e-003 -1.675e-003 -1.605e-003 FeS
         N2(g) -4.541e-004 -4.766e-004 -3.853e-004 N2
        CH4(g) -1.721e-000 -1.746e-003 -1.706e-003 CH4

Redox mole transfers:
          C(-4) -1.721e-003
          Fe(3)  4.175e-003
          N(-3) -7.140e-007
           N(0) -9.082e-004
          S(-2) -1.630e-003
```

Fig. 5.7 Selected output of inverse modeling at Hnevice site

5.3.3 Forward geochemical modeling

5.3.3.1 Principles and modeling strategy

This type of models, also called reaction path models, is used for prediction of water chemistry evolution along a flowline. In this case, initial water chemistry is known and the aim is to predict water chemistry at some downgradient point along flow path. We have to stipulate reacting mineral phases which dissolve and also mineral phases which precipitate when their SI values are higher than 0. The input of model comprises the initial water chemistry and reacting mineral

phases. This type of model also can equilibrate a water sample with a gas with specified partial pressure (for example, with P_{CO2}). The output is similar to the output of speciation model (e.g., list of dissolved species and saturation indices), but the amount of dissolved or precipitated minerals during equilibration is also indicated. The concept of modeling is

Initial water + Reacting phases = Predicted water + Products (5.7)

Let us assume dissolution of halite, NaCl, and barite, $BaSO_4$, in an initial water. In MINTEQA2, for example, both minerals can be included in input as "infinite phase" (which means that their amount in solid phase is large and is not influenced very much by their dissolution) and "finite phase" (in this case we stipulate their amount in contact with 1L of water). In PHREEQC input, amounts of minerals are entered in EQUILIBRIUM_PHASES bloc, where default value for large ("infinite") concentration is 10 mol/L. When initial amount of a mineral is zero, only precipitation, but not dissolution is allowed. The amount of a mineral S [mol/L] can be determined by conversion of solid phase analyses data, usually in wt %, using equation

$$S[mol/L] = [(\rho_b/n).(wt\ \%/100)]/MW \quad (5.8)$$

where ρ_b is bulk density of solid phase in g/dm^3, n is porosity, and MW is molecular weight of a mineral.

Problem: Convert concentration of calcite in solid phase of 0.5 wt % to mol/L.
Use ρ_b = 1800 g/dm^3, n = 0.3, and MW of calcite is 100 g.
Solution: [(1800/0.3).(0.5/100)]/100 = 0.3 mol/L

In the problem above, a program will dissolve in each reaction step

$$\Delta NaCl + \Delta BaSO_4 \quad (5.9)$$

where Δ is mass transfer coefficient in mol/L, which is a small number. In each step, the program adds into water ΔNa^+, ΔCl^-, ΔBa^{2+}, ΔSO_4^{2-}, and then there is speciation calculation. If saturation index for a dissolving phase is still negative, then dissolution continues. The transfer coefficient is kept small to avoid sudden supersaturation of water and conversion of reactants into products. In the meantime, other pre-determined reactive minerals can be precipitated if their saturation indexes values become positive.

Programs for forward modeling can be used in "batch mode", e.g., there is equilibration of water with given phases in a closed vessel. The program PHREEQC

can also be used in 1-D transport mode, e.g., water flows through a column and is equilibrated with minerals and adsorbing phases in the column. This type of modeling already belongs to the reactive transport modeling. Inverse models and forward models are complementary because when we want to determine down-gradient evolution of water chemistry, then we need to know which processes have already influenced water chemistry upgradient.

Surface complexation modeling of adsorption implemented in forward modeling programs is based on diffuse double layer model in PHREEQC. There are more options in MINTEQA2, where also constant capacitance model and triple layer model, (Langmuir, 1997), are available. In the most common diffuse double layer model the following steps are performed:

a) After water chemistry input concentration of Fe(III) converted to HFO as Fe(III) [g/L] × 1.589 is entered.
b) Then specific surface in [m^2/g] is entered, which is 600 m^2/g for freshly precipitated HFO, but is lower for older precipitates.
c) Finally, concentration of adsorption sites in [mol of sites/L] is entered, which is 0.2 mol sites/mol HFO x concentration of HFO [mol HFO/L] for weak adsorption sites, and 0.005 mol sites/mol HFO × concentration of HFO [mol HFO/L] for strong adsorption sites.

For description of input in PHREEQC see previous text.

In some programs (for example, PHREEQC, Version 2) kinetics can also be included. Generally, rate of a reaction is expressed as a function of deviation from equilibrium, e.g.,

$$Rate = k.(1 - W) \tag{5.10}$$

where $W = IAP/K_{sp}$ (Chapter 4.2). The term in parenthesis is multiplied by rate constant k and by ratio A/V, which is the ratio of surface A of a mineral and V is volume of solution in contact with the surface. The ratio A/V is sometimes dropped when unimportant (e.g., in oxidation of organic matter). Complete equation is

$$Rate = \frac{A}{V}.k.(1 - \Omega) \tag{5.11}$$

Typical problems solved by forward modeling are: (a) Reactions of contaminated water with aquifer solids like calcite and $Fe(OH)_3$. (b) Determination of water

chemistry after mixing with water in the stream, equilibration with gases with specified partial pressures and after completion of chemical reaction. (c) Evaporation of contaminated water in a discharge area with precipitation of minerals etc. Examples of forward geochemical modeling include determination of natural background concentrations of dissolved metals (Runnells et al., 1992), modeling of sulfate contamination at abandoned mine in Wisconsin (Toran, 1994), modeling of reactions in aquifer contaminated by acid mine drainage (Stollenwerk, 1994), calculation of radionuclide retardation under changing pH conditions (Saunders and Toran, 1995), modeling of Na-HCO_3 ground water evolution in fractured aquifer in Tennessee (Toran and Saunders, 1999), and modeling of geochemical evolution in regional flow system in southwestern France (André et al., 2005).

5.3.3.2 Case study: neutralization of acid mine drainage in a batch

This example shows neutralization of acid mine drainage by calcite in a batch (closed recipient, e.g., a beaker). This means that there is no flow, just adding of calcite into solution. Composition of water is entered in SOLUTION 1. Then calcite is added and equilibration with several minerals is forced in EQUILIBRIUM_PHASES module.

First number after the name of mineral is saturation index, and second number is its initial amount of mineral in mol in contact with 1L of water. Initially, there is only calcite in contact with acid water, i.e. only calcite can dissolve. All other minerals including gypsum, siderite etc. are not present at the beginning of the batch calculation, which means that they can only precipitate. Input file is in Fig. 5.8.

The complete input file:

```
TITLE AMD-neutralization_graph
PRINT
SOLUTION 0 AMD
units mmol/kgw
temp 25.0
pH 2.4
Na 2
Al 2
Fe(2)   2
Fe(3)   1
S(6)   15
EQUILIBRIUM_PHASES
Calcite 0 0.25
Gypsum 0 0
Siderite 0 0
```

```
Al(OH)3(a)  0  0
Fe(OH)3(a)  0  0
END
```

Fig. 5.8 Input file of neutralization of acid mine drainage in a batch

Selected output is in Fig. 5.9. Value of pH increased and reached 6.466. Principal result of modeling is in the table of mass transfer of mineral phases. Calcite dissolved is calculated as a difference between the final and initial amounts of the mineral. Water has not reached supersaturation with respect to gypsum and mass transferred delta was 0. On the other hand, $Al(OH)_3(a)$, $Fe(OH)_3(a)$ and siderite precipitated and their delta values were positive.

```
pH = 6.466
…
Phase       SI log   IAP  log KT   Initial     Final      Delta
Al(OH)3(a) -0.00  10.80  10.80  0.000e+00  1.992e-03  1.992e-03
Calcite     0.00  -8.48  -8.48  2.500e-01  2.366e-01 -1.339e-02
Fe(OH)3(a)  0.00   4.89   4.89  0.000e+00  9.999e-04  9.999e-04
Gypsum     -0.08  -4.66  -4.58  0.000e+00  0.000e+00  0.000e+00
Siderite    0.00 -10.89 -10.89  0.000e+00  1.940e-03  1.940e-03
```

Fig. 5.9 Selected output of neutralization in a batch

5.3.3.3 Case study: titration of acid mine drainage water

Sample of acid mine drainage water from a site in Czech Republic has low pH and high concentrations of Al, Fe, Mn, and SO_4. The sample is titrated with calcite in 10 steps. Precipitation of $Fe(OH)_3(a)$, $FeCO_3$, $Al(OH)_3(a)$, $MnCO_3$, and gypsum is allowed, when their respective SI values reach positive values. Input file for this problem is in Fig. 5.10.

First SOLUTION 1 is specified. Note that total Fe concentration is entered and program will split it to Fe(II) and Fe(III) on the basis of pe calculated from field Eh value.

The sample has no carbonate alkalinity because its pH < 4.5. Then REACTION 1, addition of calcite in 10 steps is specified, in each step 0.36 g of calcite is added. In EQUILIBRIUM_PHASES there is a list of minerals, which should precipitate when their SI values become positive.

```
SOLUTION 1 Site A - titration of AMD sample with calcite
    temp      9.1
    pH        3.6
    pe        11.5
    redox     pe
    units     mg/kgw
```

```
    density  1
    Ca       159
    Mg       558
    Na       1160
    K        114
    Fe       455
    S(6)     6500 as SO4
    Cl       68 charge
    Al       293
    Mn       40.9
REACTION 1
    Calcite  1.0
    0.036 moles in 10 steps #360 mg/l of calcite in each step
EQUILIBRIUM_PHASES
Siderite 0 0
Rhodochrosite 0  0
Al(OH)3(a) 0  0
Fe(OH)3(a) 0  0
Gypsum 0  0
```

Fig. 5.10 Input file for titration of acid mine drainage sample with calcite

Output in the form of pH-buffering graph and the amount of precipitated minerals is shown in Fig. 5.11. First plateau at pH of about 3.6 corresponds to the precipitation of $Fe(OH)_3(a)$, which buffers pH by production of $3H^+$ moles for precipitation of 1 mole of $Fe(OH)_3(a)$. Then from pH of about 5.2 to pH of about 5.5 there is precipitation of siderite and $Al(OH)_3(a)$. Only after the precipitation is completed, pH starts to rise, but equilibrium with calcite is not reached even in last step.

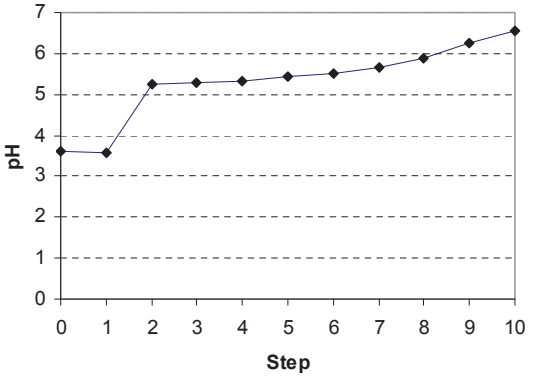

Fig. 5.11 Graph of forward modeling of acid mine drainage water titration. In each step 360 mg/L of calcite are added

6 Reactive transport modeling

6.1 Principles and modeling strategy

We have discussed so far purely geochemical models, which do not include physical processes like dispersion. Now we will introduce **reactive transport models** briefly. In this type of models, transport and chemical steps are generally separated. The advection-dispersion equation (ADE) with chemical reactions for species dissolved in water is

$$\frac{\partial}{\partial x_\alpha}\left(D_{\alpha\beta}\frac{\partial C_i}{\partial x_\beta}\right)-\frac{\partial}{\partial x_\alpha}\left(v_\alpha C_i\right)+r_{reac,i}=\frac{\partial C_i}{\partial t} \tag{6.1}$$

For minerals in solid phase we obtain

$$r_{reac,i}=\frac{\partial C_i}{\partial t} \tag{6.2}$$

In equations above, v_a is advective velocity in direction x_a, $D_{\alpha b}$ is hydrodynamic dispersion coefficient tensor, and $r_{reac,i}$ is source/sink term due to chemical reaction. Generally so called **split operator** approach is used, when a program solves in transport step the ADE for each of dissolved species, and then in chemical step a set of chemical reactions based on forward modeling takes place (formation of complexes, precipitation of pre-determined minerals etc.). Some coupled codes use common forward modeling codes, for example, the code MINTRAN (Walter et al., 1994) uses MINTEQA2 in its geochemical module. Similarly, programs PHT3D (Prommer et al., 2003) and PHAST (Parkhurst et al., 2004) use program PHREEQC in their geochemical modules. Again, examples of reactive transport modeling in contaminant hydrogeology are numerous, including, for example, modeling of acid mine drainage plume attenuation (Zhu et al., 2001), modeling of neutralization reactions in a column (Jurjovec et al., 2004), modeling of acid mine drainage generation in a waste rock pile (Molson et al., 2005), modeling of biodegradation of hydrocarbon plume under transient flow conditions (Prommer et al., 2002), modeling of natural attenuation of phenolic compounds in deep sandstone aquifer (Mayer et al., 2001), and modeling of geochemical reactions during artificial recharge (Greskowiak et al., 2005). Applications of reactive transport modeling in regional ground water flow investigation are less common, but they do exist (for example, Keating and Bahr, 1998).

6.2 Case study: modeling of acid mine drainage neutralization

When acid mine drainage enters an aquifer with carbonates like calcite in solid phase, several neutralization reactions take place (Zhu et al., 2002): (1) dissolution of calcite, (2) dissolution of siderite, (3) dissolution of $Al(OH)_3$, and dissolution of $Fe(OH)_3$. Each reaction buffers pH at different region. Only calcite may be initially present in aquifer and all other minerals are formed in preceding steps of neutralization (for example, when calcite dissolves, pH is buffered above 6.0 and siderite, $Al(OH)_3$, and $Fe(OH)_3$ precipitate; when siderite dissolves, $Al(OH)_3$ is stable or may still precipitate and so on). Simulation can be performed in column mode and output can be plotted as a function of pore volumes (PV) or as a function of distance in the version of PHREEQC with graphical capabilities prepared by Vincent Post.

Initial solution in column entered in SOLUTION 1–200 is pure water. SOLUTION 0 is flushing solution with low pH and high concentrations of Al, Fe(II), Fe(III) and sulfate. An essential module is the input of minerals in solid phase in bloc EQUILIBRIUM_PHASES.

First number after name of a mineral is saturation index SI. Value of 0 indicates that water will be pushed to equilibrium with that mineral. Second number indicates the amount of the mineral in moles in contact with 1 L of water prior to the injection of SOLUTION 0. When the amount is 0 (for example, for siderite), this means that the mineral is not initially present in the column at the beginning of simulation and may only precipitate later. Thus, in the example above only calcite is initially present.

Transport parameters are defined in the bloc TRANSPORT. Command –cells indicate 200 cells in column, -lengths indicate that each cell is 0.5 m long, e.g., total column length is 100 m. Command -time step [s] indicate residence time in a cell, which is linked to the advective velocity v as

$$v\ [m/s] = \text{lengths/time step} \tag{6.3}$$

Command –boundary_conditions indicate flux boundary conditions at both inlet and outlet ends of the column. Command –punch cells indicate that results will be written for cells 1–200, e.g., for all cells in the column.

Block USER_GRAPH can be used for plotting of results in Vincent Post's version of PHREEQC. Results are plotted as a function of distance. In that case, TRANSPORT module commands –punch cells and –print cells include all cells, e.g., cells 1–200. Then commands –punch frequency and –print frequency are numbers,

which are equal to the number of –shifts (here 100). This means that only concentrations after last shift (e.g., after complete simulation run) will be plotted. Then in SELECTED_OUTPUT –distance is set true and in USER_GRAPH headings and axis titles are indicated and information about axis are included in Visual Basic commands on lines libeled 10, 20, and 30.

Complete input file is in Fig. 6.1.

```
TITLE AMD-neutralization
SOLUTION 0 Acid water
units mmol/kgw
temp 25.0
pH 2.4
pe 10.0
Na 12 charge
Al 2
Fe(2)  2
Fe(3)  1
S(6)   10
SOLUTION 1-200 Initial water #use background water
units mmol/kgw
temp 25.0
pH 6.9
pe 6.0
Ca 0.1 charge
C(4) 0.2
EQUILIBRIUM_PHASES 1-200
Calcite 0 0.01 #initial CaCO3 content
Gypsum 0 0
Siderite 0 0
Al(OH)3(a) 0 0
Fe(OH)3(a) 0 0
PRINT -reset false
TRANSPORT
-cells 200
-lengths 0.5 #total length 200*0.5 = 100m
-shifts 100
-time_step 86400 #lengths of a cell/advective velocity
-flow_direction forward
-boundary_conditions flux flux
-diffusion_coefficient 1.0e-9
-dispersivities 0.05 #longitudinal dispersivity 0.05m
-correct_disp true
-punch_cells 1-200
```

```
-punch_frequency 100
-print_cells 1-200
-print_frequency 100
SELECTED_OUTPUT
-file  AMD
-reset false
-step true
-pH true
-totals Al Fe(2) Fe(3) pH
-distance true
USER_PUNCH
-head m_Fe(2), m_Fe(3), m_Al, pH
10 PUNCH tot("Fe(2)"), tot("Fe(3)"), tot("Al"), -LA("H+")
PRINT -reset false
USER_GRAPH
-headings distance(m) pH
-chart_title "Acid neutralization"
-axis_titles "distance(m)" "pH"
-axis_scale x_axis 0 100 5
-axis_scale y_axis 0 10 1
-axis_scale sy_axis 0 14 1
-initial_solutions false
-plot_concentration_vs x
-start
10 graph_x dist
20 graph_y tot("Fe(2)")*1000, tot("Fe(3)")*1000, tot("Al")*1000
30 graph_y -LA("H+")
END
```

Fig. 6.1 Input of reactive transport modeling of acid mine drainage plume

Results of modeling (input modified compared to Fig. 6.1 due to convergence problems) are plotted in Fig. 6.2. Three different peaks of dissolved Fe(3), Al, and Fe(2) (from left to right) correspond to regions of neutralization by respective dissolution of $Fe(OH)_3(a)$, $Al(OH)_3(a)$, and siderite. Where these minerals dissolve, concentrations of Fe(3), Al, and Fe(2) are higher than in input acid water (for example, Al concentration at about 19 m is 4.0 mmol/l compared to 2.0 mmol/l at the inflow boundary). In pH graph, there are changes of slope at distances about 15 m, 19 m, and 29 m, corresponding to different neutralization regions. However, concentrations used in this modeling are relatively low and these regions are not very developed.

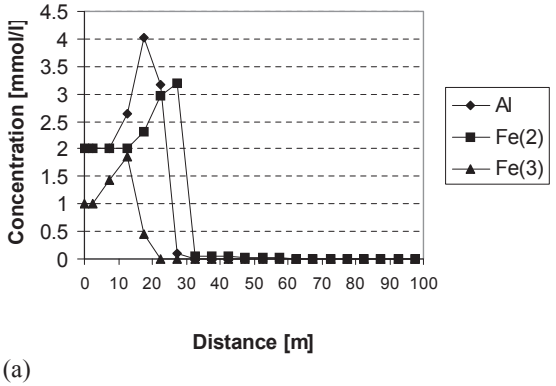

(a)

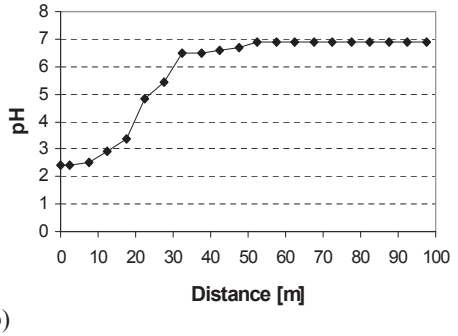

(b)

Fig. 6.2 Results of modeling: (a) dissolved concentrations of Al, Fe(2), and Fe(3), and (b) groundwater pH as a function of distance from source

6.3 Case study: modeling of Cd adsorption in a column

Input file for modeling of Cd transport with adsorption a soil column is shown in Fig. 6.3. Compared to the previous case, there is an additional command SURFACE. Here the Hfo_sH indicate strong adsorption sites and Hfo_wH indicate weak adsorption sites on the surface of hydrous ferric oxide (HFO) adsorbent. First parameter after names of sites is number of sites in moles of sites/L of water, second parameter is specific surface of HFO adsorbent in m^2/g, and third parameter is the amount of HFO in contact with 1 L of water. The second parameter is from literature (but note that with aging of a mineral the degree of crystallinity generally increases and the value of specific surface decreases; for example, 600 m^2/g applies for freshly precipitated $Fe(OH)_3(a)$, but value of about 100 m^2/g applies for goethite, Langmuir (1997)). However, there is a relation between first

and third number: for strong sites applies that (third parameter/89) × 0.005 = first parameter, for weak sites applies that (third parameter/89) × 0.2 = first parameter, where 0.005 and 0.2 are moles of strong and weak sites, respectively, per mole of HFO based on Dzombak and Morel (1990). The value of 89 is molecular weight of HFO with composition of goethite (FeOOH). Meaning of other parameters is the same as in acid mine drainage example.

In this case, output is plotted in Vincent Post's version of PHREEQC as a function of pore volumes PV (e.g., as a breakthrough curve) instead of a function of distance. In USER_GRAPH commands –axis scale first number and second number indicate minimum and maximum on the axis of a graph, other numbers are auxiliary markers on axis. Line 10 graph_x (step_no + 0.5)/10 indicates that points on x-axis will be related to pore volumes, for example, for step number 5 the point on x-axis will indicate mid-point of the column, for step number 10 this is one pore volume (PV) etc. The 0.5 is added because concentrations are calculated for the middle point of a cell.

```
TITLE Cd-PV_graph
SOLUTION 0 CdCl2
units mmol/kgw
temp 25.0
pH 6.3
Cd 5
Cl 10 charge
END
SOLUTION 1-10 Pure water
units mmol/kgw
temp 25.0
pH 4.9 charge
SURFACE 1-10
-equilibrate surface with solution 1-10
Hfo_sH 0.0064 600.0 115.0
Hfo_wH 0.258 600.0 115.0
END
PRINT -reset false
TRANSPORT
-cells 10
-lengths 0.01
-shifts 90
-time_step 7200
-flow_direction forward
-boundary_conditions flux flux
-diffusion_coefficient 1.0e-9
-dispersivities 0.02
```

```
-correct_disp true
-punch_cells 10
SELECTED_OUTPUT
-file Cd-PV_graph
-reset false
-step true
-pH true
-totals Cd Cl
USER_GRAPH
-headings PV Cd Cl
-chart_title
-axis_titles "PORE VOLUME" "Concentration (mmol/l)"
-axis_scale x_axis 0 9 1 0.1
-axis_scale y_axis 0 10 1 0.1
-initial_solutions false
-plot_concentration_vs time
-start
10 graph_x (step_no + 0.5)/10
20 graph_y tot("Cd")*1000, tot("Cl")*1000
END
```

Fig. 6.3 Input file of Cd-adsorption modeling in C vs. PV mode

Results are in Fig. 6.4. Cl as a conservative tracer appears at the end of column after only 0.2 PV and reaches 0.5 of initial concentration after 0.5 PV. After 2.0 PV concentration of Cl becomes constant. Cd starts to appear at the end of column only after 3.3 PV because it is retarded by adsorption. After about 9 PV an initial concentration of 5.0 mmol/L is reached and then there is no more change.

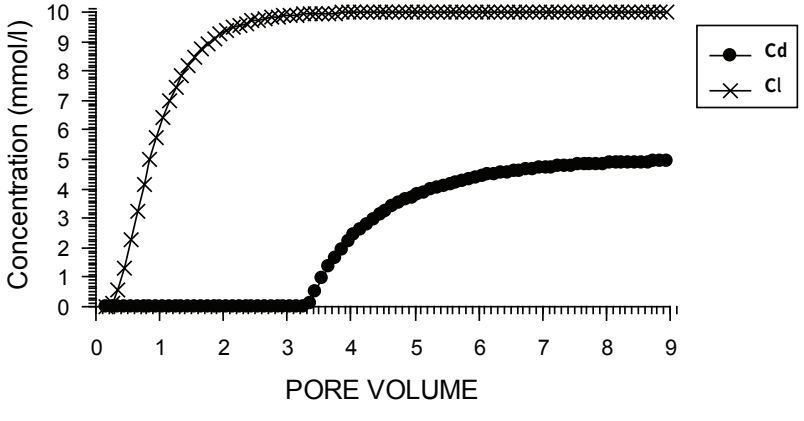

Fig. 6.4 Results of Cd transport modeling in C vs. PV mode

6.4 Case study: modeling diffusion of tritium with decay in landfill liner

Diffusion of tritium is modeled as diffusion of a conservative species, but 1st order decay with half-life of 12.3 years is added. Input file is in Fig. 6.5. Tritium has to be added in modules SOLUTION_MASTER_SPECIES and SOLUTION_SPECIES because is not included in standard PHREEQC database. Decay parameters are entered in RATES and KINETICS modules. Boundary condition is considered as constant tritium concentration. Obviously, this is oversimplified because tritium concentration in precipitation decreases in time. In PHREEQC variable concentration at a boundary can be used and program performs convolution of input data. An example is modeling of artificial recharge of Rhine water by van Breukelen et al., (1998).

The line 10 in RATES corresponds to the equation of 1st order decay.

The half-life in [s] is defined in bloc KINETICS, in –parms.

The rest of input is the same as in the case of conservative diffusion.

```
TITLE Diffusion-tritium decay
SOLUTION_MASTER_SPECIES
T  T  0T 1.008
SOLUTION_SPECIES
T = T
log_k 0
SOLUTION 0   Tritium
      units  mmol/kgw
      pH     7.0 charge
      temp   25.0
      T      100
SOLUTION 1-40 Initial solution for column
units mmol/kgw
pH 7.0 charge
temp 25.0
RATES
T
-start
10 rate = mol("T")*-(0.693/parm(1))
20 moles = rate*time
30 save moles
-end
KINETICS 1-40
```

```
T
-parms 3.8745e8 #12.3 years in seconds
TRANSPORT
       -cells 40
       -lengths 0.1
       -shifts 40
       -time_step 8.64e6                #100 days
       -flow_direction diffusion_only
       -boundary_conditions constant
       -diffusion_coefficient 2.59e-9   # in m2/s
       -punch_cells 1-40
       -punch_frequency 40
       -print_cells 1-40
       -print_frequency 40
PRINT
       -reset false
SELECTED_OUTPUT
       -file Dif-tritium
       -totals T
USER_GRAPH
-headings distance(m) tritium
-chart_title "Diffusion"
-axis_titles "distance(m)" "TU"
-axis_scale x_axis 0 4.5 0.5
-axis_scale y_axis 0 100 10
-initial_solutions false
-plot_concentration_vs x
-start
10 graph_x dist
20 graph_y tot("T")*1000
END
```

Fig. 6.5 Input for tritium diffusion with decay

Results are in Fig. 6.6. There is a parabolic profile typical for diffusion. The influence of decay is limited due to short time of diffusion. Decay would be become more important in longer term.

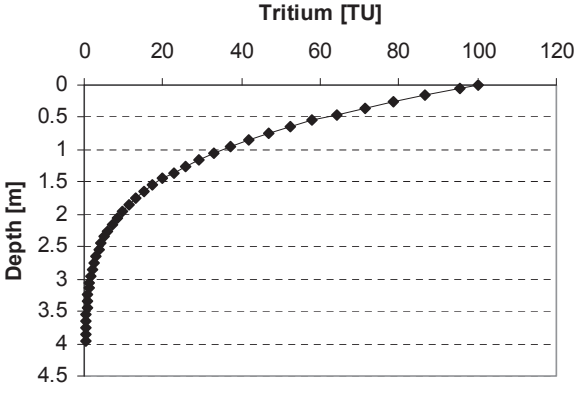

Fig. 6.6 Results of tritium diffusion modeling (TU – tritium units)

6.5 Case study: modeling of natural attenuation and iron cycling at Hnevice site, Czech Republic

Results of inverse geochemical modeling presented in Chapter 5.3.2.3 were used as the choice of suitable phases for modeling of reactive transport. The reactive transport modeling was performed using the program PHT3D (Prommer et al., 2003). The complex mixture of hydrocarbons in the field was approximated by toluene and residual fraction of low solubility. Initial fraction of toluene in the mixture was set to 0.5. The dissolution of the 2-component mixture was calculated by Raoult's Law. The degradation of toluene was modeled by 1st order kinetics, where toluene was first transferred to the pool available for degradation and then degraded. The dissolution/precipitation of ferrihydrite, siderite and mackinawite were modeled as kinetic processes depending on saturation index SI. De-gassing of CO_2, N_2 and CH_4 was allowed when their partial pressures exceeded hydrostatic pressure at a given sampling point.

A 2-D cross-sectional area 80 m and 2 m thick oriented in the direction of groundwater flow and shown in Fig. 5.5 was used in modeling scenarios. Horizontal discretisation was 1.0 m and vertical discretisation was 0.1 m. The finer vertical discretisation was necessary to account for much steeper vertical concentration gradients at lower plume fringe. Hydraulic conductivity of 1.9×10^{-3} m/s and effective porosity of 0.25 were constant over the domain and constant head boundary conditions were used at the inflow and outflow boundaries. Running time was 10 years.

Selected results of the reactive transport model in 2-D domain are shown in Fig. 6.7. In base case (a) intermediate dispersivities $\alpha_L = 0.1$ m and $\alpha_V = 0.001$ m were used, which were based on performed tracer test results. In high dispersivities case (b) values of $\alpha_L = 0.5$ m and $\alpha_V = 0.005$ m were used and in low dispersivities case (c) values of $\alpha_L = 0.05$ m and $\alpha_V = 0.0005$ m were used. The highest concentrations of toluene were calculated for low dispersivities values, while the lowest concentrations were calculated for the highest dispersivities values. In high dispersivities case the end of dissolved plume was located about 42 m from upstream end of the domain. The depletion of ferrihydrite started at about 31 m. Upstream of this location presence of dissolved oxygen and nitrate prevented the use of ferrihydrite as an electron acceptor. Enrichment in ferrihydrite, which is secondary with respect to the onset of contamination, started at lower fringe of the plume at elevation of about 151.5 m. This was a consequence of re-oxidation of ferrous iron transported out of the plume and precipitation of ferrihydrite,

$$Fe^{2+} + 0.25\,O_2 + 2.5\,H_2O = Fe(OH)_3 + 2\,H^+ \qquad (6.4)$$

The thickness of the secondary ferrihydrite precipitation zone was lowest in the case of smallest value of vertical dispersivity because less Fe(II) is transported out of the plume. Re-oxidation of reduced species (i.e. secondary redox reactions (SRR)) at a plume fringe was found to be important also in several other modeling studies (e.g. Hunter et al., 1998; Van Breukelen and Griffoen, 2004; etc.).

It is evident that the values of dispersivities have a strong impact on the amount of precipitated Fe(II) minerals. The amount of precipitated siderite is the highest for lowest dispersivities values and lowest for higher dispersivities values. High dispersivity decreases dissolved Fe(II) concentrations, thus decreasing the amount of precipitated ferrous minerals such as siderite and vice versa.

The same trends as those observed for siderite are for FeS, but no precipitation is observed for highest dispersivities values because dispersion caused low dissolved iron concentrations. Furthermore, the FeS precipitation zone is located closer to the plume core than siderite precipitation zone and, for this reason, FeS precipitation occurs in more reducing environment. This is consistent with the onset of sulfate reduction after the ferrihydrite reduction in redox ladder.

Another important factor determining the amounts of precipitated siderite and FeS are values of kinetic rate constants. An extreme case are equilibrium reactions with maximum precipitated amounts, but with low Fe(II) concentrations in groundwater. However, based on high dissolved iron concentrations in the field both phases precipitate and dissolve kinetically. In this modeling, kinetic rate constants were adjusted to fit dissolved iron concentrations.

The modeling was also able to reproduce partial overlap of several electron acceptors consuming zone suggested in both field observations and previous reactive transport modeling studies (Cozzarelli et al., 2001; Schreiber et al., 2004). Possible explanations were adsorption of Fe(II) and heterogeneity of Fe(III) availability in solid phase.

The modeling also confirmed an important role of re-oxidation zone of previously reduced zone in mass balance of electron acceptors. After retreat of free phase plume (e.g. by free phase pumping) large amounts of minerals such as siderite and FeS are left behind and their oxidation consumes a significant portion of dissolved oxygen and nitrate, which are not available for attenuation of recent free phase plume (Vencelides et al., 2007). For example, when kinetic constants based on dissolved iron best-fit were applied, only about 90 % of electron acceptors reached the recent plume during the re-oxidation period. This means that the presence of zone with reduced minerals in the rear zone of recent plume increases time necessary for natural attenuation.

In summary, reactions at the plume fringe and in the re-oxidation zone have a strong impact on natural attenuation because they influence the availability of electron acceptors within a plume. The presented modeling indicated a significant role of Fe(II) re-oxidation at the lower plume fringe. However, this remains a controversial issue (Van Breukelen and Griffoen, 2004) and supporting field data are limited. Some modeling studies included cation exchange of Fe(II), which eliminated re-precipitation of iron (Brun et al., 2002).

This study shows an important role of modeling in the identification of processes in contaminant plumes and prediction of contaminant plumes behavior. The approach used in this study including collection and analysis of water from multilevel piezometers, calculation of saturation indices combined with mineralogical investigation of solid phase, inverse geochemical modeling supported by isotopic data and finally reactive transport modeling can be used in similar conditions at other contaminated sites.

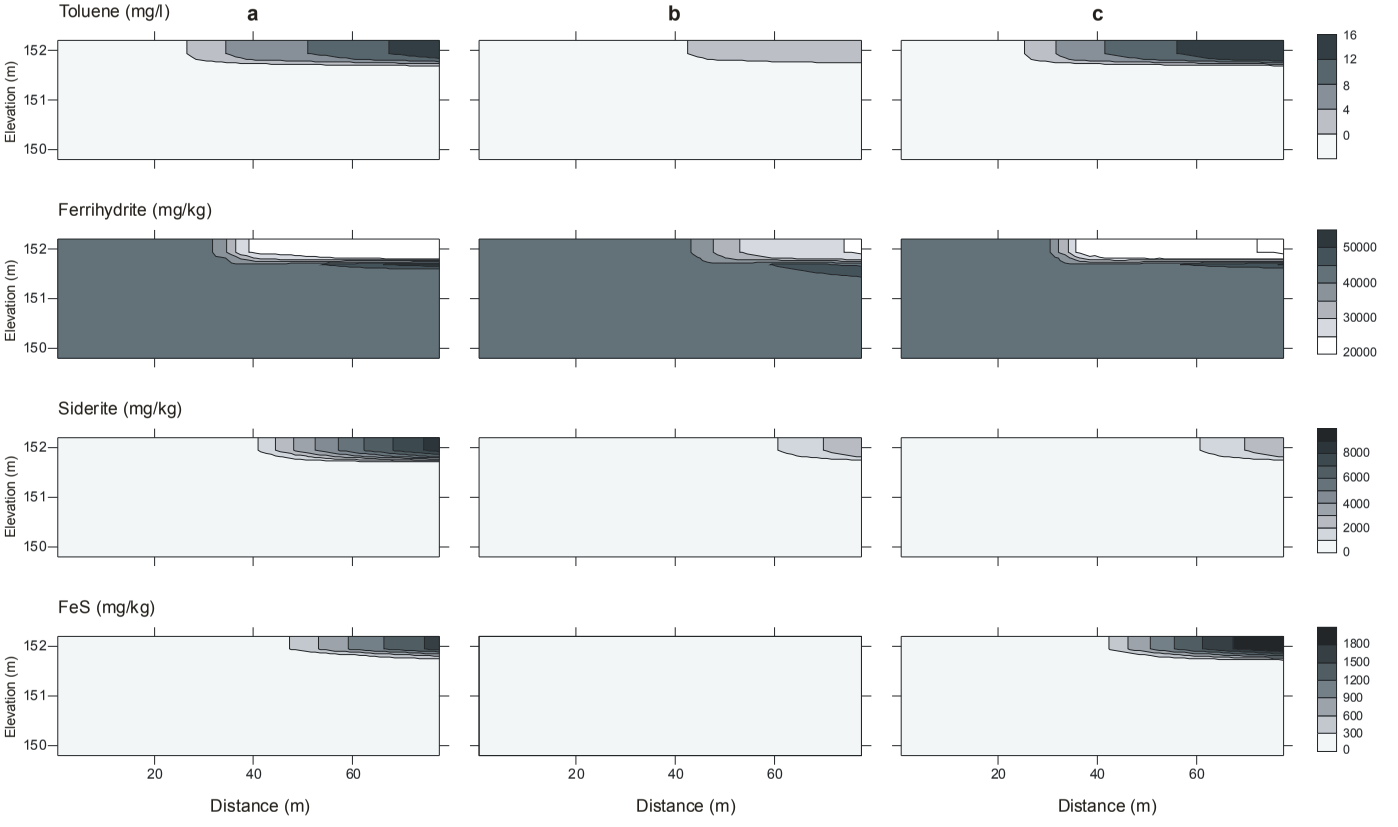

Fig. 6.7 Selected results of reactive transport modeling at Hnevice site (see text) (Published with permission of Elsevier, License Number 3265971254628)

6.6 Case study: reactive transport modeling of acid plume in sandstones

This example is based on study of hydrogeochemical processes linked the presence of acid solutions in sandstone aquifer. Although this example is based on real situation, presented results are aimed at demonstrating the importance of the hydrogeochemical interactions only and do not represent a real site.

6.6.1 Site geology and hydrogeology

The acid plume is hosted in sediments of a Sedimentary Basin. Bedrock is composed of Proterozoic and Lower Paleozoic metamorphic rocks and it is possible to consider it as impermeable. The sandstone formation, which has been the main subject of leaching, is about 20 meters thick and it is located at the bottom of sedimentary sequence of the basin. The sandstones affected by acid plume are overlaid by 40 m thick layer of silty sandstones and this formation is confined by 60 m thick layer of marlstone, muddy limestone and marly siltstone.

The Lower sandstone formation contains no carbonates, the cement consist only of SiO_2 and clay minerals (kaolinite and illite). Pyrite with a significant amount of As is present here in contents in range 0.2–8.3 % wt.

Upper part of the lithologic profile (about 80 m thick) is build of fine to coarse grained sandstones with clayey and carbonaceous cement.

6.6.2 Hydrogeology

Hydrogeological conditions of the site area are complicated. Two aquifers are developed in the sedimentary complex.

The Lower Aquifer is formed mainly by marine sandstones and silty sandstones and it has an artesian water level. It is possible to distinguish two layers with different values of the hydraulic conductivity within this aquifer. The lower part (ca 20 thick) has 50 times higher value of hydraulic conductivity comparing to the upper part, ca 40 m thick layer of silty sandstones. The Upper Aquifer is formed by fine to coarse sandstones and it has a free surface water level. The Upper Aquifer is unconfined.

These two aquifers are separated by 60 m thick Aquitard, which is formed of marlstone, muddy limestone and marly siltstone.

The main component of the leaching solution was sulphuric acid at an average concentration of about 5 %. The leaching solution was also enriched in an oxidant, i.e. NO^{3-} ions.

Baseline, natural conditions before leaching assumed in modeling were:

The median baseline chemical composition and maximum concentrations of major components in groundwater in the Upper and Lower Aquifer are in Table 6.1. The hydrochemical water type is Ca – SO_4 – HCO_3. Water is often slightly acidic with increased concentrations of Al and Fe.

Table 6.1 Median and maximum concentration of major components in mg/L

Aquifer	Ca	Na	Mg	K	HCO_3	SO_4	Cl	NO_3
Upper (median)	100	6	6	2	260	47	13	11
Upper (max)	407	211	175	23	530	1590	120	108
Lower (median)	31	7	3	1	91	30	5	0.5
Lower (max)	65	14	30	4	278	118	16	23

Redox conditions in both aquifers are also different. In Upper Aquifer detectable concentrations of oxygen and nitrate are found. In contrast, in Lower Aquifer, in the zone unaffected by leaching, there is no oxygen and nitrate. Iron is typically present in the form of reduced minerals, mostly sulfides.

Application of acid leaching changed baseline conditions completely. Currently total amount of dissolved solids is almost 5 Mt including 3.72 Mt of sulfate, 467 kt of aluminum, 118 kt of iron, 82.7 kt ammonia ions and 40 kt of nitrate. Most serious contaminants from human health viewpoint are As, Be, Cr, V, and Cd. Except sulfate, nitrate, chloride, fluoride and ammonia ions, which were injected in leaching solutions, other contaminants have the origin in mineral phases of the Lower Aquifer.

Principal reactions with primary minerals are:

Dissolution of kaolinite:

$$Al_2Si_2O_5(OH)_4 + 6\,H^+ \leftrightarrow 2\,Al^{3+} + 2\,H_4SiO_4 + H_2O \tag{6.5}$$

Dissolution of muscovite and illite:

$$KAl_3Si_3O_{10}(OH)_2 + 10\,H^+ \leftrightarrow K^+ + 3\,Al^{3+} + 3\,H_4SiO_4 + 6\,H_2O \tag{6.6}$$

All minerals produce Al and muscovite is also a source of Be and Cd. As a consequence of acid solution application, value of pH in the affected area drop by more than 6 units and there was a shift of redox equilibrium to the level buffered by the N(V)/N(0) redox couple. Due to the shift of redox equilibrium, significant part of present sulfidic minerals was oxidized. The process produced additional acidity:

$$FeS_2 + 2\,NO_3^- + 2\,H_2O \leftrightarrow 2\,SO_4^{2-} + N_2(g) + Fe^{2+} + 4\,H^+ \quad (6.7)$$

A common accessory of pyrite is As (contents about 0.15 wt%), which is mobilized in the process of pyrite dissolution. Generally, the difference in pH between affected part and background zone of the Lower Aquifer is 5–6 units, in redox potential Eh 300–400 mV and in concentrations of dissolved species from 3 to 4 orders of magnitude.

6.6.3 Reactive transport modeling

After the end of remediation pumping residual solutions will start spreading into uncontaminated parts of the aquifer. Due to strong geochemical contrast between leaching area and pristine aquifer it is evident that application of transport model without considering geochemical reactions would provide incorrect results from viewpoint of contaminant attenuation and potential input of other contaminants from the rock environment (Bain et al., 2001; IAEA, 2005).

For this reason, reactive transport model has been used. The aim of the modeling was to evaluate the impact of on-going geochemical reactions on potential exposition to harmful components. Two model scenarios were considered.

Both modeling scenarios have identical input data, geometry of modeling domain and boundary conditions. The only difference is in implementation of geochemical reactions in second model. Model (a) simulates conservative (i.e. advective) transport and model (b) also includes dissolution/precipitation of minerals, cation exchange, and surface complexation.

Reactive transport was modeled by code PHAST (Parkhurst et al., 2004). Program PHAST uses "operator splitting" technique and in each time step calculates transport of dissolved species and speciation and chemical reactions for each cell of the modeling grid.

The aim of model was to calculate the potential negative impact of residual solutions after uranium leaching on the overlying Upper Aquifer used for water supply, especially taking into account the possibility of limited integrity of the Aquitard. For this reason, the model was set as 2-D cross-section oriented in

flow direction and located in the axis of contaminant plume. Code ModelMuse (Winston, 2009) was used to construct input files and program ModelViewer (Hsieh and Winston, 2002) was used for visualization of output results (Fig. 6.8).

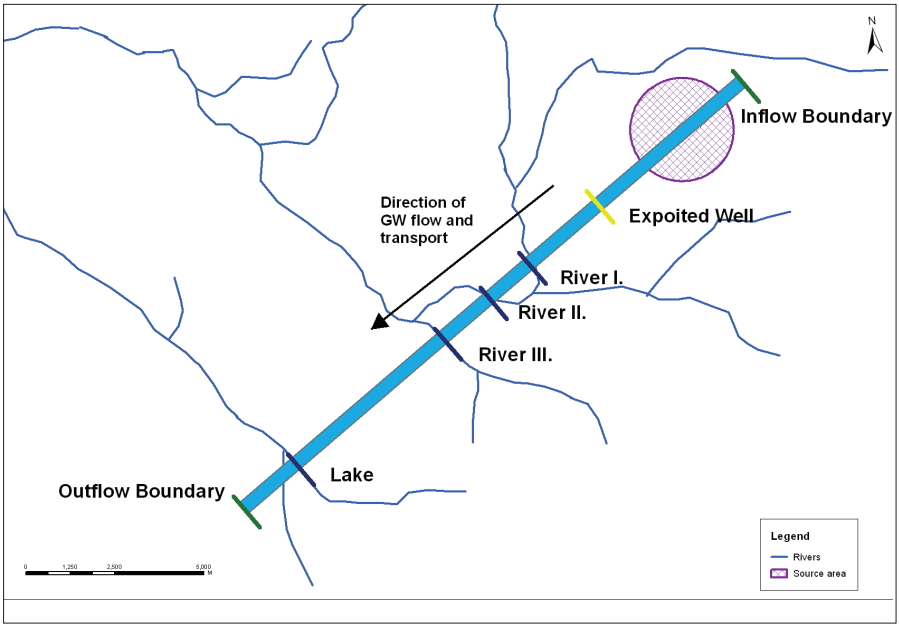

Fig. 6.8 Study area with location of modeling profile

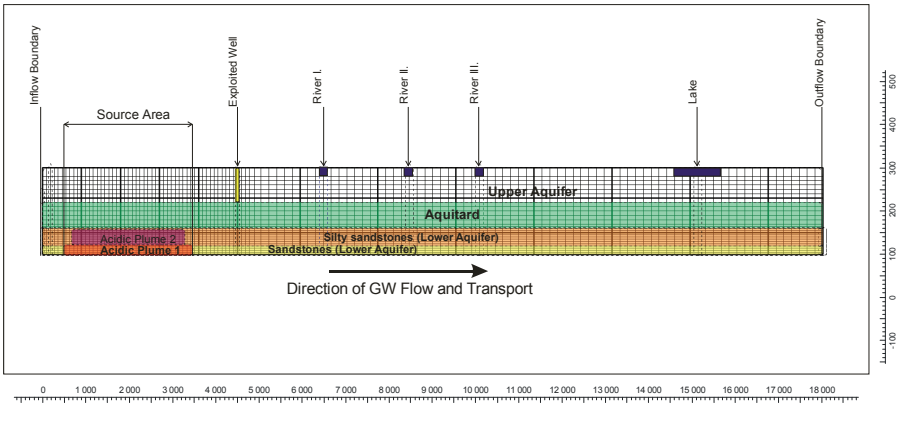

Fig. 6.9 Modeling cross section with the main geological units

Modeling domain has a length of 18,000 m, total thickness of 200 m and comprises (in upward direction) 20 m of sandstone, 40 m of silty sandstone, 60 m of aquitard and 80 m of principal Upper Aquifer (Fig. 6.9). Space discretization step of modeling grid in flow direction was 180 m ($\Delta x = 180$ m). In the leaching fields the grid step was reduced to $\Delta x = 90$ m. In vertical direction the discretization was $\Delta z = 10$ m except the lower aquifer sandstones at the base of modeling domain, where vertical grid step was $\Delta z = 5$ m.

Horizontal hydraulic conductivity k_h was 2.0 m.day^{-1} for Lower Aquifer sandstone, 0.1 m.day^{-1} for silty sandstone, 0.0001 m.day^{-1} for Aquitard and 4.32 m.day^{-1} for principal Upper Aquifer. Vertical hydraulic conductivity k_z was linked to horizontal hydraulic conductivity in such a way that it was set to be 10× lower. Considering possible tectonic disruption in aquitard, two zones with increased vertical hydraulic conductivity were created in the model with a value of 0.432 m.day^{-1}, which are zones of preferential communication between Lower and Upper Aquifers.

A sensitivity analysis of the influence of aquitard vertical hydraulic conductivity k_z on the model results was performed. Value of longitudinal dispersivity was set to 90 m, value of vertical transversal dispersivity was 1 m and value of diffusion coefficient was 1.0×10^{-9} m^2.day^{-1}.

Four different solutions were used in the model: (1) background groundwater from the Lower Aquifer, (2) background groundwater from the Upper Aquifer, (3) acid solutions with variable composition in lower aquifer sandstones, and (4) in overlying layers (silty sandstones). Composition of solutions used in modeling is in Table 6.2.

Table 6.2 Composition of modeling solutions in mg.L^{-1}

Parameter	IC Upper	IC Lower	AS 60g	AS
pH	7.5	7.3	1.5	1.9
pe	14.3	–2.8	13.5	13.0
Al	0.0	0.0	6356.5	2015.7
HCO_3	130.0	173.6	0.0	121.6
Ca	46.1	41.0	257.8	110.5
Cl	5.5	4.2	1759.4	560.8
F	0.0	0.1	242.1	76.8
Fe	0.2	5.6	1098.0	352.1
K	0.9	1.3	66.7	22.1
Mg	0.8	7.5	55.9	23.0

Mn	0.0	0.1	18.1	5.8
NO_3	2.3	0.0	368.5	117.2
NH_4	0.0	0.0	1073.6	340.4
Na	1.1	5.4	20.8	10.3
SO_4	13.2	21.5	42823.5	13592.5
Si	1.6	1.5	38.9	13.4
$O_2(g)$	9.0	0.0	0.0	0.0

Note: Upper background groundwater in Upper Aquifer
Lower background groundwater in Lower Aquifer
AS 60g acid solution in Lower Aquifer sandstones, current stage
AS acid solution in silty sandstones

Initially, residual technological solutions are located in the area of leaching fields and then they start spreading in the direction of groundwater flow. Simultaneously, they interact with primary minerals in the Lower Aquifer, Upper Aquitard and overlying Upper Aquifer. Processes included in the model were equilibrium and/or kinetically constrained dissolution/precipitation of primary and secondary minerals, ion exchange and surface complexation on the surface of hydrous ferric oxide (HFO). Number of surface complexation sites was linked to the amount of goethite in the aquifer matrix. Used mineral phases are in Table 6.3.

Table 6.3 Reactive mineral phases

Phase	Formula	Type	Kinetics	M_0 (mol.L^{-1})
Pyrite	$FeS_{1,9976}As_{0,0024}$*	P/S	kinetics	0,25
Goethite	FeOOH	P/S	equilibrium	0,05
Kaolinite	$Al_2Si_2O_5(OH)_4$	P/S	kinetics	1,36
Muskovite (illite)	$KAl_3Si_3O_{10}(OH)_2$	P	equilibrium	0,08
Jurbanite	$AlOHSO_4$	S	equilibrium	0
K-Jarosite	$KFe_3(SO_4)_2(OH)_6$	S	equilibrium	0
Gypsum	$CaSO_4.2\,H_2O$	S	equilibrium	0
Gibbsite	$Al(OH)_3$	S	equilibrium	0
SiO_2(am)	SiO_2	S	equilibrium	0
Fluorite	CaF_2	S	equilibrium	0
Calcite	$CaCO_3$	P	equilibrium	0.1

Notes: P primary mineral
S secondary mineral
M_0 initial amount

Kinetics of dissolution and potential precipitation of kaolinite was based on Sverdrup and Warfving, (1995):

$$rate = 1000\, A\, \frac{r}{6} \left(\frac{m}{m_0}\right)^{0.67} \left(1 - \frac{IAP_{kaolinit}}{K_{kaolinit}}\right) \tag{6.8}$$

where:

$$r = 10^{-15,1}\, [H^+]^{0,7} \left[1 + \frac{(Al^{3+})}{4\ 10^{-6}}\right]^{-0,4} + 10^{-17,6} \left[1 + \frac{(Al^{3+})}{4\ 10^{-6}}\right]^{-0,2} \tag{6.9}$$

A	surface area of kaolinite [m²/L]
m0	initial amount of kaolinite [mol/L]
m	current amount of kaolinite [mol/L]
IAP	Ion activity product
K	equilibrium constant for dissolution of kaolinite

For precipitation of kaolinite reaction rate was set 10× lower than for its dissolution (Appelo and Postma, 2005).

Kinetics of pyrite oxidation by nitrate was based on Williamson and Rimstidt (1994), adapted by Eckert and Appelo (2002) and Prommer and Stuyfzand (2005):

$$rate = ((O_2)^{0,5} + (NO_3)^{-0,5})\, [H^+]^{-0,11} \left(10^{-10,19} \frac{A}{V}\right) \left(\frac{m}{m_0}\right)^{0,67} \tag{6.10}$$

Arsenic was included in simulation as an accessory in pyrite with initial molar fraction of 0.0024.

6.6.4 Simulation results

When conservative and reactive transport modeling outputs are compared, there are significant differences between both versions of modeling. Relatively small is the difference in concentration of sulfate, which is a dominant component in the system (Fig. 6.11). However, even in this case heterogeneous reactions, mainly pyrite oxidation, producing additional sulfate and coupled with precipitation of jarosite, alunite, or ettringite have some impact.

Large differences are in behavior of principal ions (K^+, Na^+, Mg^{2+} a Ca^{2+}). In reactive version of the model there is replacement of cations from exchange sites at pH about 4.2 by protons H^+.

In the frontal zone of contaminant plume a narrow zone of increased concentration of cations is created. As a consequence, supersaturation with respect to gypsum is reached temporarily and this mineral precipitates. However, this gypsum is not stable in advancing plume and later dissolves. Another Ca source is calcite (Fig. 6.12), which is not present in Lower Aquifer, but is found in Upper Aquitard and Upper Aquifer. For this reason, gypsum precipitates at the contact between the Aquitard and Lower Aquifer (Fig. 6.13).

Ion exchange sites remain saturated by H^+ after contaminant plume was transported downgradient and they represent an additional pool of acidity. This is evident from comparison of pH and sulfate concentrations (Figs 6.10 and 6.11). Low pH zone is advancing in slower rate compared to advective velocity and sulfate transport. Ion exchange maintains low pH in previously contaminated area even when all sulphate was flushed out by inflowing background groundwater.

Precipitation and dissolution of Fe and Al hydroxides has a strong impact on behavior of whole system. Both Fe and Al are present in residual solutions in high concentrations (1100 mg/L and 6350 mg/L, respectively), Figs. 6.14 and 6.15. Source of aluminum is kinetically restricted dissolution of kaolinite, source of iron and also arsenic and sulfate is the oxidation of autochthonous pyrite by nitrate, also modeled as kinetically restricted reaction. Precipitation of aluminum minerals is affected by complexation of Al with fluoride ions. When pH reaches about 3.0, iron starts to precipitate as ferric hydroxide/goethite (Fig 6.16),

$$Fe^{3+} + 3\,H_2O = Fe(OH)_3 + 3\,H^+ \qquad (6.11)$$

When pH reaches about 4.0, aluminum starts to precipitate as amorphous aluminum hydroxide (Fig. 6.17),

$$Al^{3+} + 3\,H_2O = Al(OH)_3 + 3\,H^+ \qquad (6.12)$$

This reaction produces acidity and buffers pH at low region. A part of Fe and Al is during contaminant plume advance bound in metastable minerals such as jarosite, ettringite and alunite.

Precipitation of ferric hydroxide, modeled as equilibrium process, keeps pH at 3.0–3.5, precipitation of aluminum hydroxide at 4.0–4.5. In contrast, presence of ferric hydroxides in the Upper Aquifer increases its neutralization capacity to acidification by residual solutions. This is evident at places where aquitard is not tight and background Upper Aquifer groundwater is mixed with acid solutions penetrating from the Lower Aquifer. Hydrous ferric oxides (HFO) also provide capacity for surface complexation of many toxic metals (Dzombak and Morel, 1990).

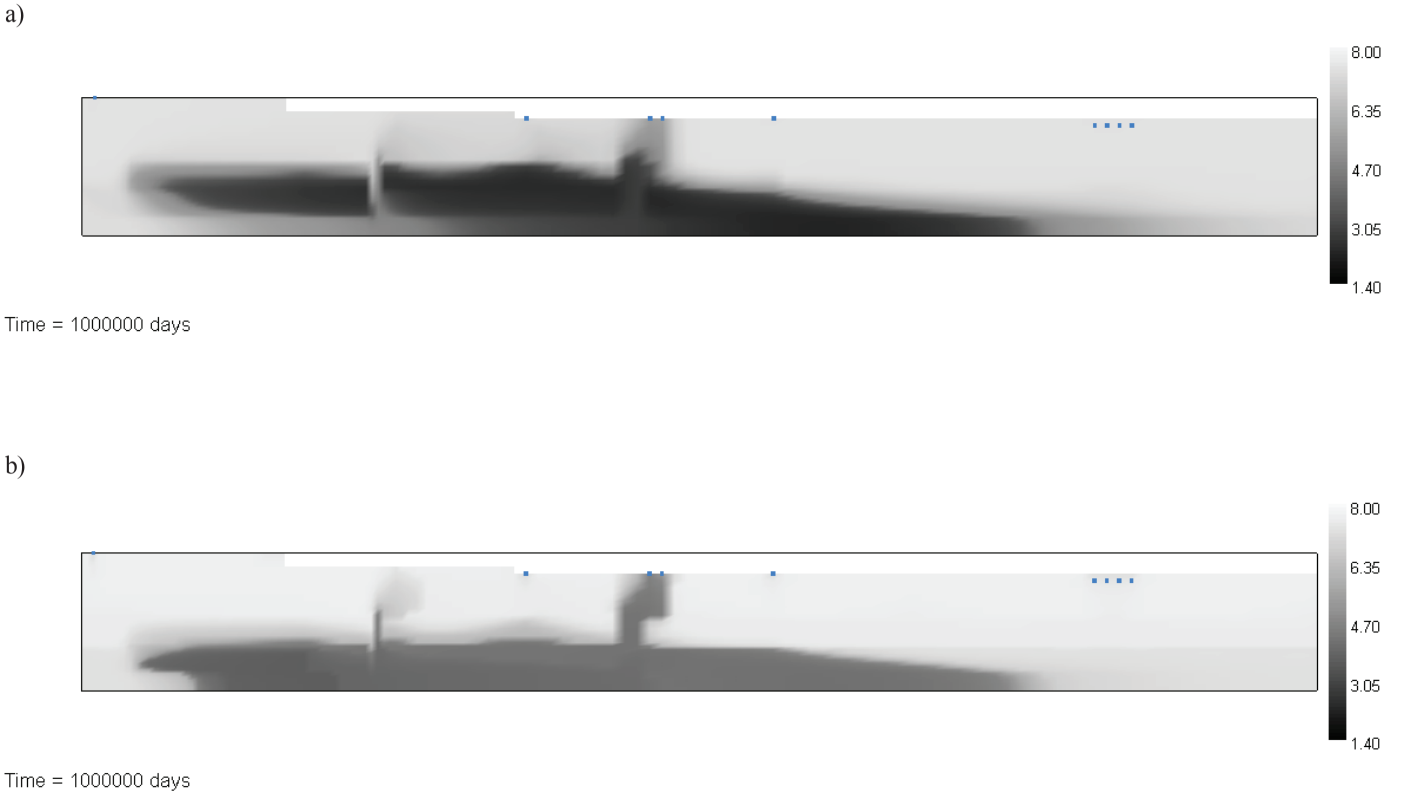

Fig. 6.10 Modeling results – pH (a) conservative case, (b) reactive case

a)

b)

Fig. 6.11 Modeling results – Sulfate (mol.L^{-1}) (a) conservative case, (b) reactive case

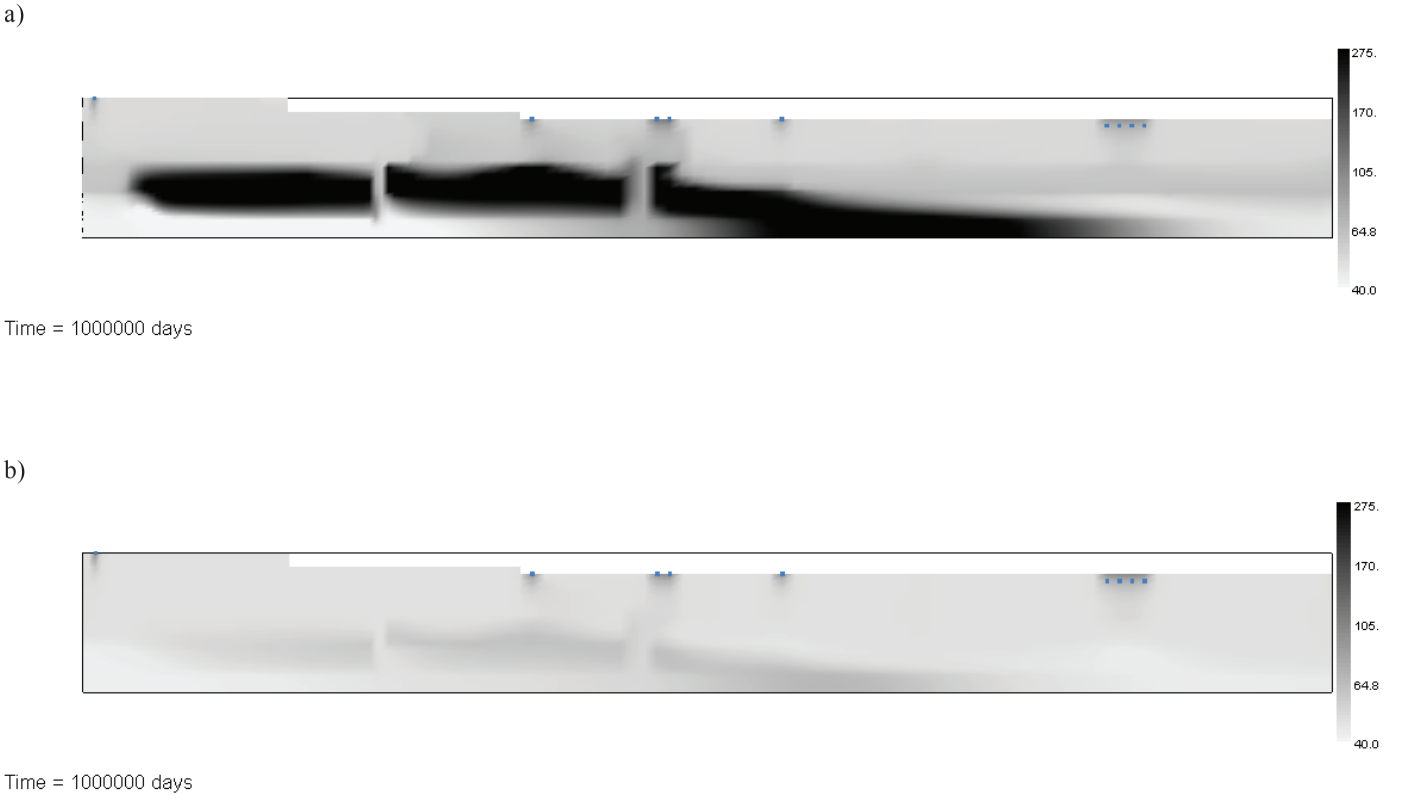

Fig. 6.12 Modeling results – Ca (mol.L^{-1}) (a) conservative case, (b) reactive case

a)

b)

Fig. 6.13 Modeling results – Gypsum (mol.L^{-1}) (a) conservative case, (b) reactive case

Fig. 6.14 Modeling results – Al (mol.L^{-1}) (a) conservative case, (b) reactive case

a)

b)

Fig. 6.15 Modeling results – Fe (mol.L^{-1}) (a) conservative case, (b) reactive case

Fig. 6.16 Modeling results – Goethite (mol.L^{-1}) (a) conservative case, (b) reactive case

a)

b)

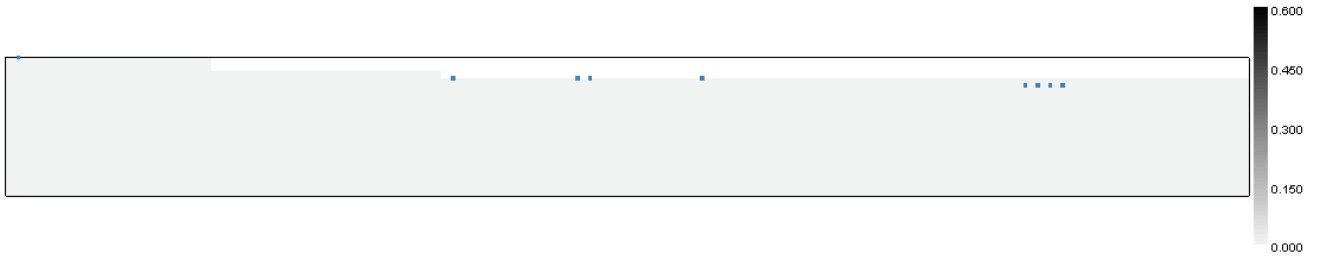

Fig. 6.17 Modeling results – Gibbsite (mol.L^{-1}) (a) conservative case, (b) reactive case

6.6.5 Conclusions

Behavior of contaminant plume can be approximated by transport of sulfate, which is dominant component in acid solutions. In the Lower Aquifer, cation exchange is an important process, resulting in frontal zone of the plume enriched in Ca and Mg. In this zone, irreversible precipitation of secondary minerals such as jarosite, ettringite and gypsum may occur. Dissolution of primary minerals such as pyrite and kaolinite is also significant because these minerals represent sources of metals and metalloids. Solid phase surface in the zone affected by acid solutions represents a source of H^+ limiting the increase of pH after retreat of acid plume.

In the Upper Aquifer dominant processes are dissolution of calcite and precipitation of gypsum and ferric and aluminum hydroxides. This case study demonstrates clearly that reactive transport modeling is a necessary prerequisite for studies of complex contaminant plumes.

Literature

Ahmed K. M., Bhattacharya P., Hasan M. A., Akhter S. H., Alam S. M. M., Bhuyian M. A. H., Imam M. B., Kham A. A., Sracek O., 2004. Arsenic enrichment in groundwater of the alluvial aquifers in Bangladesh, Appl. Geoch. 19, pp. 181–200.

Albarède F., 1995. Introduction to Geochemical Modeling, Cambridge University Press.

Allison J. D., Brown D. S., Novo-Gradac K. J., 1991. MINTEQA2, A Geochemical Assessment Data Base and Test Cases for Environmental Systems, Athens, GA, U.S. EPA.

Anderson M. P., Woessner W. W., 1992. Applied Groundwater Modeling, Simulation of Flow and Advective Transport, Academic Press Inc., 381 p.

André L., Franceschi M., Pouchon P., Atteia O., 2005. Using geochemical data and modelling to enhance the understanding of groundwater flow in a regional deep aqufer, Aquitaine Basin, south-west of France, J. Hydrology 305, pp. 40–62.

Appelo C. A. J., Postma D., 2005. Geochemistry, groundwater and pollution, 3rd Edition, A. A. Balkema, Rotterdam/Brookfield.

Baedecker M. J., Cozzarelli I. M., Eganhouse R. P., Siegel D. I., Bennett P. C., 1993. Crude oil in a shallow sand and gravel aquifer-III. Biogeochemical reactions and mass-balance modeling in anoxic groundwater, Appl. Geochemistry, 8, pp. 569–586.

Bain J., Mayer K. U., Blowes D. W., Frind E. O., Molson J. W, Kahnt R., Jenk U., 2001. Modelling the closure-related geochemical evolution of groundwater at a former uranium mine. Journal of Contaminant Hydrology, Vol. 52, No. 1–4, pp. 109–135.

Bethke C. M, 1996. Geochemical Reaction Modeling, New York, Oxford University Press, 397 p.

Blowes D. W., Jambor J. L., 1990. The pore-water geochemistry and the mineralogy of the vadose zone of sulfide tailings, Waite Amulet, Quebec, Canada, Appl. Geoch., 5, pp. 327–346.

Bredehoeft J., 2005. The conceptualization model problem – surprise, Hydrogeol. J. 13, 1, 37–46.

Brun A., Engesgaard P., 2002. Modelling of transport and biogeochemical processes in pollution plumes: literature review and model development, J. Hydrol. 256, pp. 211–227.

Chapelle F. H., 1993. Ground Water Microbiology and Geochemistry, John Wiley & Sons, New York.

Christensen T. H., Bjerg P. L., Banwart S. A., Jakobsen R., Heron G., Albrechtsen H.-J., 2000. Characterization of redox conditions in groundwater contaminant plumes, J. Contam. Hydrol. 45, pp. 165–241.

Cozzarelli I. M., Bekins B., Baedecker M. J., Aiken G. R., Eganhouse R. P., Tuccillo M. E., 2001. Progression of natural attenuation processes at a crude oil spill site: I. Geochemical evolution of the plume, J. Contam. Hydrol. 52, 369–385.

Deutsch W. J., 1997. Groundwater Geochemistry, Fundamentals and Applications to Contamination, Lewis Publishers, Boca Raton, New York.

Drever J. I., 1997. The Geochemistry of Natural Waters, Surface and Groundwater Environments, 3rd Edition, Prentice Hall, Upper Saddle River, NJ 07458.

Domenico P., Schwartz F. W., 1998. Physical and Chemical Hydrogeology, 2nd Edition, John Wiley & Sons, New York.

Dzombak D. A., Morel F. F. M., 1990. Surface Complexation Modeling: Hydrous Ferric Oxide, New York, John Wiley & Sons, 393 p.

Eckert, P., Appelo C. A., 2002. Hydrogeochemical modeling of enhanced benzene, toluene, ethylbenzene, xylene (BTEX) remediation with nitrate. Water Resources Research, Vol. 38, No. 8.

Fetter C. W., 1999. Contaminant Hydrogeology, Prentice Hall, New York, 500 p.

Freeze R. A., Cherry J. A., 1979. Groundwater, John Wiley & Sons, 604 p.

Fritz S. J., 1994. A survey of charge-balance errors on published analyses of potable ground and surface waters, Groundwaters 32, pp. 539–546.

Gerla P. J., 1992. Pathline and geochemical evolution of groundwater in a regional discharge area, Red River Valley, North Dakota, Groundwater 30, pp. 743–754.

Greskowiak J., Prommer H., Massmann G., Johnston J. D., Nützmann G., Pekdeger A., 2005. The impact of variably saturated conditions on hydrogeochemical changes during artificial recharge of groundwater, Appl. Geoch. 20, pp. 1409–1426.

Heron G., Christensen T. H., Tjell J. C., 1994. Oxidation capacity of aquifer sediments, Envir. Sci. Technol. 28, pp. 153–158.

Hunter K. S., Wang Y., Van Capellen P., 1998. Kinetic modeling of microbially-driven redox chemistry of subsurface environments: coupling transport, microbial metabolism and geochemistry, J. Hydrol. 209, 56–80.

Hsieh P. A., Winston R. B., 2002. User's guide to Model Viewer, a program for threedimensional visualisation of ground-water model results. U.S.G.S. Open File Report 02-106. Menlo Park. USGS.

IAEA. 2005. Guidebook on environmental impact assessment for in situ leach mining projects. IAEA-TECDOC-1428. Vienna: IAEA.

Jurjovec J., Blowes D. W., Ptacek C. J., Mayer K. U., 2004. Multicomponent reactive transport modeling of acid neutralization reactions in mine tailings, Water Res. Research 40, W11202, 17 p.

Keating E. H., Bahr J. M., 1998. Using reactive solutes to constrain groundwater flow models at a site in northern Wisconsin, Water Res. Research, Vol. 34, No. 12, pp. 3561–3571.

Kehew A. E., 2000: Applied Chemical Hydrogeology, Prentice Hall, Upper Saddle River, NJ 07458.

Kharaka Y. K., Gunter W. D., Aggarwal P. K., Perkins E. H., DeBraal J. D., 1988. Solmineq. 88: A computer program for geochemical modeling of water-rock interactions, U.S. Geological Survey Water Resources Investigation Report 88-4227.

Konikow L. F., Bredehoeft J. D., 1992. Ground-water models cannot be validated, Advances in Water Resources 15, 75–83.

Langmuir D., 1997. Aqueous Environmental Geochemistry, Prentice Hall, Upper Saddle River, NJ 07458.

Mayer K. U., Frind E. O., Blowes D. W., 2002. Multicomponent reactive transport modeling in variably saturated media using generalized formulation for kinetically controlled reactions, Water Res. Research, 38(9), article no. 1174.

Mayer K. U., Benner S. G., Frind E. O., Thornton S. F., Lerner D. N., 2001. Reactive transport modeling of processes controlling the distribution and natural attenuation of phenolic compounds in a deep sandstone aquifer, J. Contam. Hydrology 53, pp. 341–368.

McDonald M. G., Harbaugh, 1988. A modular three-dimensional finite-difference groundwater flow model, Techniques of Water-Resources Investigations 06-A1, USGS, 576 p.

Molson J. W., Fala O., Aubertin M., Bussière B., 2005. Numerical simulations of pyrite oxidation and acid mine drainage in unsaturated waste rock piles, J. Contam. Hydrol. 78, pp. 343–371.

Palmer C. D., Cherry J. A., 1984. Geochemical evolution of groundwater in sequences of sedimentary rocks, J. Hydrol., 75, pp. 27–65.

Parkhurst D. L., Appelo C. A. J., 1999. PHREEQC-2, a Hydrogeochemical Computer Program, U.S. Geological Survey, Water Res. Inv.

Parkhurst, D. L., Kipp, K. L., Engesgaard, Peter, and Charlton, S. R., 2004. PHAST—A program for simulating ground-water flow, solute transport, and multicomponent geochemical reactions: U.S. Geological Survey Techniques and Methods 6–A8, 154 p.

Plummer L. N., Jones B. F., Truesdall A. H., 1976. WATEQ4F-A Fortran IV Version of Wateq, a Computer Program for Calculating Chemical Equilibria of Natural Waters, U.S. Geological Survey Water Resources Investigations Report 76-13.

Plummer L. N., 1984. Geochemical modeling: A comparison of forward and inverse methods. First Canadian/American Conference on Hydrogeology, Eds. B. Hitchon, E. I. Wallick, Dublin, Ohio, National Water Well Assoc., pp. 149–177.

Plummer L. N., Parkhurst D. L., Fleming G. W., and Dunkle, S. A., 1988, A computer program incorporating Pitzer's equations for calculation of geochemical reactions in brines: U.S. Geological Survey Water-Resources Investigations Report 88-4153, 310 p.

Plummer L. N., Prestemon E. C., Parkhurst D. L., 1994. An Interactive Code (NETPATH) for Modeling Geochemical Reactions along a Flow Path, Version 2.0, U.S. Geological Survey Water Resources Investigation Report 94-4169.

Prommer H., Barry D. A., Zheng C., 2003. MODFLOW/MT3DMS-Based Reactive Multicomponent Transport Modeling, Groundwater, Vol. 41, No. 2, pp. 247-257.

Prommer H., Barry D. A., Davis G. B., 2002. Modeling of physical and reactive processes during biodegradation of a hydrocarbon plume under transient groundwater flow conditions, J. Contam. Hydrology 59, pp. 113–131.

Prommer, H., Stuyfzand P. J., 2005. Identification of temperature-dependent water quality changes during deep well injection experiment in pyritic aquifer. Environmental Science & Technology, Vol. 39, No. 7, pp. 2200–2209.

Reardon E. J., 1990. An ion interaction model for determining ion equilibria in cement/water systems, Cement Concrete Research 20, pp. 175–192.

Robertson W. D., Cherry J. A., Sudicky E. A., 1991. Ground-Water Contamination from Two Small Septic Systems on Sand Aquifers, Groundwater, Vol. 29, No. 1, pp. 82–92.

Runnells D. D., Shepherd T. A., Angino E. E., 1992. Determining natural background concentrations in mineralized areas, Envir. Sci. Technol. 26, pp. 2316–2323.

Saunders J. A., Toran L. E., 1995. Modeling of radionuclide and heavy metal sorption around low- and high-pH waste disposal sites at Oak Ridge, Tennessee, Appl. Geoch. 10, pp. 673–684.

Schecher W. D., McAvoy D. C., 1998. A Chemical Equilibrium Modeling System: Version 4.0 for Windows User's Manual, Environmental Research Software, Hallowell, Maine.

Schreiber M. E., Carey G. R., Feinstein D. T., Bahr J. M., 2004. Mechanism of electron acceptor utilization: implications for stimulating anaerobic biodegradation, J. Contam. Hydrol. 73, 99–127.

Sracek O., Bhattacharya P., Jacks G., Gustafsson J. P., 2001. Mobility of arsenic and geochemical modeling in groundwater environment, In: Jacks G., Bhattacharya P., Khan A. A. (Ed.): Groundwater arsenic contamination in the Bengal Delta Plain of Bangladesh, KTH Special Publication, TRITA-AMI REPORT 3084, pp. 9–20.

Sracek O., Bhattacharya P., Jacks G., Gustafsson J.-P., von Bromssen M., 2004. Behavior of arsenic and geochemical modeling of arsenic enrichment in aqueous environments, Appl. Geoch. 19, pp. 169–180.

Sracek O., Bhattacharya P., von Bromssen M., Jacks G., Ahmed K. M., 2005. Natural enrichment of arsenic in groundwaters of Brahmanbaria district, Bangladesh: geochemistry, speciation modeling and multivariate statistics, In: J. Bundschuh, P. Bhattacharya, D. Chandrasekharam (Ed.): Natural Arsenic in Groundwater: Occurrence, Remediation and Management, A. A. Balkema Publishers, pp. 133–143.

Sracek O., Hirata R., 2002. Geochemical and stable isotopic evolution of the Guarani Aquifer System in the state of São Paulo, Brazil, Hydrogeology J. 10, pp. 643–655.

Šráček O., Datel J., Mls J., 2002. Kontaminační hydrogeologie (Contaminant Hydrogeology), 2nd Edition, Karolinum, UK Praha.

Šráček O., Kuchovský T., 2003. Základy hydrogeologie (Introduction to Hydrogeology), Masaryk University.

Šráček O., Zeman J., 2004. Introduction to Environmental Hydrogeochemistry, Masaryk University.

Stollenwerk K. G., 1994. Geochemical Interactions between Constituents in Acidic Groundwater and Alluvium in an Aquifer near Globe, Arizona, Appl. Geochemistry, 9, pp. 353–369.

Stumm W., 1992. Chemistry of the Solid-Water Interface, New York, John Wiley & Sons, 428 p.

Stumm W., Morgan J. J., 1996. Aquatic Chemistry, 3rd Edition, John Wiley & Sons, Inc.

Sverdrup H. U., Warfvinge P., 1995. Estimating field weathering rates using laboratory kinetics. In: Min. Rev. pp. 485–541.

Tipping E., 1994. WHAM – A Chemical Equilibrium Model and Computer Code for Waters, Sediments and Soil, Incorporating a Discrete Sites/Electrostatic Model of Ion-Binding by Humic Substances, Computers and Geosciences 20, pp. 973–1023.

Toran L., 1994. Sulfate contamination in groundwater from a carbonate-hosted mine, J. Contam. Hydrol., 2, pp. 1–29.

Toran L. E., Saunders J. A., 1999. Modeling alternative paths of chemical evolution of Na-HCO_3-type groundwater near Oak Ridge, Tennessee, USA, Hydrogeology J. 7, 4, pp. 355–364.

Tuccillo M. E., Cozzarelli I. M., Herman J. S., 1999. Iron reduction in the sediments of a hydrocarbon-contaminated aquifer, Appl. Geochem. 14, pp. 655–667.

Van Breukelen B. M., Appelo C. A. J., Olsthoorn T. N., 1998. Hydrogeochemical transport modeling of 24 years of Rhine water infiltration in the dunes of the Amsterdam water supply, J. Hydrol. 209, pp. 281–296.

Van Breukelen B. M., Röling W. F. M., Groen J., Griffioen J., van Verseveld H. W., 2003. Biogeochemistry and isotope geochemistry of a landfill leachate plume, J. Contam. Hydrol. 65, pp. 245–268.

Van Breukelen B. M., Griffioen J., 2004. Biogeochemical processes at the fringe of landfill leachate plume: potential for dissolved organic carbon, Fe(II), Mn(II), NH_4, and CH_4 oxidation, J. Contam. Hydrol. 65, 245–268.

Vencelides Z., Sracek O., Prommer H., 2006. Iron cycling and its impact on the electron balance at a petroleum hydrocarbon contaminated site in Hnevice, Czech Republic, J. Contam. Hydrol., 89, 245–268.

Walter A. L., Frind E. O., Blowes D. W., Ptacek C. J., Molson J. W., 1994. Modeling of Multicomponent Reactive Transport in Groundwater, I. Model Development and Evaluation, Water Res. Research, 30, pp. 3137–3148.

Weaver T. R., Bahr J. M., 1991. Geochemical Evolution in the Cambrian-Ordovician Sandstone Aquifer, Eastern Wisconsin: 1. Major Ion and Radionuclide Distribution, Groundwater, Vol. 29, No. 3, pp. 350–356.

Williamson M. A., Rimstidt J. D., 1994. The kinetics and electrochemical rate-determining step of aqueous pyrite oxidation. Geochimica et Cosmochimica Acta, Vol. 58, pp. 5443–5454.

Winston R. B. 2009., ModelMuse — A graphical user interface for MODFLOW–2005 and PHAST: U.S. Geological Survey Techniques and Methods 6–A29. Reston. USGS.

Wolery T. J., 1988. EQ3/6, A Software Package for Geochemical Modeling of Aqueous Systems: Package Overview and Installation Guide (Version 7.0), Lawrence Livermore National Laboratory.

Yeh, G.-T. and V. S. Tripathi, 1990. HYDROGEOCHEM, A Coupled Model of HYDROlogic Transport and GEOCHEMical Equilibria in Reactive Multicomponent Systems. ORNL-6371. Oak Ridge National Laboratory.

Zheng C., Wang P. P., 1999. MT3DMS: A modular three-dimensional multispecies model for simulation of advection, dispersion and chemical reactions of contaminants in groundwater systems: Documentation and user's guide. Contract Report SERDP-99-1. Vicksburg, Mississippi, U.S. Army Engineer Research and Development Center.

Zhu C., Hu F. Q., Burden D. S., 2001. Multi-component reactive-transport modeling of natural attenuation of an acid ground water plume at a uranium mill tailings site, J. Contam. Hydrol. 52, pp. 85–108.

Zhu C., Anderson G. M., Burden A. S., 2002. Natural attenuation reactions at a uranium mill tailings site, western USA, Groundwater, Vol. 40, No. 1.–2.

Zhu C., Anderson G., 2002. Environmental Applications of Geochemical Modeling, Cambridge University Press, 284 p.

Ondřej Šráček
Miroslav Černík
Zbyněk Vencelides

Applications of Geochemical and Reactive Transport Modeling in Hydrogeology

Executive Editor Tomáš Opatrný
Responsible Editor Lucie Loutocká
Layout Anna Petříková
Cover Design Jiří Jurečka

Published by Palacký University, Olomouc
Křížkovského 8, 771 47 Olomouc
www.vydavatelstvi.upol.cz
www.e-shop.upol.cz
vup@upol.cz

Printed by TISKSERVIS Jiří Pustina
Gen. Sochora 1764/22
708 00 Ostrava-Poruba
www.tiskservis.cz

First Edition

Olomouc 2013

Book Series – Textbooks

ISBN 978-80-244-3781-1

Not for sale

VUP 2013/667